Mechanisms and modelling of sonochemically-mediated free radical degradation of contaminants

Author:
Han, Hyungjin

Publication Date:
2009

DOI:
https://doi.org/10.26190/unsworks/14628

PLEASE TYPE

THE UNIVERSITY OF NEW SOUTH WALES
Thesis/Dissertation Sheet

Surname or Family name: **HAN**

First name: **HYUNGJIN** Other name/s:

Abbreviation for degree as given in the University calendar: **Ph. D**

School: **School of Civil & Environmental Engineering** Faculty: **Engineering**

Title:

Mechanisms and Modelling of Sonochemically-Mediated Free Radical Degradation of Contaminants

Abstract 350 words maximum: (PLEASE TYPE)

Hazardous and recalcitrant pollutants in the environments have led to a great many environmental issues these days. Many researchers have focused on the approaches to treatment of these pollutants which contaminate environments such as soil, surface and groundwater. As an advanced oxidation processes (AOPs), sonolysis which is the oxidation technology involving the use of ultrasonic irradiation, has proven to be successful for the treatment and remediation of contaminated environments. In this thesis, hydrogen peroxide formation and formic acid degradation by ultrasonic irradiation of well-characterised solutions are described under various conditions in order to determinate reaction mechanism by which peroxide degradation and contaminant degradation occur. The effect of gas properties and frequency on hydrogen peroxide and formic acid degradation are examined. Experimental results obtained are analyzed in light of the reactions occurring. Successful mathematical modeling of the results obtained confirms that, for the most part, hydrogen peroxide and formic degradation occur by free radical generation within bubbles with subsequent transfer of these radicals to the bubble-water interface where the majority of the degradation occurs. The effect of Fe(II) addition which can lead to Fenton reactions in the bulk solution are also investigated. Experimental and model results show that the heterogeneous reactions can enhance the degradation of formic acid in the presence of Fe(II). Oxidation of phenol by ultrasonic irradiation under a variety of initial conditions and solution environments is also described and validated by a simple kinetic model. The model developed will be useful for improving our understanding of free radicals behaviour and the interplay between free radical generation and contaminant degradation.

FOR OFFICE USE ONLY Date of completion of requirements for Award:

26-03-2009

THIS SHEET IS TO BE GLUED TO THE INSIDE FRONT COVER OF THE THESIS

Mechanisms and Modelling of Sonochemically-Mediated Free Radical Degradation of Contaminants

by

Hyungjin HAN

BSc, MEng

A thesis submitted in partial fulfilment

of the requirements for the degree of

Doctor of Philosophy

School of Civil and Environmental Engineering

The University of New South Wales

2009

ORIGINALITY STATEMENT

'I hereby declare that this submission is my own work and to the best of my knowledge it contains no materials previously published or written by another person, or substantial proportions of material which have been accepted for the award of any other degree or diploma at UNSW or any other educational institution, except where due acknowledgement is made in the thesis. Any contribution made to the research by others, with whom I have worked at UNSW or elsewhere, is explicitly acknowledged in the thesis. I also declare that the intellectual content of this thesis is the product of my own work, except to the extent that assistance from others in the project's design and conception or in style, presentation and linguistic expression is acknowledged.'

Signed

Date

Abstract

Hazardous and recalcitrant pollutants in the environments have led to a great many environmental issues these days. Many researchers have focused on the approaches to treatment of these pollutants which contaminate environments such as soil, surface and groundwater. As an advanced oxidation processes (AOPs), sonolysis which is the oxidation technology involving the use of ultrasonic irradiation, has proven to be successful for the treatment and remediation of contaminated environments.

In this thesis, hydrogen peroxide formation and formic acid degradation by ultrasonic irradiation of well-characterised solutions are described under various conditions in order to determinate reaction mechanism by which peroxide degradation and contaminant degradation occur. The effect of gas properties and frequency on hydrogen peroxide and formic acid degradation are examined. Experimental results obtained are analyzed in light of the reactions occurring. Successful mathematical modeling of the results obtained confirms that, for the most part, hydrogen peroxide and formic degradation occur by free radical generation within bubbles with subsequent transfer of these radicals to the bubble-water interface where the majority of the degradation occurs. The effect of Fe(II) addition which can lead to Fenton reactions in the bulk solution are also investigated. Experimental and model results show that the heterogeneous reactions can enhance the degradation of formic acid in the presence of Fe(II).

Oxidation of phenol by ultrasonic irradiation under a variety of initial conditions and solution environments is also described and validated by a simple kinetic model. The model developed will be useful for improving our understanding of free radicals behaviour and the interplay between free radical generation and contaminant degradation.

ACKNOWLEDGEMENTS

I am sincerely grateful to my supervisor, Professor David Waite for his guidance and comments. This study would not have been completed without his enthusiastic encouragement and constant support.

The friendship and support of my colleagues within the School is greatly acknowledged. I would like to thank to Dr. Gautam Chattopadhyay for his assistance in the laboratory work. I also appreciate administrative assistance to Pattie MacLaughlin, Julie O'Keefe and Karenne Irvine. In particular, I wish to extend my warmest thanks to Dr Shikha Garg for her valuable advices, kind discussion and friendship. I would not have been able to accomplish much of work in the study.

Finally, I owe my deep thanks to my wife, Junghwa Lee, and lovely princesses, Sebin, Seyoung, and Yoojung, who provided great love and support during the entire period of my study, especially in the last year prior to completion. I also wish to thank my parents for their absolute love and support over the years.

Hyungjin HAN
2009

TABLE OF CONTENTS

LIST OF FIGURES

LIST OF TABLES

Chapter 1

Introduction

1.1 Background

With increasing concerns about the risks posed by organic contaminants in water supplies, in part related to the desire to recycle wastewaters, a need exists to upgrade water treatment processes such that the concentration of such contaminants is reduced to levels at which risk is minimal. While many organic compounds can be degraded and/or removed by traditional methods of biological treatment or activated carbon adsorption, some compounds (including herbicides, pesticides, pharmaceuticals and natural and synthetic hormones) will require more powerful degradative technologies.

Treatment technologies known as Advanced Oxidation Processes (AOPs) represent one approach to degradation of organic contaminants which show potential for wider use in water and wastewater treatment. AOPs generally act through formation of hydroxyl radical. Because, the hydroxyl radical has a strong oxidation potential (E_o = 2.73 V; Pignatello *et al.*, 2006) and high reactivity for most organic compounds (typically exhibiting second order rate constants in the range 10^7 ت 10^{10} $M^{-1}s^{-1}$; Buxton *et al.*, 1988), AOPs would appear to hold considerable promise for removal of recalcitrant organic compounds.

Possible AOPs include UV irradiation, high pH ozonation, ozonation combined with hydrogen peroxide addition (the ـپperoxoneـپ process), Fenton and photo-Fenton

oxidation, electrochemical oxidation and sonolysis. Each of these technologies has their own particular advantages and disadvantages but all represent possible approaches to oxidative degradation of organic compounds in aqueous solution.

While investigations to date have been, for the most part, at bench-scale only, the technology of sonolysis appears particularly promising. Sonolysis is the application of ultrasound to chemical reactions and processes. The chemical effects of ultrasound derive from the phenomenon of acoustic cavitations; the formation, growth and implosive collapse of bubbles in a liquid (Suslick, 1988). The collapse of these bubbles produces high local temperatures and pressures. Locally, temperature and pressure may reach up to and above 5000 K and 1000 atm, respectively (Makino *et al.*, 1983, Suslick, 1989, Suslick, 1990, Serpone and Colarusso, 1994). These critical conditions result in homolysis of water producing highly reactive species such as hydroxyl (•OH) and hydrogen (•H) atom radicals. These radicals react with each other leading to other species such as water, hydrogen and hydrogen peroxide (reactions (1) to (6)).

$$H_2O \rightarrow OH\bullet + H\bullet \quad (1)$$

$$OH\bullet + H\bullet \rightarrow H_2O \quad (2)$$

$$OH\bullet + OH\bullet \rightarrow H_2O_2 \quad (3)$$

$$H\bullet + H\bullet \rightarrow H_2 \quad (4)$$

$$H_{2}\bullet + O_2 \rightarrow HO_{2}\bullet \quad (5)$$

$$HO_{2}\bullet + HO_{2}\bullet \rightarrow H_2O_2 + O_2 \quad (6)$$

The radicals produced by application of ultrasonic radiation can be used for initiating a wide range of oxidation reactions, particularly as a result of generation of the hydroxyl radical. In addition to hydroxyl radical attack, compounds that are particularly volatile may partition into the gaseous bubble and be degraded by pyrolysis.

While many investigations have demonstrated the effectiveness of sonolysis, our understanding of the mechanism(s) underlying degradation is often limited and very little attempt has been made, in part due to the inherent complexity of these heterogeneous processes, to develop mathematical models of the degradation kinetics.

1.2 Objectives

The main objective of this study is to provide a better understanding of the free radical reactions initiated by ultrasonic irradiation of aqueous solutions and, where possible, to use kinetic modelling approaches to validate our hypotheses pertaining to key reaction pathways. Particular attention is given to the generation of hydrogen peroxide, a relatively stable end product of free radical reactions, and to degradation of formic acid, a simple ب model contaminant پ chosen for the simplicity of its degradation pathway via hydroxyl radical attack. The impact of variation in key parameters such as frequency and background gas on sonochemical activity are investigated by examining the impact on hydrogen peroxide production and formic acid degradation kinetics. As noted above, mathematical modelling is undertaken as an aid to hypothesis development and testing.

More specifically, the aims of this study are to:

1) Advance our understanding of the ultrasonic irradiation phenomena in aqueous solution.
2) Improve understanding of free radical production pathways, reactions of the produced radicals both with themselves and with selected target compounds.
3) Develop mathematical models that adequately describe the time dependence of generation and/or decay of measurable species in solution. To this end, analysis is focussed on the kinetics of hydrogen peroxide formation and formic acid degradation.
4) Investigate the implications of the proposed reaction pathways to other contaminants. To this end, attention is given to measuring (and modelling) the degradation kinetics of phenol.

1.3 Outline

The structure of the thesis is as follows.

Chapter 2 critically reviews the relevant literature relating to both the general principles of sonochemistry and application of sonolysis in degradation of organic compounds in aqueous solution.

Chapter 3 documents the experimental procedures used in all studies described in the thesis and provides an introduction to the kinetic modelling approaches used.

Chapter 4 presents the experimental results of hydrogen peroxide formation and formic acid degradation under different frequencies and background gases by ultrasonic irradiation. Hydrogen peroxide formation rates under a variety of experimental conditions are presented as are formic acid degradation rates under a similar range of conditions. Likely chemical reactions accounting for both hydrogen peroxide formation and formic acid degradation are presented in this chapter as is empirical discussion of the effect of reaction conditions on hydrogen peroxide formation and formic acid degradation.

Chapter 5 presents a mathematical model for hydrogen peroxide formation and formic acid degradation. Model outputs are developed and compared with rates of hydrogen peroxide formation rate and formic acid degradation described in Chapter 4. Discussion is presented of the agreement (or disagreement) between measured and modelled results.

Chapter 6 reviews the effect of addition of ferrous iron (Fe(II)) on formic acid degradation. The effect of Fe(II) addition is probed by measurement of Fe(II) concentrations as a function of time as well as H_2O_2 generation rate and rate of formic acid degradation.

Chapter 7 presents the results of studies of phenol degradation by sonolysis. The rates of degradation of phenol as a function of ultrasonic frequency, background gas and added ferrous iron concentration are reported. The applicability of a model for phenol degradation based on the principles developed earlier in the thesis (and that was found suitable for description of hydrogen peroxide generation and formic acid degradation) is assessed in this chapter.

Chapter 8 summarises the major conclusions drawn from this study and also outlines recommendations for further research.

Chapter 2

Literature Review

2.1 Introduction

The main objective of this chapter is to decisively review the literature and present an overview of recent research related to ultrasonic irradiation. In this chapter, the fundamental concept of ultrasound and its potential to degrade contaminants are introduced. Uses and applications of ultrasonic irradiation are also reviewed.

The fundamentals of ultrasound are introduced in Section 2.3 while the many factors and conditions that affect the sonochemical phenomena are described in Section 2.4. The use of hydrogen peroxide as an indicator of sonochemical reactions, and the application of sonochemistry for the destruction of compounds via both hydroxyl radical attack and thermolytic degradation are described in Section 2.5.

2.2 General concept of ultrasound

Ultrasound is defined as radiation of frequencies higher than 16 kHz where the average person can not hear (Ensminger, 1973, Mark *et al.*, 1983). The upper limit of the ultrasonic frequency range is not well defined but it is typically taken to be 5 MHz for gases and 500 MHz for liquids and solids. Uses of ultrasound may be generally divided into two areas according to its purpose and frequency range. Firstly, low power or high frequency (2 to 10 MHz) is normally applied for diagnostic purposes such as medical scanning and chemical analysis, while high-power or low frequency (20 to 100 kHz) is generally used for cleaning, plastic welding, and initiating chemical reactions. Common applications and uses of ultrasound are shown in Table 2.1 (Mason and Lorimer, 1988).

Table 2.1 Industrial uses of ultrasound (Mason and Lorimer, 1988).

Field	Applications
Biology, biochemistry	Homogenization and cell disruption: Power ultrasound is used for rupture cell wall in order to release contents for further studies
Engineering	Ultrasound has been used to assist drilling, grinding and cutting. It is particularly useful for processing hard, brittle materials such as glass and ceramics. Other uses of ultrasound are welding (both plastics and metals) and metal tube drawing. High-frequnecy (MHz) ultrasound is used in nondestructive material and flaw detection.
Dentistry	For both cleaning and drilling of teeth
Geography, geology	Pulse/echo techsniques are used in the location of mineral and oil deposits and in depth gauges for seas and oceans. Echo ranging at sea has been used for many years.
Industrial	Pigments and solids can be easily dispersed in paint, inks, and resins. Engineering tools are often cleaned and depressed by immersion in ultrasonic baths. Two less widely used applications are acoustic filtration and ultrasound drying.

Medicine	Ultrasound imaging (2-10MHz) is used, particularly in obstetrics, for observing the fetus and for guiding subcutaneous surgical implements. In physiotherapy lower frequencies (20-50 kHz) are used in the treatment of muscle strains.
Plastics, polymers	The welding of thermoplastics is effectively achieved using power ultrasound. Polymerization initiation and polymer degradation are also affected. Cure rates of resins and their decomposition can be measured with frequency ultrasound.

2.3 Fundamentals of sonochemistry

Reactions caused by ultrasound are not the result of the direct input of energy to molecules, as is the case in photochemistry. Ultrasonic irradiation produces an alternating adiabatic compression and expansion of the liquid media. In the expansion phase of the ultrasonic wave, microbubbles form due to reduced pressure (i.e., sufficiently negative pressures). These microbubbles are filled with vaporised liquid or gas that was previously dissolved in the aqueous solution. The microbubbles can either be stable about their average size for many cycles or transient, growing to a certain size then violently collapsing or imploding through the compression phase as shown in Figure 2.1. The collapse or implosion of these microbubbles creates extreme local conditions such as high local pressures (up to 1000 atm) and high local temperatures (up to 5000K) that can induce chemical reactions (Makino *et al.*, 1983, Suslick, 1989, Suslick, 1990, Serpone and Colarusso, 1994). This phenomenon of bubble formation and collapse, which leads to energy release and extreme local conditions, is termed acoustic cavitation (or, in some instances, just "cavitation").

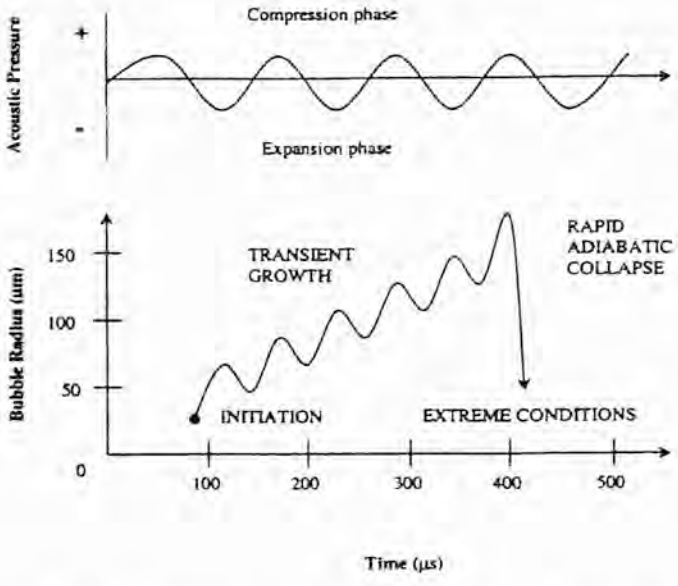

Figure 2.1 Schematic of the acoustic cavitation process during ultrasonic irradiation (Suslick, 1988). Fluctuations in pressure due to sound waves induce microcavities that expand and compress until a critical size is reached and the cavity implodes.

The localized conditions caused by cavitation are very short-lived, but they have been shown to result in the generation of highly reactive species including hydroxyl (OH•), hydrogen (H•) and hydroperoxyl free radicals (HO_2•). Hydrogen peroxide (H_2O_2), formed by the recombination of hydroxyl and hydroperoxyl radicals, has also been observed and used as an indicator of free radical species generated during ultrasonic irradiation (Weissler, 1958, Anbar and Pecht, 1964, Makino *et al.*, 1983, Riesz *et al.*, 1985).

Riesz *et al.* (1985) provided evidence of hydroxyl and hydrogen atom radicals generated during ultrasound using ESR spin trapping techniques. By generating such free radical species ultrasound offers the potential to initiate and promote oxidation and reduction reactions for a range of chemical, biological, industrial, and remediation applications.

Many researchers have investigated the reaction sites of radical reactions mediated by ultrasonic irradiation and developed mechanisms of reaction of radical species both with themselves and with target species (Hart and Henglein, 1985, Henglein and Kormann, 1985). Suslick and Hammerton (1986) describe the available sonochemical reaction

sites in aqueous media and indicate that the sonochemical decomposition of compounds proceeds in the three different reaction zones in aqueous media: (i) the inside of the cavitation bubble at a high temperature (approximately 5000 K) and pressure (several 100 atm), (ii) the interfacial zone surrounding the bubble cavity where large temperature and pressure gradients exist, and (iii) in bulk solution at ambient temperature.

Free radicals produced by the thermolytic decomposition may either react with each other to form new molecules and radicals or diffuse into the interfacial zone, leading to possible further reactions with solution phase species. Volatile compounds such as trichloroethylene and chlorobenzene may degrade by pyrolytic decomposition within the cavity itself. These compounds readily enter the gaseous phase within the microbubble and can undergo thermolytic degradation as a result of the high temperature and pressure within the bubble (Dewulf *et al.*, 2001, Goel *et al.*, 2004)

Hydroxyl radicals accumulate at the interfacial layer surrounding the hot bubble and may react with hydrophilic compounds like phenol. A local concentration of 4×10^{-3} M of OH• in the interfacial region was proposed by Gutierrez and Henglein (1991).

Suslick and Hammerton (1986) investigated thermolytic degradation in the gaseous region relative to solution phase degradation by measuring the rate of decomposition of volatile metal carbonyls with varying substituted ligands. In their study, the overall system vapour pressure was kept constant and only the vapour pressure of the metal carbonyl was varied, causing the concentration of the metal carbonyl to increase linearly in the vapour phase according to its partial pressure. Under such conditions, if decomposition occurs in the gas phase only, a plot of the reaction rate coefficient versus the vapour pressure of the metal carbonyl species will be linear with a zero intercept. If degradation occurs in the bulk liquid only, such a plot will have a non-zero intercept with a zero slope. First order rate constants were found to depend linearly on vapour pressure of the metal carbonyl complex, with plots resulting in a non-zero intercept. While Henry's law explains the linear dependence of the decomposition rate on the concentration of the substrate in the vapour phase, the non-zero intercept indicates additional decomposition sites. From their data, Suslick and Hammerton (1986) calculated temperatures and zone thickness for the cavity and interfacial regions.

Such data indicates that chemical decomposition by ultrasound involves both thermolytic degradation in the vapour phase and chemical degradation in the solution phase, most likely in the interfacial zone. While pyrolytic decomposition might be expected at high solute concentrations and for volatile substrates, at lower solute concentrations and/or for less or non-volatile species, decomposition by free radical species, is more likely to dominate (Riesz *et al.*, 1985, Serpone *et al.*, 1994).

The bulk solution region was estimated to extend ~ 200 nm from the bubble surface and had a lifetime of < 2 μs (Suslick, 1989). In the bulk liquid, no primary reactions with ultrasonically generated radicals have been observed to occur, though it is possible that a small number of free radicals produced in the cavities or at the interface may diffuse into the bulk solution and react with species present (Adewuyi, 2001). Reactions mediated by hydroxyl radicals could take place in the bulk solution at low concentration while, at high concentration, the reaction could also take place at the interface (Kondo *et al.*, 1989b, Kotronarou *et al.*, 1991).

The location of the sonochemical formation of hydrogen peroxide was investigated by Anbar and Pecht (1964) who suggested that hydrogen peroxide is produced not in the liquid phase but in the bubble phase. They used OH• scavengers to ascertain the location of hydrogen peroxide formation by sonolysis and found that non-volatile OH• scavengers did not affect the production of hydrogen peroxide while volatile ones did.

Ashokkumar *et al.* (1999) investigated the role of interfacially adsorbed molecules on multibubble sonoluminscence using the solution pH. They proposed that the solutes are adsorbed at the bubble/solution interface and then evaporated into the bubble inside during reactified diffusion, leading to the quenching of the sonoluminescence.

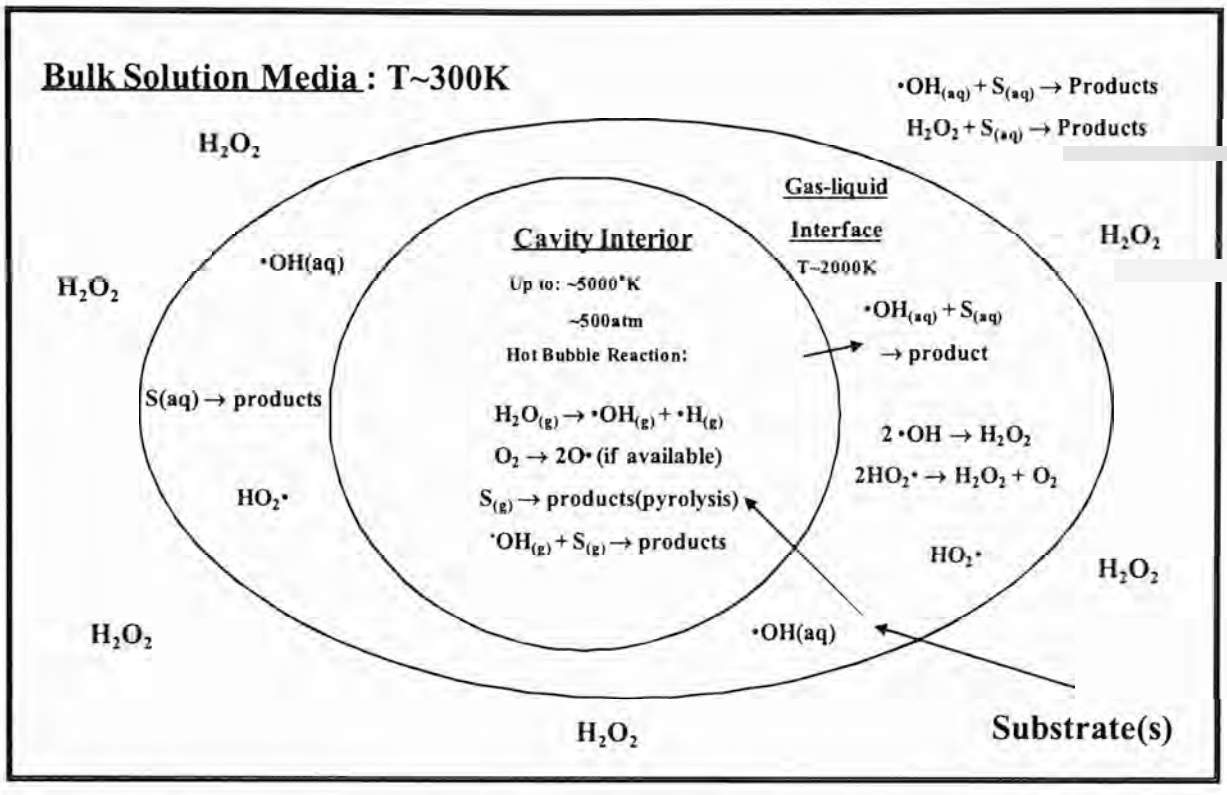

Figure 2.2 Proposed three reaction zones in the cavitation process (Adewuyi, 2001).

2.4 Factors Affecting Sonochemistry

2.4.1 Presence and nature of dissolved gases

There are several properties of gases that can affect sonochemistry. The specific heat ratio ($\gamma = C_p/C_v$ where C_p is the specific heat capacity at constant pressure and C_v is the specific heat capacity at constant volume) of the gas in the bubble affects the amount of heat released and the temperature reached when the bubble collapses. Assuming adiabatic implosion, maximum temperatures and pressures within collapsed cavitation bubbles were predicted by Noltingk (1950) and Nepprias (1980) from approximate solutions of the Rayleigh-Plesset equations:

$$T_{max} = T_0\left(\frac{P_m(\gamma - 1)}{P}\right) \quad (1)$$

$$P_{max} = P\left(\frac{P_m(\gamma - 1)}{P}\right)^{\frac{\gamma}{\gamma-1}} \quad (2)$$

where T_0 is the ambient liquid temperature or temperature of bulk solution, P is the pressure in the bubble at its maximum size or the vapour pressure of the solution, P_m is pressure in the bubble at the moment of transient collapse, and γ ($= C_p/C_v$) is the ratio of specific heats. As can be seen from equations 1 and 2, higher temperatures and pressures are generated with monatomic gases (such as argon and helium) with higher γ than those with diatomic gases (such as nitrogen and oxygen) with lower γ. Specific heat ratios of various gases are given in Table 2.2 (Mason and Lorimer, 1988).

Table 2.2 Characteristics of various gases of interest

Gas	Specific heat ratio(γ)	Thermal conductivity (10^{-2} W m^{-1} K^{-1})
Argon	1.66	1.73
Neon	1.66	4.72
Helium	1.66	14.30
Oxygen	1.39	1.64
Nitrogen	1.40	2.52
Carbon monoxide	1.43	2.72

The solubility of the gas in the liquid used is also an important parameter. Since the bubbles formed may re-dissolve before collapse occurs, gases with high solubility in the reaction mixture may decrease the cavitational effect. The bubbles which do not dissolve often become large as a result of the facile penetration of gas into the bubble and, in some instances, may float to the surface and explode (Thompson and Doraiswamy, 1999).

Entezari *et al.* (1997) studied the dependence of cavitational intensity on the nature of the background gases by investigating the rate of carbon disulfide dissociation. They concluded that the major factor determining the rate of ultrasonically-mediated carbon disulfide dissociation was the gas solubility in their system.

Another parameter that affects cavitational collapse and sonochemistry is the thermal conductivity of the gas. A gas with low thermal conductivity prevents heat dissipation from the cavitation site resulting in a higher localized temperature compared to a gas with a high thermal conductivity (Table 2). As the thermal conductivity of the gas increases, the amount of heat loss due to thermal dissipation also increases (Thompson and Doraiswamy, 1999).

2.4.2 Acoustic power

Many researchers have found that during ultrasound, increasing the power applied to the aqueous solution increases the rate of the reaction to a certain maximum, above which continued increases in power input actually decreases decomposition rate (Gutierrez and Henglein, 1990). Ratoarinoro *et al.* (1995a) hypothesized that this behaviour is due to the formation of a dense cloud of cavitation bubbles near the probe tip that prevents transmission of energy further into the liquid. Sehgal and Wang (1981) investigated the threshold intensities and kinetics of sonoreaction of thymine in aqueous solution and observed that cavitation chemistry of thymine was significantly reduced at relatively higher acoustic intensities (> $3W/cm^2$). The exact threshold intensity for sonochemical activity will vary according to reactor configuration and conditions.

2.4.3 Frequency

Operating frequency significantly influences the cavitation process by affecting the size of the bubbles being formed (Francony and Pétrier, 1996, Hua and Hoffmann, 1997, Kang *et al.*, 1999, Beckett and Hua, 2001, Jiang *et al.*, 2006). Generally, the oscillating pressure waves caused by ultrasonic irradiation cause the formation of microbubbles of a particular resonant size before collapsing. The size of the acoustic bubble is inversely correlated to the frequency applied (Mason and Lorimer, 1988, Hua and Hoffmann, 1997) as is expressed by the following equation :

$$R_r^2 = \frac{3\gamma P_0}{\rho\omega_r^2} \qquad (3)$$

where R_r is the resonant bubble radius, ρ is the density of the liquid, ω_r is the resonant frequency, P_0 is the hydrostatic pressure (1 atm), and γ (= C_p/C_v) is the specific heat ratio.

At very high frequencies, the extent of cavitation is diminished as either (1) the rarefaction period of the sound wave is insufficient in its duration and/or intensity to initiate cavitation, or (2) the compression cycle occurs faster than the time required for the microbubble to collapse. In the past, most sonochemical reactions were carried out at frequency between 20 and 50 kHz. This could be due to the fact that alteration of frequency has no significant effect in certain reactions such as the dissociation of carbon disulfide (Entezari *et al.*, 1997). However, current research is showing that higher reaction rates of sonolytic oxidation can be expected at higher frequencies (Entezari and Kruus, 1994, Hua and Hoffmann, 1997).

Petrier *et al.* (1994) found that the rate of sonochemical degradation of phenol was enhanced at higher frequency irradiation (487 kHz) compared to that at low frequency (20 kHz). They suggested that at the higher frequency, greater release of hydroxyl radicals into solution contributes to increased degradation. At high frequency, more cavitational events occur due to the smaller resonance radius of cavitation bubbles (6.6 μM at 486 kHz and 170 μM at 20 kHz) and their shorter collapse time (4.1×10^{-7} s at 487 kHz and 100×10^{-7} s at 20 kHz). Under such conditions, more hydroxyl radicals are generated and released into the liquid phase.

At low frequencies, larger cavitation bubbles and more violent implosions lead to higher localized temperatures and pressures at the site of collapse. However, more cavitational events occur and more free radicals are likely to be generated at higher frequencies. Higher frequencies have been shown to increase the number of free radicals such as hydroxyl, hydrogen atom radicals and hydroperoxyl radicals produced under oxic conditions (Cum *et al.*, 1991). Also, this frequency effect increases the mass transfer of hydroxyl radicals into the surrounding medium and concurrently increases the transport of gases and volatile organic compounds into the bubbles (Hung and Hoffmann, 1999).

Kanthale *et al.* (2008) investigated the effect of frequency and power on sonoluminescence and hydrogen peroxide yields using four different frequencies (213, 355, 647, 1056 kHz) and a wide range of acoustic powers. The used the numerical simulations on the basis of single bubble dynamics and found that the dependence of hydrogen peroxide formation on frequency was controlled by the average bubble temperature, heat and mass transfer effects and the number of cavitation bubbles.

2.5 Sonochemical Generation of Compounds

2.5.1 Hydrogen peroxide formation

Hydrogen peroxide formation is considered indirect evidence of the generation of free radical species by ultrasonic irradiation. Hydroxyl and hydrogen atom radicals are generated by the thermolytic decomposition of water in the bubble cavity ($H_2O \rightarrow OH\bullet + H\bullet$). In the presence of oxygen, hydrogen atom radicals react with oxygen to form hydroperoxyl radicals ($H\bullet + O_2 \rightarrow HO_2\bullet$) in competition with recombination reactions to regenerate water ($OH\bullet + H\bullet \rightarrow H_2O$). Hydrogen peroxide is formed by the recombination of hydroxyl radicals ($OH\bullet + OH\bullet \rightarrow H_2O_2$) at the interfacial zone and/or in the bulk solution. As oxygen is a well known scavenger of hydrogen radicals (H•), the recombination reaction ($OH\bullet + H\bullet \rightarrow H_2O$) is prevented in the presence of oxygen, and increased concentrations of hydrogen peroxide (due to the hydroxyl radical recombination reaction) are observed when oxygen is present in solution (Harada and Kumagai, 2003).

Due to such reactions, hydrogen peroxide formation has been used as an indicator of the production of free radicals. Much research has been undertaken on the mechanisms and kinetics of H_2O_2 production during ultrasound (Weissler, 1958, Wakeford *et al.*, 1999, Anbar and Pecht, 1964, Hart and Henglein, 1985, Gutierrez *et al.*, 1986, Harada and Kumagai, 2003).

As mentioned above, Anbar and Pecht (1964) studied the location of the sonochemical formation of hydrogen peroxide and suggested that it is produced not in the liquid phase

but in the vapour phase. Hart and Henglein (1985) concluded that hydroxyl radicals produced in the gas phase form hydrogen peroxide in the interfacial zone, suggesting that hydrophobic compounds enter the interfacial zone and react with OH• radicals, lowering hydrogen peroxide yields. They also found that hydroperoxyl radicals (HO_2•) formed in the presence of oxygen do not react with iodide but produce hydrogen peroxide. Similar results were presented by Henglein and Kormann (1985) who found that the enrichment of hydrophobic solutes in the bubble or interfacial zone more easily scavenged the OH• radicals produced under argon.

Increased oxygen concentrations generate more HO_2• and subsequently more hydrogen peroxide (HO_2• + HO_2• → H_2O_2 + O_2). However, when the oxygen concentration increases above a certain point, the localized temperature at the cavitation site decreases as the specific heat of oxygen is about 1.8 times that of argon at 1500K. Thus the dissociation mechanisms become less effective, less reactive radicals are generated during bubble collapse, and less H_2O_2 is produced at higher oxygen concentrations (Gong and Hart, 1998).

Gutierrez *et al.* (1986) found that oxygen was generated as a product like hydrogen and hydrogen peroxide from ultrasonic irradiation of pure water under argon. Hydroxyl radicals are a pathway of hydrogen peroxide formation. Also OH• radicals disproportionate in the gas phase at higher temperatures (OH• + OH• → O• + H_2O) and oxygen might be formed by the combination reaction (O• + O• → O_2). They proposed a 'structured hot spot' model with, as mentioned before, three potential regions for chemical reactions: (1) a hot gaseous nucleus, (2) an interfacial zone with gradient in temperature and local radical density, and (3) the bulk solution at ambient temperature. According to their study, hydroxyl radicals form H_2O_2 close to these 'hot spots', with the percentage of OH• radicals escaping the areas being small.

Radical scavenging reactions can also occur under air present conditions. Nitrous species like HNO_2 and HNO_3 produced in the gas phase by nitrogen decomposition by ultrasound irradiation can dissolve and then dissociate to form ions (NO_2^- and NO_3^-) in the bulk solution. Nitrite can then react with hydrogen peroxide to form nitrate (Supeno and Kruus, 2000).

Harada and Kumagai (2003) suggested that nitrogen present in the air may scavenge hydrogen peroxide formed during ultrasonic irradiation. Nitrogen is oxidized to nitric ion or nitrous ion in water, and then oxidized by hydrogen peroxide to nitrate, NO_3^-.

Gutierrez *et al.* (1991) undertook radical scavenging studies in the sonolysis of aqueous solutions of I^-, Br^-, and N_3^-. They found that the total yield of oxidised products such as hydrogen peroxide and iodine was independent of solute concentrations and equal to the hydrogen peroxide yield in pure water. They concluded that the hydroxyl radicals barely escape into bulk solution and calculated a localized concentration of 4×10^{-3} M for OH• radicals in the interfacial region between the cavitation bubbles and the bulk liquid.

2.5.2 Sonolytic Degradation of Organic Compounds

Volatile aromatic compounds are degraded mainly by thermolytic decomposition in the bubble cavity, where critical conditions of high temperature and pressures occur (Drijvers *et al.*, 1996, Francony and Pétrier, 1996, Drijvers *et al.,* 1998, Drijvers *et al.*, 1999, Gondrexon *et al.*, 1999, Okuno *et al.*, 2000, Jiang *et al.*, 2005).

Francony and Petrier (1996) investigated the sonochemical degradation of carbon tetrachloride in aqueous solution at two different frequencies (20 kHz and 500 kHz) and found that it was completely decomposed into Cl^- and CO_2. The results suggested that carbon tetrachloride decomposed thermolytically inside the cavitation bubble to form trichloromethyl radicals and dichlorocarbene. More rapid mineralization was achieved at 500 kHz than 20 kHz.

Drijvers *et al.* (1999) carried out experiments involving the sonolysis of aqueous solutions containing the volatile hydrophobic compounds trichloroethylene and chlorobenzene. Both organics were decomposed by thermal degradation inside the cavitation bubble though indirect evidence of free-radical mediated degradation was also observed.

Drijvers *et al.* (1996) investigated the effects of pH and saturating gas on the ultrasonic degradation of trichloroethylene (TCE) at 520 and 20 kHz. They found that more efficient TCE degradation was achieved at 520 kHz and with increasing pH up to 10 and argued that the pH effect could be attributable to the changing dominance of different carbonate species. Under neutral and alkaline pH conditions, carbonate and bicarbonate are the dominant species while under acidic conditions inorganic carbon is present as dissolved carbon dioxide. The specific heat ratio, an important parameter for critical bubble collapse (see Section 2.2.1), is significantly lower for CO_2 (γ_{CO_2} = 1.034) than it is for air (γ_{air} = 1.403). The lower heat capacity ratio leads to lower temperatures at implosion of the cavitation bubble resulting in a decrease in the number of free radicals formed thereby lowering the efficiency of TCE degradation under acidic conditions.

Kotrounarou and Hoffmann (1991) investigated the kinetics and mechanisms of the sonochemical reactions of *p*-nitrophenol in oxygenated solution at 20 kHz. They found that p-nitrophenol was decomposed by high-temperature reactions at the interface region of cavitation bubbles and hydroxyl radical reactions were secondary reaction channel. In their work, the average effective temperature of the interfacial region was estimated to be about 800 K.

Okuno *et al.* (2000) investigated the rate of degradation of various aromatic compounds by ultrasonic irradiation (benzene, chlorobenzene, 1,2-, 1,3-, 1,4-dichlorobenzene, biphenyl, and polychlorinated biphenyls) at 200 kHz and under an argon atmosphere and found that the rate increases according to increasing vapour pressure of the compounds under investigation. They suggested that the main decomposition pathways of benzene, chlorobenzene, and 1,3-dichlorobenzene, which more easily penetrate the gas phase due to their relatively high vapour pressures, are pyrolysis either inside collapsing cavitation bubbles or in the interfacial region. In contrast, the decomposition pathways of biphenyl and polychlorinated, which exhibit relatively low vapour pressures, seem to be via a combination of pyrolysis in the interfacial region and OH radical reactions.

Gonderxon *et al.* (1999) reported on the degradation of pentacholorphenol using a three-stage sonochemical reactor operating in continuous flow mode and investigated the effect of a variety of parameters including ultrasonic power, reactor volume and flow rate. They showed that pentacholorphenol was degraded by hydroxyl radical reactions at high frequency (500 kHz) and that decomposition rates were linearly related to the ultrasonic power input. They suggested that increased power input leads to enhancement of the cavitation zone and its associated chemical effects.

Jiang *et al.* (2006) investigated the degradation of 4-chlorophenol in oxygen saturated conditions under various operating conditions. They suggested that its degradation rate is dependent on the initial concentration of 4-chlorophenol. Degradation occurs in the bulk solution at low concentrations, while at high concentrations 4-cholorophenol is predominantly degraded at the bubble-liquid interface. They also found that the solution temperature significantly influences the reaction rate.

Dewulf *et al.* (2001) investigated the sonolytic degradation of trichloroethylene and chlorobenzene at micro molar concentrations. They found that the reaction rate increased with decreasing initial concentration of organic compound. They found that OH• radicals induced degradation together with pyrolysis at micro molar concentrations of these volatile compounds accounted for the removal of these compounds from solution. They deduced that hydroxyl radical attack contributed 48.5% of the total degradation at chlorobenzene concentrations between 1 and 5 μM.

Lim *et al.* (2007) examined the effect on rates of sonochemical degradation of carbon tetrachloride, trichloroethylene and 1,2,3-tri-chloropropane in aqueous solution of various parameters including temperature, power density, saturating gas and chemical characteristics. They found that the reaction rates were higher at low temperatures with larger rate constants observed for contaminants with high vapour pressure and low activation energy. Also they found that higher power intensity and the saturating gas of low specific heat ratio, high solubility and low thermal conductivity resulted in faster reaction.

Ayyildiz *et al.* (2007) investigated the effect of mass transfer on the sonolytic degradation of halogenated organic compounds (trichloroethylene and ethylene dibromide) at 20 kHz. From both theoretical and experimental results, they suggested that Henry's constant positively influenced the sonolytic degradation for less volatile compounds ($H_v < 0.1$), while the influence of Henry's constant on the degradation of high volatile compounds ($H_v > 1$) was negligible. They also found that the liquid phase diffusion coefficient was an important parameter in the degradation process.

Beckett and Hua (2000) examined the degradation of 1,4-dioxane by ultrasound irradiation at four difference frequencies (205, 358, 618 and 1071 kHz) under argon and oxygen saturated conditions. They observed the maximum decomposition rate of 1,4-dioxane at 358 kHz. They proposed that free radical mechanisms are significant over the entire range of frequencies due to major by-product formation.

2.5.3 Sonolytic Degradation with Coupled System

As free radicals are the root cause of the oxidizing behaviour of ultrasonic systems, many efforts have been given to improve or maximize the efficiency of free radical production during ultrasonic irradiation (Barbier and Pétrier, 1996, Fung *et al.*, 2001, Abdelsalam and Birkin, 2002, Dutta *et al.*, 2002, Beckett and Hua, 2003). Many researchers have tried to enhance or maximize the sonolytic production of free radicals by coupling the ultrasonic aspect with other so-called Advanced Oxidation Processes. A brief review of such coupled processes is given below.

2.5.3.1 Fenton's reagent

As described in Section 2.1, when ultrasonic waves irradiate an aqueous solution, hydrogen peroxide is generated by recombination of hydroxyl radicals and hydroperoxyl radicals (when oxygen is present) produced following the thermolytic decomposition of water. Addition of Fe(II) should enhance the production of hydroxyl radicals since the combination of Fe(II) and the H_2O_2 produced during sonolysis leads to the Fenton reaction:

$$Fe^{+2} + H_2O_2 \rightarrow Fe^{+3} + OH\bullet + OH^- \quad (4)$$

Joseph *et al.* (2000) examined the sonochemical degradation of aqueous solutions of azobenzene and related azo dyes by ultrasonic irradiation at 500 kHz and 50 W under air, O_2, or argon saturation conditions combined with the addition of Fe(II). They observed a 3-fold increase of the reaction rate at an optimal Fe(II) concentration in the range between 0.1mM and 0.5 mM.

Jiang and Waite (2003) investigated the effect of Fe(II) addition on the ultrasonic degradation of phenol. They conducted the experiments using 30 W ultrasonic irradiation at 608 kHz in air-equilibrated solutions and at various concentrations of ferrous iron. Compared with the rate constant of 0.0165 min^{-1} for the decomposition of phenol by ultrasonic irradiation only, the rate constant for phenol degradation in the presence of 500 μM Fe(II) approximately doubled to 0.0355 min^{-1}. Ferrous iron concentrations up to 2 mM were investigated with optimum degradation rate of phenol being achieved at Fe(II) concentrations between 400 to 1000 μM with pH in the range 3.5-4.2. Increase of Fe(II) concentration above 2 mM was found to result in a rate constant decrease presumably due to the direct reduction of hydroxyl radicals by Fe(II).

Nam *et al.* (2003) also investigated the sonolytic degradation of non-volatile organic compound by ultrasonication coupled with Fe(II). They observed enhancements of 2.8-fold and 3.6-fold in the p-chlorobenzoic acid degradation rate at Fe(II) concentrations of 10 and 20 μM, respectively. They found that the coupled Fe(II)/ultrasound process enhanced the OH radical production rate by 70% compared to ultrasound alone. They also suggested that the Fenton reaction most likely occurs in the interfacial region rather than in the bulk solution.

Ben *et al.* (2005) investigated the oxidation of diethylstilbestrol (DES) in aqueous solution by ultrasound irradiation (665 kHz) and Fe(II) addition and found that oxidation of diethylstilbestrol is significantly enhanced by Fe(II) addition. They found that the rate of degradation of 30 μM diethylstilbestrol increased to 25 and 50% in the presence of 10 and 15 μM of Fe(II) respectively. They also found that the concentration

of hydrogen peroxide in solution decreased with the addition of Fe(II) along with an increase in the degradation of DES.

2.5.3.2 Ozone

The concurrent use of ozone and ultrasound has been shown to improve decomposition rates for a variety of environmentally relevant compounds relative to the application of either method alone (Barbier and Pétrier, 1996, Kang and Hoffmann, 1998, Weavers and Hoffmann, 1998, Weavers *et al.*, 1998, Destaillats *et al.*, 2000, Pétrier *et al.*, 2002, Lesko *et al.*, 2006,). The combined application of ultrasound with ozone, otherwise known as sonozone, has also been shown to oxidize natural organic matter to levels difficult to achieve by means of either method alone. Thus, Olson and Barbier (1994) examined the oxidation of natural organic matter by ultrasonic irradiation in the presence of ozone achieving 91% removal of TOC while only 40% removal was obtained with ozone alone.

Barbier and Petrier (1996) carried out experiments on 4-nitrophenol degradation by ultrasound irradiation (at frequencies of 500 and 20 kHz) combined with ozone. They found that the coupling of ultrasound and ozone could enhance the mineralization of 4-nitrophenol even at low pH, conditions normally unsuitable for oxidation by ozone alone. Their study went on to show that the ultrasonic irradiation plays an important role in the efficiency of ozone decomposition.

Weavers *et al.* (1998) examined the degradation of nitrobenzene, 4-nitrophenol and 4-chlorophenol in aqueous solutions using a combination of sonolysis and ozone. They found that sonolytic ozonation enhanced the loss of total organic carbon at both 20 kHz and 500 kHz with all three compounds. They concluded that an increase in the concentration of hydroxyl radicals formed during the thermal decomposition of ozone was the major reason for the enhancement evident in the combined system rather than simply an enhancement in mass transfer of ozone in aqueous solution due to sonolysis.

Ozone itself decomposes in water through a series of complex reactions. During its decomposition free radicals such as O• and OH• are generated and they may further

react with ozone until it is completely depleted. During sonolysis, ozone is thermolytically decomposed within the gas phase of the cavitation bubble in the following reactions:

$$O_3 \rightarrow O_2 + O\bullet \quad (5)$$

$$O\bullet + H_2O \rightarrow OH\bullet + OH\bullet \quad (6)$$

The radical products formed may then diffuse into the interfacial region next to the bubble where they can then react with solution phase species. In the absence of radical scavengers in the gas phase, oxygen radicals may also attack ozone, inhibiting the production of further radicals by generating dioxygen ($O\bullet + O_3 \rightarrow 2O_2$). The additional hydroxyl radicals formed from the decomposition of ozone in the vapor phase, coupled with hydroxyl radicals created during the thermolytic dissociation of water during sonication, explain the improved degradation rates observed in combined sonolysis and ozone systems.

2.5.3.3 Photocatalysis

Besides ozone, much research has also been directed towards the combination of ultrasonic irradiation and ultraviolet irradiation in an effort to improve oxidation efficiency. Sierka and Amy (1985) analyzed the catalytic effects of combining UV and sonolysis with ozone for the oxidation of humic acid and trihalomethane precursors and found that the combination of all three systems (UV/ultrasound/ozone) was the most effective process for the decomposition of organic compounds. The results of Petrier *et al.* (2002) supported this finding, showing the most effective decomposition of an azo dye occurred with all three applications combined. Toy (1990) showed that the oxidation of 1,1,1-trichloromethane was improved by combining sonoloysis and photolysis relative to either process alone.

Shirgaonkar and Pandit (1998) examined the destruction of 2,4,6-trichlorophenol using a combination of ultrasound and photocatalysis under different operating conditions such as ultrasonic intensity, solution temperature, and UV transmission. They found that the synergetic effects of the combined system were more marked at lower intensity. As the ultrasonic intensity was increased, however, no significant improvement in

oxidation rates was observed compared to ultrasonic irradiation alone. Degradation rates by the combined system were entirely independent of the mode of UV transmission.

Kubo *et al.* (2005) investigated the degradation of phenol by ultrasonic irradiation in the presence of TiO_2 under dark conditions. Phenol degradation rates varied with the amount of TiO_2 and the level of dissolved oxygen present. The kinetic model they proposed to explain their results included OH• radical formation by thermolytic water dissociation, oxygen atom formation by thermolytic decomposition of oxygen and TiO_2 catalysis. The latter effect occurred as a result of positive holes generated in the vicinity of the TiO_2 surface on sonication. The positive hole reacts with water to produce a hydroxyl radical. The physical effects of ultrasonic irradiation have been shown in separate photocatalysis studies (Mrowetz *et al.*, 2003, Harada, 2005). These studies show that the dechlorination rate of PCBs using TiO_2 in the presence of ultrasound is dramatically increased. This improvement in process efficiency could be explained by a variety of factors including continual particle cleaning, increased mass transfer rates and reduction in TiO_2 particle size which increases the effective surface area of the semiconductor.

Chapter 3

Materials and Methods

3.1 Introduction

A series of experiments were conducted in which frequencies, initial concentration of substrate and solution composition including pH were varied for different background gases (air, argon, oxygen, and nitrogen). Hydrogen peroxide, ferrous iron, and concentration of the model organic compounds formic acid and phenol were monitored over the duration of the reaction. All experiments were conducted at 25 °C. In this chapter the chemicals, instruments and analytical techniques used in acquiring the data are described. In addition, computational approaches used for mathematical modelling are summarised. Details specific to particular studies are described in subsequent chapters.

3.2 General Reagents

All solutions were prepared with 18 MΩ.cm Milli-Q water unless otherwise stated. Chemicals were used as received. Glassware and plasticware was soaked in a 10% HNO_3 acid bath for at least 3 days and rinsed with Milli-Q water prior to use. All pH adjustments were performed using high purity 30% w/v HNO_3 and 0.1 N NaOH (Fluka puriss p.a. plus).

3.3 Instruments

3.3.1 Ultrasonic system

The ultrasound equipment used in this study was supplied from Radiocom Systems (France) and contained three generators emitting radiation of 300, 600 and 800 kHz. Accompanying the generators were reactors equipped with transducers to produce the three different ultrasonic frequencies of interest. The generators as well as the transducers and reactors are shown in Figure 3.1.

The sonochemical device incorporates a radio frequency generator-amplifier connected to 4 cm diameter piezo-electric disc transducers (PZT) fixed on a titanium plate at the bottom of a 400 mL Pyrex glass reactor. A low voltage connection (12 V) activates an electric fan in order to dissipate excess heat generated by the transducer.

In order to optimize frequency control, the power input was increased progressively until the designed acoustic power was achieved. Acoustic power is converted from the electric power by the relationships shown in Figures 3.2 to 3.4 at each frequency. Frequency adjustment is obtained using the ADJUST button which on turning has to indicate the highest value on the vu-meter. If the transducer becomes noisy, it indicates that operation at this particular frequency is unworkable.

In order to maintain consistent temperature in the reaction solution, the reactor was fitted with a threaded cooling jacket attached to a constant temperature water bath which enabled control of solution temperature between 0 and 35°C.

Studies were undertaken under air, argon, oxygen or nitrogen atmospheres with the gas of interest sparged continuously through the reaction solution for 20 to 30 minutes prior to ultrasonic irradiation. Silicon lid with sampling port and gas inlet has been used to prohibit the any influx of air. Gas sparging was stopped during experiments.

Figure 3.1 Reactors with underlying ultrasonic transducers (top) and ultrasonic generators (bottom) used in all studies reported here.

3.4 Methods

3.4.1 Calorimetric measurement

The sonochemical reaction results from the formation, growth and sudden implosion of microbubbles (a process known as "cavitation"). Generally, applied electrical power cannot be transferred to aqueous media without loss. Therefore, measurement of the actual power input to the solution, or acoustic power, is necessary. A simple calorimetric method has been frequently used to measure acoustic power in ultrasonic applications (Mason, 1992). Actual power can be calculated using the following equation:

$$\text{Power} = \frac{dT}{dt} \cdot C_P \cdot M \qquad (1)$$

where dT/dt is the temperature variation over a particular time interval, C_p is the heat capacity of the solvent (4.184 J kg^{-1} K^{-1}) and M is the mass of solvent used (kg).

To implement the calorimetric method described above, the temperature was recorded at certain time intervals using a thermocouple placed in the reactor. The temperature variation during sonication was then plotted versus time, and dT/dt calculated by linear regression of the data. As the power is dissipated into solution via the PZT transducer of a certain area, the acoustic intensity (W/cm^2) supplied by the ultrasonic irradiation can be calculated using:

$$\text{Intensity} = \frac{\text{Acoustic Power(W)}}{\text{Area}(cm^2)} \qquad (2)$$

Intensity used in this study was about 2.4 W/cm^2 at 30W of acoustic power.

3.4.2 Characteristics of ultrasonic irradiation

As electrical power input cannot be directly transferred without loss to ultrasound waves in aqueous solution and as the extent of power loss may vary with frequency, the applied power was normalized using the calorimetric technique described above. The electrical power input was used to control the acoustic intensity input to the solution. Experiments with deionized water were conducted in order to generate calibration curves relating electrical power input to acoustic intensity in a relationship known as the acoustic yield.

For each frequency, the acoustic intensity in solution can be calculated using the calibration curves shown in Figure 3.2 to 3.4. The figures show that the acoustic yield is 54% at 300 kHz, 56% at 600 kHz, and 46% at 800 kHz. Using these results, a normalized acoustic power of 30 W was applied in order to compare results of experiments at different frequencies.

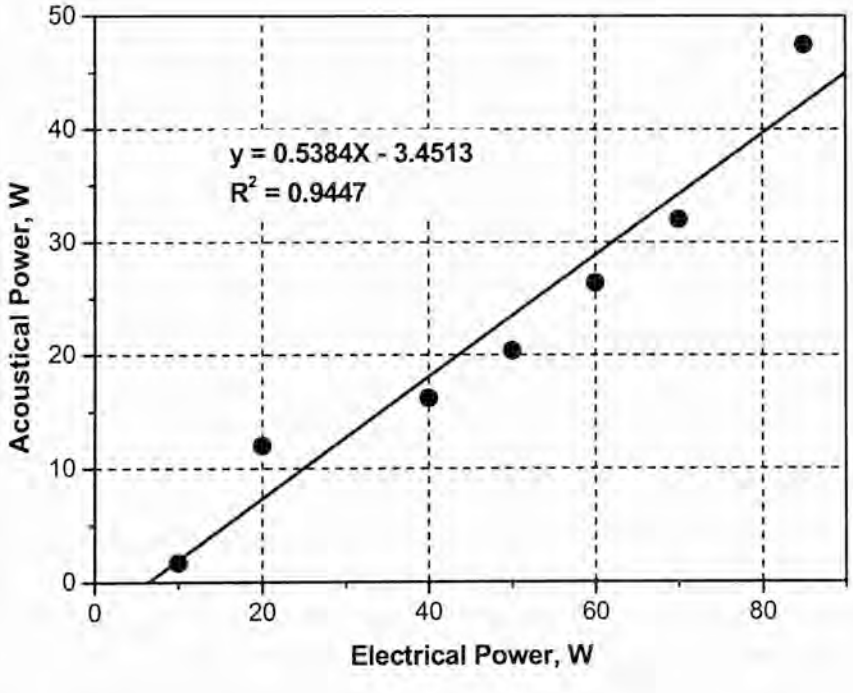

Figure 3.2 Acoustic yield from the calorimetric method at 300 kHz

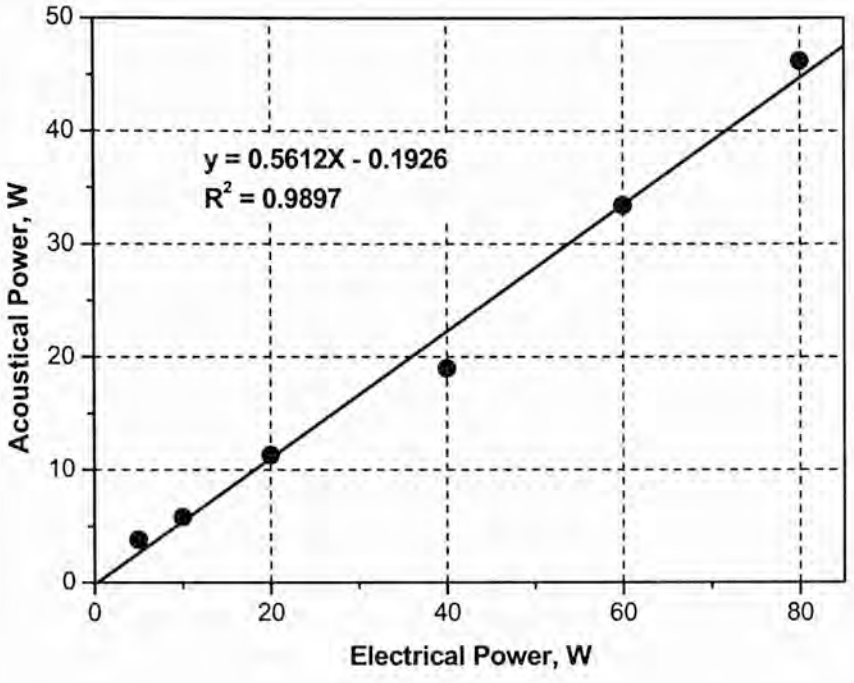

Figure 3.3 Acoustical yield from the calorimetric methods at 600 kHz

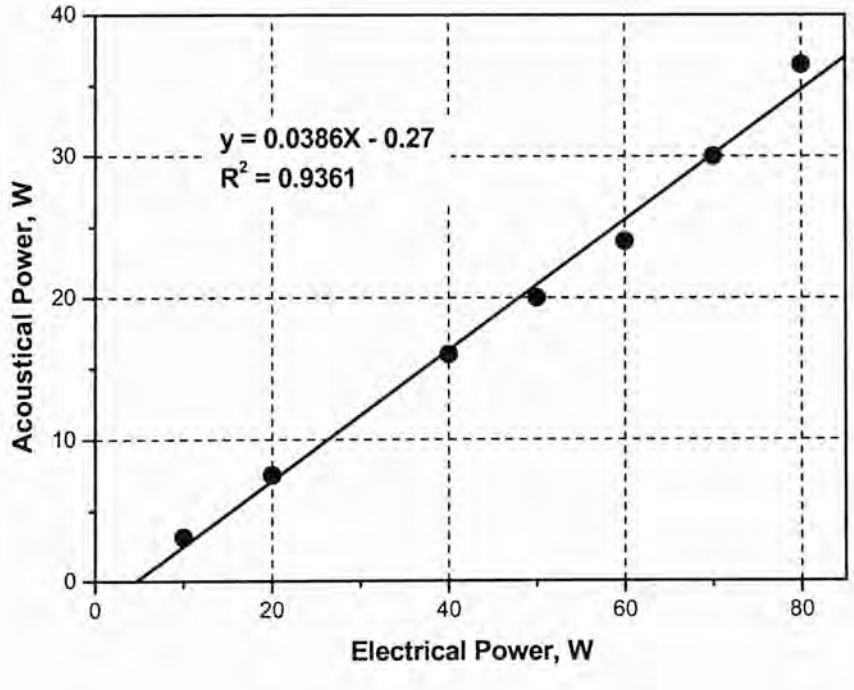

Figure 3.4 Acoustical yield from the calorimetric methods at 800 kHz

3.4.3 Hydrogen peroxide measurement

Hydrogen peroxide generation is considered indirect evidence of free radical species produced by ultrasonic irradiation with hydrogen peroxide formation arising from both the recombination of hydroxyl radicals and of hydroxperoxyl radicals (these reactions are discussed further in Chapter 4).

$$OH\bullet + OH\bullet \rightarrow H_2O_2 \quad (3)$$

$$HO_2\bullet + HO_2\bullet \rightarrow H_2O_2 + O_2 \quad (4)$$

The concentration of H_2O_2 was determined either by the iodomeric method or, if Fe(II) was present, by the DPD method. Both methods are described below.

3.4.3.1 Iodometric method

The concentration of H_2O_2 in solution was determined spectrophotometrically using the iodometric method (Allen *et al.*, 1952, Kormann *et al.*, 1988) provided Fe(II) was not presented. Samples (0.5 mL to 2.0 mL) from the reactor were diluted with Milli-Q water to 2.0 mL and mixed with 2.0 mL of 0.1 M potassium biphthalate and 2 mL of a solution containing 0.4 M KI, 0.06 M NaOH, and 2×10^{-4} M ammonium molybdate. The sample was then placed in a quartz cuvette (1.0 cm path length) and absorbance measured at a wavelength of 350 nm ($\varepsilon_{I_3^-}$ = 26400 M^{-1} cm^{-1}) using a Cary 1E UV-Vis spectrometer.

3.4.3.2 DPD method

The DPD method was used to analyze hydrogen peroxide in experiments in which Fe(II) was present (Bader *et al.*, 1988). In this study, the method was modified in order to minimize interference by ferrous and ferric iron. 1,10-phenanthroline was used as complexing agent for ferrous iron while ferric iron was quenched by EDTA (0.5M Na_2EDTA); such modifications have been used in previous studies for H_2O_2 analysis in the presence of iron (Duesterberg *et al.*, 2005). 1 mL of sample was quenched by 2 mL of 1,10-phenanthroline solution followed by addition of 750 µL of a phosphate buffer (pH 6.5, 0.5 M phosphate) to establish the appropriate pH for DPD analysis. 400 µL of

the EDTA solution was then added to complex any Fe(III) present. The sample was then placed in a quartz cuvette to which 30 μL of DPD reagent (1% in 0.1M H_2SO_4) was added, followed by 30 μL of horseradish peroxidase (≈0.8 mg/mL). The absorbance was then measured at 551 nm (ε = 21000 M^{-1} cm^{-1}) using a Cary 1E UV-Vis spectrometer. The peroxidase and DPD solutions were stored for no more than two weeks.

3.4.4 Phenol and intermediates measurement

Phenol and its oxidation byproducts were measured using a Hewlett-Packard 1100 series HPLC system with a diode array detector and fluorescence detector and equipped with an Alltech ODS-2 250mm column. Detection wavelengths for the diode array detector (DAD) were set at 290 nm (for hydroquinone), 275 nm (for phenol and catechol) and 254 nm (for benzoquinone). Emission and excitation wavelengths for the fluorescence detector (FLD) were 310 nm and 270 nm for phenol, 330 nm and 290 nm for hydroquinone, and 320 nm and 275 nm for catechol. An acetonitrile/water (20%/80%) mixture containing 1% acetic acid was used for the mobile phase at a flow rate of 1 mL/min. Comparing retention times with standards confirmed the identity of the byproducts, and their concentrations were calculated using calibration curves generated from standard solutions. Calibration curves were updated whenever a new stock solution of phenol was used for experiments. Calibration curves for phenol and phenolic by-products developed with both the diode array detector and the fluorescence detector are shown in Figures 3.5 and 3.6.

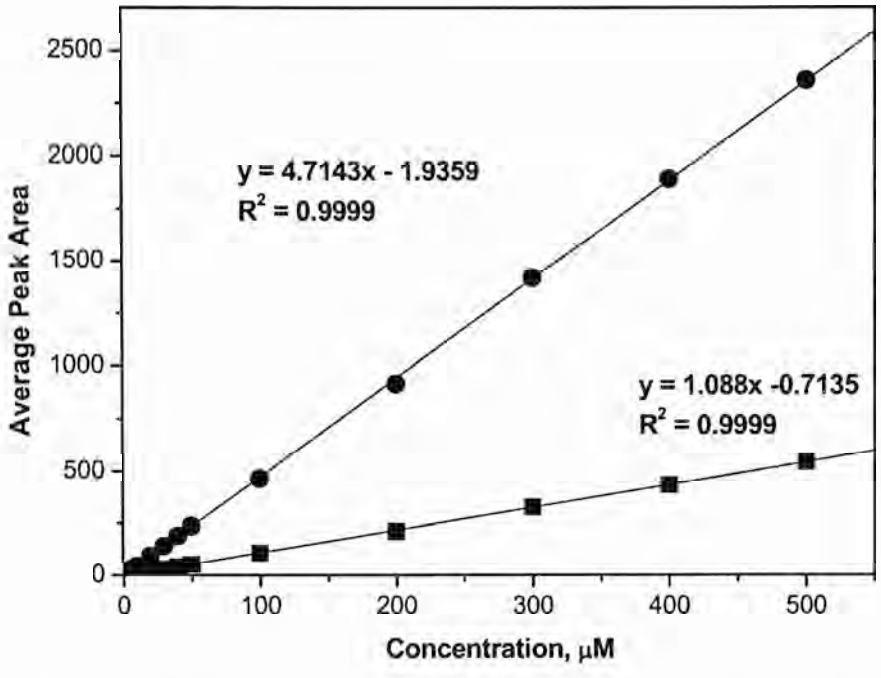

Figure 3.5 Calibration curve for phenol analysis by HPLC using either the DAD (•) or the FLD (■)

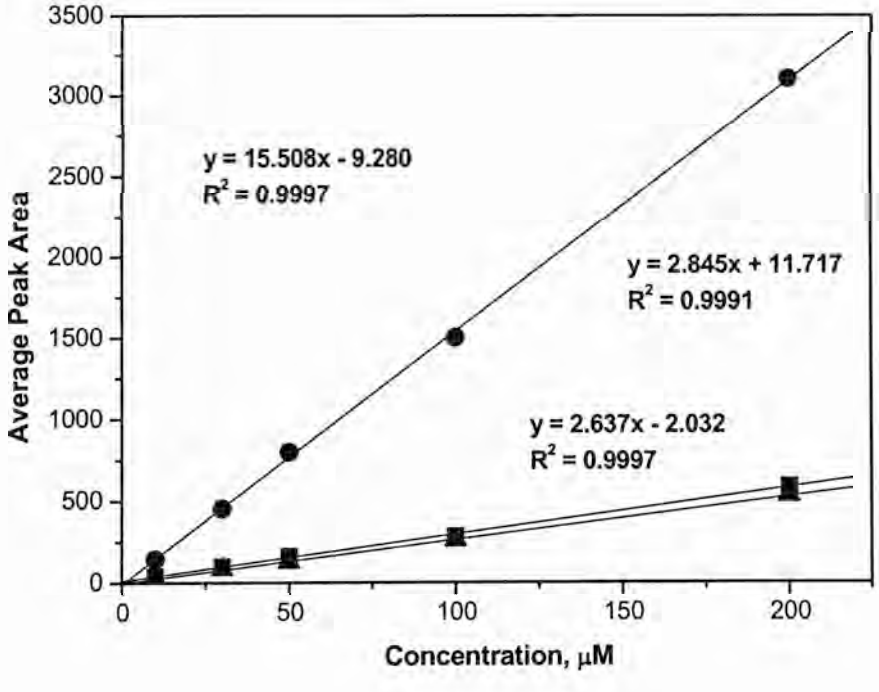

Figure 3.6 Calibration plots obtained by HPLC with DAD for phenol byproducts benzoquinone (•), hydroquinone (■) and catechol (▲)

3.4.5 C^{14} analysis

A variety of studies were undertaken utilising formic acid as a simple target organic compound with CO_2 being the major product of hydroxyl radical attack. The extent of conversion of formic acid to CO_2 was determined utilising radiolabelled formic acid. Specifically, ^{14}C-labelled formic acid ($Na^{14}COOH$, from Sigma) was added at trace levels to formic acid and analyzed using a Packard Tri-Carb 2200 TR Liquid Scintillation Counter. The samples were then vigorously sparged with air for at least 30 seconds to drive out any $^{14}CO_2$ remaining in solution from the oxidation of $H^{14}COOH$. 1 mL of the sample solution was then added to 10 mL of Beckman liquid scintillation fluid for analysis in a Packard Tri-Carb 2100TR Liquid Scintillation Analyzer. HCOOH concentrations were calculated using calibration curves determined with $H^{14}COOH$ standards. Calibration curves were updated whenever fresh stock solutions of $H^{14}COOH$ were made. Figure 3.7 shows the calibration curve obtained from a series of samples of known concentration.

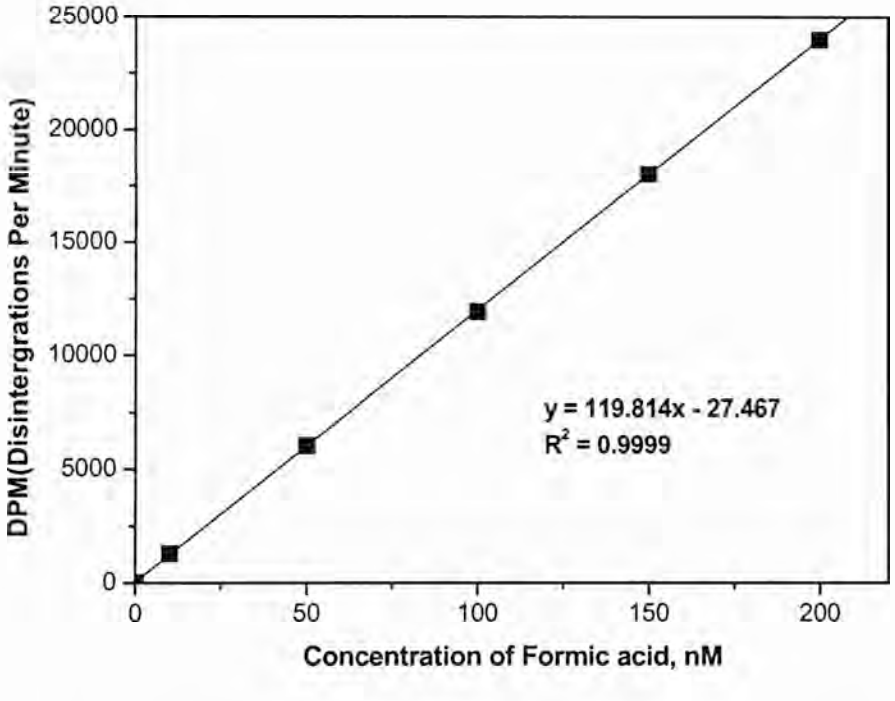

Figure 3.7 Calibration curve developed for determination of formic acid concentration

3.4.6 Fe(II) measurement

Ferrous iron (Fe(II)) was measured spectrophotometrically using 1,10-phenanthroline (Fortune and Mellon, 1938). Stock solutions of Fe(II) at 1 mM were prepared by dissolving ferrous sulfate ($Fe_2SO_4 \cdot 7H_2O$) (Ajax Chemicals, reagent grad) in 2 mM HCl. Stock solutions were prepared every three months and stored in the dark below 4°C. Determination of Fe (II) concentration in the stock solutions was undertaken regularly to ensure that Fe(II) was not oxidized during the storage period. Ferrous iron concentrations were calculated using calibration curves made from a series of Fe(II) standard solutions. Control experiments measuring Fe(II) in the presence of ferric iron showed negligible interference in absorbance readings at 510 nm using a Cary 1E UV-Vis spectrometer.

3.4.7 Nitrate measurement

Nitrate concentration was monitored at 220 nm using UV-VIS spectrophotometer (Greenberg *et al.*, 1992). Its concentration has been calculated by the calibration curve established by standard solution (500 μM of $NaNO_3$).

3.4.8 Computational analysis

Kinetic modelling of various chemical reaction mechanisms was undertaken using the computer modelling program KINTECUS (Ianni, 2002) and ACUCHEM (Braun et al., 1988) coupled to a MATLAB interface developed by Dr. Andrew L. Rose, unless otherwise stated. ACUCHEM provides a solution of differential equations that result from chemical reaction kinetics using implicit, variable order, linear multi-value integration methods. The integration time step is determined automatically based on the integration tolerance specified by the user, which was 0.001 in our case. Variable or unknown rate constants for modelling were optimized using numerical fitting routines built into KINTECUS.

KINTECUS (Ianni, 2002) features the ability to fit or optimize unknown or poorly defined rate constants by minimising the error between simulated and experimental data. The software provides a number of fitting/optimization algorithms as well as statistical methods for comparing experimental and simulated data. Optimized rate constants presented and discussed in this work were obtained using the Powell fitting algorithms and the relative least squares method as the comparison operator (Vetterling *et al.*, 1992). For the fitted rate constants proposed in this work, the algorithm produced optimized values within 5% of each other.

In addition to kinetic modelling and rate constant optimization, sensitivity analysis of the reaction mechanisms used was conducted to distinguish the relative importance of various reactions. Normalized sensitivity coefficients are used in accurate mechanism reduction, determining which reactions are the main sources and sinks and which also shows which reactions require accurate rate constants and which ones can have essentially guessed rate constants.

Examination of the sensitivity of the model (i.e., changes in species concentrations) to perturbations in various rate constants was undertaken using normalized sensitivity coefficients (NSCs) and by performing principal component analysis (PCA) (Vajda *et al.*, 1985). A reaction that has a very small NSC for a species indicates that it has negligible influence on the species regardless of the rate constant or the concentration of reactant species (Gautier *et al.*, 1985).

$$NSC = \left(\frac{\frac{\partial [Species]}{[Species]}}{\frac{\partial k}{k}} \right)_k = \left(\frac{\partial \ln [Species]}{\partial \ln k} \right)_k$$

NSCs were determined numerically at 10 equally spaced time intervals over the experimental reaction time using KINTECUS. In order to gauge the overall effect of perturbations in each rate constant on each species over the entire reaction time, the sum of the squares of the NSCs was calculated using

$$\text{Sum of squares of NSCs for the } j\text{th rate constant} = \sum_{n=1}^{25}\sum_{i}(S_{i,j}(t_n))^2$$

where i represents those species whose concentration was measured experimentally.

While NSCs provide an excellent measure of the system response to varying rate constants one at a time, they do not account for the relationships between closely interacting reactions (Vajda *et al.*, 1985, Turányi, 1990). To account for such interactions, principal component analysis was undertaken according to the method of Vajda *et al.* (1985).

In the principal components analysis, the smallest eigenvalues represent eigenvectors that contribute an insignificant amount to the system response, so that only those eigenvectors with the largest eigenvalues need to be considered. Inspection of these eigenvectors reveals which rate constants, or principal components, contribute the most to the systems behaviour. PCA was performed by considering only the NSCs calculated for species whose concentrations were experimentally determined. PCA was performed automatically using the KINTECUS add-on software package, ATROPOS (Ianni, 2002).

Chapter 4

Hydrogen Peroxide Generation and Formic Acid Degradation By Ultrasonic Irradiation

4.1 Introduction

As mentioned in Chapter 2, hydrogen peroxide formation has been considered indirect evidence of free radical generation by ultrasonic irradiation (Weissler, 1958, Wakeford *et al.*, 1999). The ultrasonic irradiation of aqueous solutions generates small cavitation bubbles which may grow and suddenly collapse and, in so doing, create localised regions of high temperature (over 5000 K) and pressure (up to 1000 atm) (Mason and Lorimer, 1988, Suslick *et al.*, 1986, Henglein, 1993). Under these conditions, hydroxyl and hydrogen atom radicals are generated by the thermolytic decomposition of water within the cavity; i.e.

$$H_2O \rightarrow OH\bullet + H\bullet \qquad (1)$$

From here-on in our discussion, we will refer to the reaction shown in eq.(1) as the *initiation reaction.*

While the radicals generated by the initiation reaction may recombine to form water, i.e.

$$OH\bullet + H\bullet \rightarrow H_2O \qquad (2)$$

both hydroxyl radicals and hydrogen atom radicals may also react with themselves to generate, respectively, hydrogen peroxide and hydrogen gas; i.e.

$$OH\bullet + OH\bullet \rightarrow H_2O_2 \qquad (3)$$

$$H\bullet + H\bullet \rightarrow H_2 \qquad (4)$$

Due to the direct link between hydrogen peroxide formation and hydroxyl radical generation, considerable interest has been shown in using the relatively easily measured (and relatively stable) hydrogen peroxide as an indicator of the behaviour of the hydroxyl radicals.

While there have been a number of studies on the sonochemical generation of hydrogen peroxide, the analysis of the underlying processes leading to H_2O_2 formation have been relatively cursory. Anbar and Pecht (1964) researched the location of the sonochemical formation of hydrogen peroxide by using hydrophobic and hydrophilic hydroxyl radical scavengers. The results showed that non-volatile OH• scavengers do not affect the production of hydrogen peroxide while volatile OH• scavengers significantly inhibited hydrogen peroxide production suggesting that hydrogen peroxide is produced in the bubble rather than the bulk solution. This result was further supported by Hart and Henglein (1985) who showed that hydroxyl radicals produced in the bubble form hydrogen peroxide in an interfacial zone with the yield of hydrogen peroxide decreasing on addition of hydrophobic compounds. Similar observations were reported by Henglein and Kormann (1985) who found that enrichment of hydrophobic solutes in the bubble or interfacial zone resulted in OH radical scavenging. These observations were further supported by a more recent study (Rassokhin *et al.*, 1994) which suggested that the non-homogenous initial spatial distribution of hydroxyl radicals in the solution accounted for the suppression of hydrogen peroxide formation by hydroxyl radical

scavengers. They found that certain hydroxyl radical scavengers (ethanol, methanol, acetate, tert-butanol, and dioxane) reduced the rate of hydrogen peroxide formation in accord with their hydrophobic nature.

The affect of the properties of the gas used in sonochemical studies on the hydroxyl radical production has also not been defined clearly. The gas property affects the temperature and pressure in the bubble and hence the sonochemical activity. In addition, depending on the gas present in the system, additional radical reactions may occur. For instance, in the presence of oxygen, the hydrogen atoms may react with oxygen leading to the formation of hydroperoxyl radicals that may in turn disproportionate to hydrogen peroxide at the interfacial zone and/or in the bulk solution; i.e.,

$$H\bullet + O_2 \rightarrow HO_2\bullet \quad (5)$$

$$HO_2\bullet + HO_2\bullet \rightarrow H_2O_2 + O_2 \quad (6)$$

As would be expected from reactions (5) and (6), $HO_2\bullet$ mediated production of hydrogen peroxide would be expected to increase as the oxygen concentration increases.

In this study, new insights into the factors influencing hydrogen peroxide formation are obtained by examining the effect of different frequencies and dissolved gases on rate and extent of hydrogen peroxide formation. Also, experiments were conducted in the presence of a simple organic, formic acid, in an effort to examine the sonochemical degradation mechanism. Formic acid was chosen as the target compound due to its simple chemical characteristics and degradation mechanism. Effects of parameters including ultrasonic irradiation frequency, dissolved gas and pH on formic acid degradation rate are investigated. The mechanism proposed in this chapter will be used to underpin discussion of the results of more complex systems presented in later chapters.

4.2 Materials and Methods

4.2.1 Experimental setup and reagents

All chemicals were reagent grade and used as received. All reagents were prepared in 18 MΩ.cm resistivity Milli-Q water unless stated otherwise. The pH of the solutions was initially set at 3.5 using 0.1 M nitric acid but with no subsequent attempt made to control the pH.

Sonolysis was performed at three different frequencies (300, 600 and 800 kHz). As described in Chapter 3, the ultrasound reactor used in this research was supplied by Radiocom Systems (France) with separate generators producing radiation of particular frequency. As described in Section 3.3.1, the ultrasonic power dissipation was controlled with acoustic power of 30W delivered in each run. Acoustic power was measured using the calorimetric methods described in Section 3.3.1. The aqueous solution was equilibrated with different dissolved gases (air, argon, oxygen and nitrogen) as required with sparging continued for at least 15 minutes prior to each run. Gas sparging was implemented using a submerged diffuser which was inserted through a hole in the silicon cover. Gas supply was discontinued during the actual run. A silicon lid with gas-tight sampling ports was used to prevent the system from resaturation by air during sonolytic irradiation.

C^{14} labeled formic acid ($Na^{14}COOH$, from Fluka) was used as received. A stock solution of 10 μM formic acid was prepared by adding 56 μL of C^{14} labelled formic acid to 100mL of Milli Q water. Solutions with formic acid concentrations ranging from 5 nM to 1 μM were made from the stock solution and used in the sonolysis experiments. Samples were taken at discrete intervals over the duration of sonolysis (typically one hour) for subsequent analysis of both hydrogen peroxide and formic acid concentrations. Samples for formic acid analysis were sparged with argon for at least 30 seconds to remove any $^{14}CO_2$ remaining in the solution.

4.2.2 Methods

Aliquots were removed from the reaction solution at selected times and the concentration of hydrogen peroxide (and nitrate in some instances) were determined spectrophotometrically using the methods described in Section 3.3.3. The concentration of C^{14} was analyzed using a Packard Tri-Carb 2200 TR Liquid Scintillation Analyzer as described in Section 3.3.5.

4.3 Results and Discussion

4.3.1 Impact of dissolved gas properties on hydrogen peroxide formation by ultrasonic irradiation

Sonolysis of water at a temperature of 25°C and applied frequencies of 300, 600 and 800 kHz under argon saturated conditions resulted in reasonably linear increase in hydrogen peroxide concentration over the duration of the experiment suggesting that the reaction follows zero order kinetics (Figure 4.1). This linear relationship was also observed under oxygen and nitrogen saturated solutions (Figures 4.10 and 4.11). Given that the pH of the reaction mixture increases from 3.5 to 4.8 over this time period, the linearity of these production plots suggests that hydrogen peroxide production rate is not influenced significantly by the solution pH.

Rates of hydrogen peroxide formation for different dissolved gases and frequencies are summarised in Table 4.1. As shown in Table 4.1, the hydrogen peroxide formation rate varies from 0.47-4.5 μM/min at 300 kHz, 0.15-2.9 μM/min at 600 kHz and 0.25-2.1 μM/min at 800 kHz depending on the gas composition. This suggests that composition of the dissolved gas is an important parameter in controlling hydrogen peroxide formation. The variation in the physical properties of the dissolved gases causes variation in the initiation reaction (eq. 1) and other radical reactions (eq. 2-6), thereby affecting hydrogen peroxide formation.

Table 4.1 Summary of hydrogen peroxide formation rate under different dissolved gases and frequencies.

Dissolved gas / Frequency	Hydrogen peroxide generation rate (μM/min)			
	Argon	Nitrogen	Oxygen	Air
300 kHz	2.6	0.47	4.5	4.3
600 kHz	2.9	0.15	2.8	2.7
800 kHz	2.1	0.25	1.8	1.6

The physical properties of the gases used in this study are shown in Table 4.2 (Lide, 2005). It is well known that gases with larger specific heat ratio (γ) demonstrate higher rates for the initiation reaction (Mason, 1991). As described briefly in Chapter 2, the maximum temperature and pressure in the cavities depends on γ and is described by:

$$T_{max} = T_0\left(\frac{P_m(\gamma-1)}{P}\right) \tag{7}$$

$$P_{max} = P\left(\frac{P_m(\gamma-1)}{P}\right)^{\frac{\gamma}{\gamma-1}} \tag{8}$$

where T_0 and P are the ambient liquid temperature and pressure in the bubble at maximum size respectively (Mason, 1991). The pressure in the bubble at the moment of transient collapse (acoustic pressure) is denoted as P_m.

The higher the maximum temperature and pressure achieved in the bubble, the higher will be the rate of generation of hydrogen atoms and hydroxyl radicals and thus the higher the rate of hydrogen peroxide generation. The maximum temperature and pressure calculated using equations (7) and (8) with different dissolved gases are presented in Table 4.3.

The solubility of the gas may also affect sonochemical activity. Gases which are more soluble in the aqueous solution may diffuse into the cavitation bubble more readily.

Dissolved gases form the nuclei for cavitation thus more soluble gases result in a greater number of cavitation nuclei and extensive bubble collapse because gases are readily forced back to the aqueous phase (Adewuyi, 2001). Due to increase in cavitation nuclei, the rate of the initiation reaction increases with increase in solubility of the gas.

Thermal conductivity is also an important parameter affecting sonochemical reactions. Although bubble collapse is modelled as an adiabatic process, a small amount of heat is transferred to the bulk solution during collapse. As the thermal conductivity of the gas increases, the amount of heat loss due to thermal dissipation also increases (Nikitenko *et al.*, 2004); hence the rate of initiation reaction decreases.

Though the dominant property (specific heat ratio, solubility and thermal conductivity) affecting initiation reaction is not clear; based on the affect of all the properties described above, it is expected that the rate constant for initiation reaction for argon, oxygen, nitrogen and air will follow the pattern given below:

$$\text{Nitrogen} \approx \text{Air} < \text{Oxygen} < \text{Argon}$$

Table 4.2 Physical Properties of dissolved gases used.

	Specific heat ratio, γ	Thermal Conductivity (m W/(m·K), 300 K)	Solubility in water (mL gas/100g water, 20 °C)
Argon	1.67	17.9	3.30
Oxygen	1.40	26.3	3.10
Nitrogen	1.40	26.0	1.54
Air	1.40	26.2	1.87

Table 4.3 Theoretically calculated values of T_{max} and P_{max} by Equations (7) and (8) for the different dissolved gases.

	T_{max}(K)	P_{max}(atm)
Air, Oxygen & Nitrogen	5100	500
Argon	8400	100

4.3.2 Impact of ultrasonic frequency on hydrogen peroxide formation

As summarized in Table 4.1, the frequency of the ultrasonic radiation also affects the hydrogen peroxide formation rate. The frequency of the ultrasonic radiation applied is recognised to be one of the main parameters influencing hydroxyl radical production and, concomitantly, hydrogen peroxide formation rates (Pétrier *et al.*, 1992, Entezari and Kruus, 1994, Hung and Hoffmann, 1999, Kang *et al.*, 1999). The resonant radius of an acoustic bubble is inversely correlated with the ultrasonic frequency applied and its relationship is represented by the following equation (Leighton, 1994) ;

$$R_r^2 = \frac{3\gamma P_0}{\rho\omega_r^2} \tag{9}$$

where ρ is the density of the solution, ω_r is the resonant frequency, R_r is the resonant radius, P_0 is the hydrostatic pressure (1 atm) and γ is the specific heat ratio. Knowing the resonant radius, the bubble collapse times (τ) at each frequency can be calculated using the equation proposed by Mason and Lorimer (1988); i.e.,

$$\tau = 0.915 R_r \sqrt{\frac{\rho}{p_a}} \tag{10}$$

where τ is the bubble collapse time, R_r is the resonant radius, ρ and p_a represent the density of the liquid and ambient pressure respectively.

At the higher frequency, collapse of bubbles occurs more rapidly due to the smaller resonator radii. The higher collapse rate of bubbles may result in a higher mass transfer

rate between the interface and the bulk solution. With increasing frequency, the pulsation and collapse of the bubble takes place more rapidly leading to more radicals escaping from the bubble. However the acoustic period is much shorter at high frequency, resulting in decreased cavitation bubble size. This can decrease the cavitation intensity and consequently reduce the rate of the initiation reaction. Considering an adiabatic collapse, lower frequencies will result in a more violent collapse than higher frequencies due to greater resonant bubble sizes (Petrier *et al.*, 1992). Thus, it is reasonable to conclude that, for each dissolved gas, there exists an optimum frequency where sufficient energy is available to release hydroxyl radicals along with fast mass transfer rate of the hydroxyl radical to the bulk solution due to rapid bubble collapse. This hypothesis is supported by our experimental results which show that hydrogen peroxide formation depends non-linearly on frequency under all conditions examined.

It should be noted that the sonochemical activity could be optimized by combining conditions such as frequency and dissolved gas. In the following section, we discuss the impact of dissolved gases and frequency in much more detail with the aim of identifying the optimum frequency under each condition examined.

4.3.3 Hydrogen peroxide formation and formic acid degradation under argon saturated solution

4.3.3.1 Formation of hydrogen peroxide by ultrasonic irradiation

4.3.3.1.1 Effect of Frequency

From the slopes of the plots shown in Figure 4.1, the rate of hydrogen peroxide generation is found to be 2.6 μM/min at 300 kHz, 2.9 μM/min at 600 kHz and 2.1 μM/min at 800 kHz. The calculated values of resonant radii and bubble collapse time (using eq. 9 and 10) in argon-saturated solution at various frequencies examined are shown in Table 4.4. As discussed earlier, at lower frequency (300 kHz in this study) more violent collapse occurs resulting in a higher hydroxyl radical generation rate from the initiation reaction. However, the mass transfer rate of hydroxyl radical and hydrogen peroxide to the interface and bulk solution is expected to be slow at this frequency,

resulting in lower levels of hydrogen peroxide in the bulk solution. Our results further demonstrate that under argon saturated solution, optimum frequency with respect to hydrogen peroxide generation in the bulk solution is close to 600 kHz

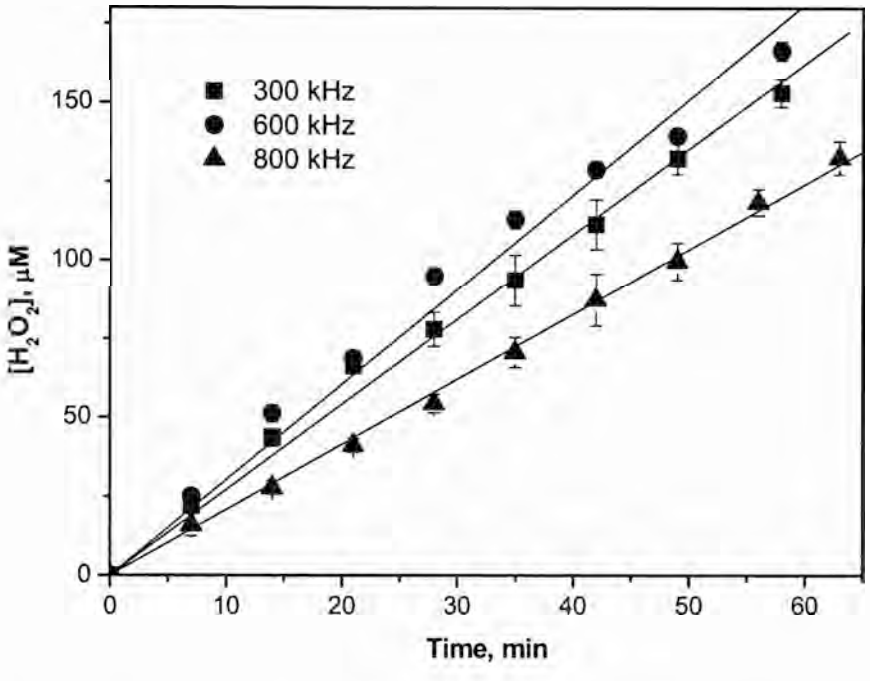

Figure 4.1 Hydrogen peroxide formation at three frequencies under argon saturated solutions for 30W(acoustical power) and pH 3.5.

Table 4.4 Properties of bubbles formed on sonication of argon saturated solution at 25°C using radiation of 300, 600 and 800 kHz frequency.

Freq. (kHz)	Resonance Radius (μm)	Surface area(A) (μm^2)	Vol.(V) (μm^3)	A/V (μm^{-1})	Bubble collapse time (μsec)
300	11.83	1.76×10^3	6.94×10^3	0.25	1.08
600	5.92	4.40×10^2	8.67×10^2	0.51	0.54
800	4.44	2.47×10^2	3.66×10^2	0.68	0.41

4.3.3.1.2 Effect of addition of hydrogen peroxide, formic acid and phenol

Given that hydrogen peroxide is itself capable of scavenging both hydroxyl ($\cdot OH + H_2O_2 \rightarrow \cdot HO_2 + H_2O$) and hydrogen atom free radicals ($H_2O_2 + \cdot H \rightarrow \cdot OH + H_2O$) (Buxton et al., 1988, Ershov et al., 2003), we examined the effect of hydrogen peroxide addition on its generation by ultrasonic irradiation. As shown in Figure 4.2 however, there is no significant effect of hydrogen peroxide addition on rate of generation of hydrogen peroxide up to 200μM.

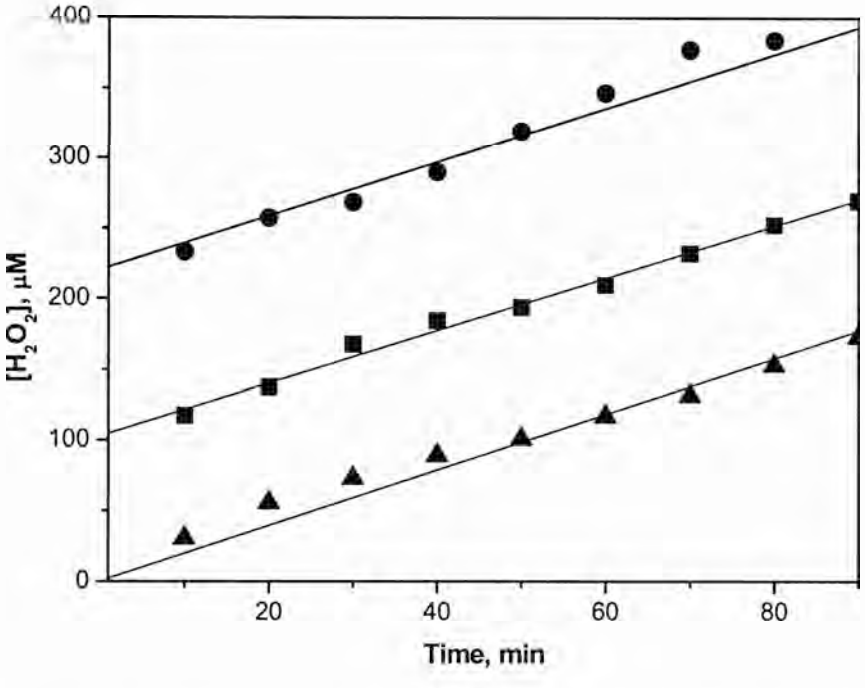

Figure 4.2 Hydrogen peroxide formation in the absence and presence of added hydrogen peroxide under argon saturated solutions at 800 kHz and 30W(● : 200 μM of H_2O_2, ■ : 100 μM of H_2O_2, ▲: no addition). Slope = 1.85 ± 0.07 μM/min.

Similarly no affect of formic acid addition on hydrogen peroxide production was observed for formic acid concentration up to 500 μM (Figure 4.3 (a)). In contrast, the presence of phenol exerted a significant effect on hydrogen peroxide formation rate (Figure 4.3 (b)). These observations support the results presented in earlier studies (Hart

and Henglein, 1985, Gutierrez and Henglein, 1991) that hydrogen peroxide is formed by free radical combination reactions either within the bubble (gaseous zone) or at the bubble-water interface with minimal effect of potential hydrophilic hydroxyl radical scavengers (such as hydrogen peroxide and formic acid) on hydrogen peroxide generation rate. However, more hydrophobic hydroxyl radical scavenger such as phenol has a significant effect on hydrogen peroxide generation.

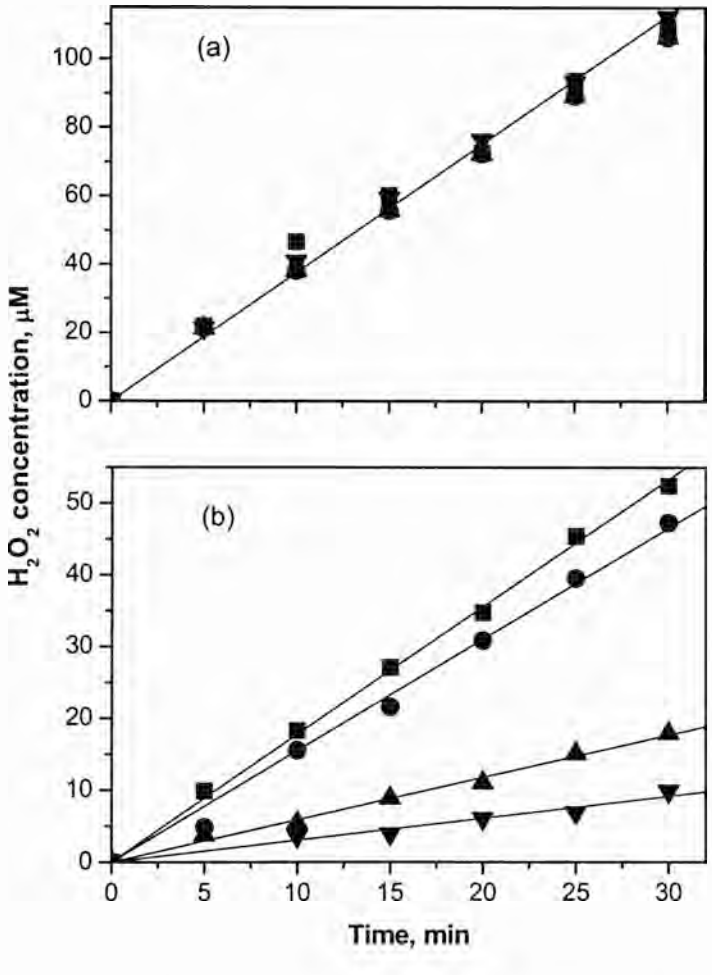

Figure 4.3 Effect of organic compounds on hydrogen peroxide formation. (a) : formic acid (b) : phenol. Conditions : 300 kHz, pH 3.5, argon saturated solutions(■: 10 μM ●: 100 μM ▲ : 300 μM ▼ : 500 μM of either phenol or formic acid).

4.3.3.2 Sonolytic degradation of formic acid under argon saturated solution

4.3.3.2.1 Effect of frequency

The results of sonolytic degradation of aqueous solutions of 200 nM formic acid under three different frequencies are shown in Figure 4.4. Formic acid degradation followed pseudo first order kinetics with the maximum pseudo first order rate constant (0.087 min^{-1}) observed at 600 kHz. Since hydrogen peroxide provides a measure of hydroxyl radical formation and formic acid degradation potentially occurs by hydroxyl radical attack, this observation is in agreement with our earlier result which showed that maximum hydrogen peroxide formation rate in argon-saturated system occurs at 600 kHz.

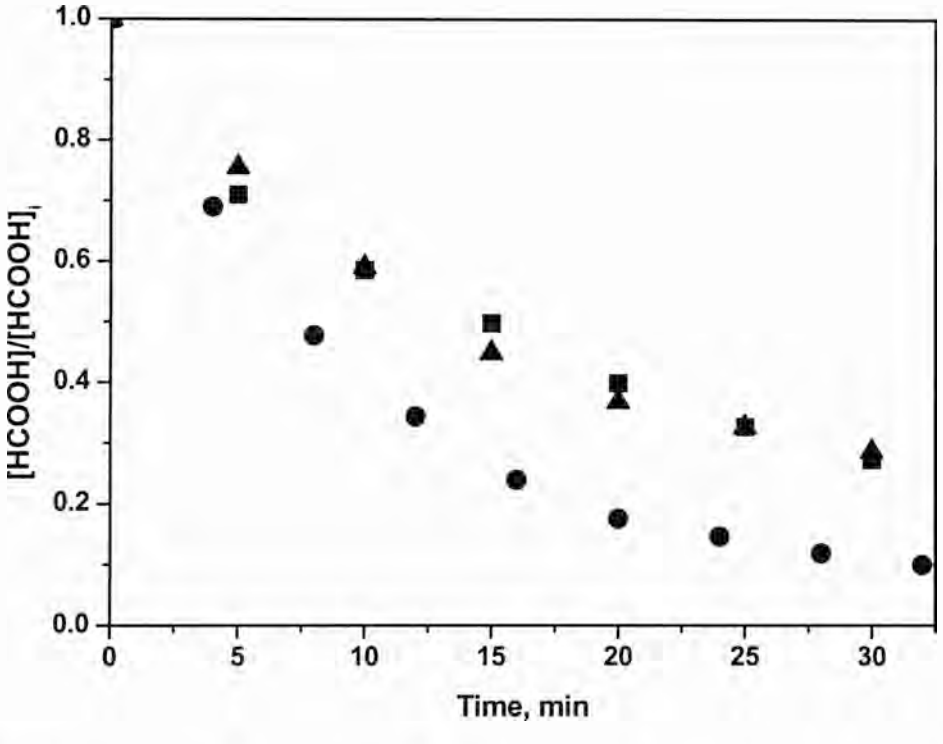

Figure 4.4 Formic acid degradation by ultrasonic irradiation under argon saturated solution (▲ : 800kHz, ● : 600 kHz, ■ : 300 kHz.

4.3.3.2.2 Effect of initial concentration on formic acid degradation

The effect of initial concentration of formic acid on the pseudo first order rate constant was investigated using formic acid concentrations in the range of 5-1000 nM at 600 kHz. The degradation of formic acid followed pseudo first-order reaction kinetics at all concentrations examined. The pseudo first order rate constant for various conditions examined are summarized in Figure 4.5. Formic acid degradation rate was shown to be dependent on the initial concentration with the rate constants decreasing on increasing formic acid concentration as depicted in Figure 4.5. The rate constant decreased sharply at low concentrations of formic acid but the rate of decrease in formic acid degradation rate slowed on increasing formic acid concentration. While formic acid degraded exponentially with time irrespective of its concentration, the observed rate constant decreased from 0.0812 min^{-1} at 5 nM to 0.0241 min^{-1} at 1 μM. A plot of log (rate constant) versus log [formic acid] yielded a straight-line relationship (r^2 = 0.90) from which the following empirical equation, $k = 0.1071[HCOOH]^{-0.2041}$, was obtained. This observation is consistent with earlier reports (Hung and Hoffmann, 1998, Dewulf *et al.*, 2001, Gogate *et al.*, 2006) which showed that the amount of hydroxyl radicals produced at the interface during ultrasonic irradiation decreases with an increase in organic concentration because of absorption of heat energy generated in the bubble due to adsorption of organic molecules to the bubble surface. Increasing organic compound concentration in the bulk solution increases the amount of organics that can penetrate into the bubble during bubble expansion. The evaporated molecules may consume part of the heat energy that is generated during pyrolysis resulting in decrease of the bubble temperature and hence reduction in extent of hydroxyl radical generation.

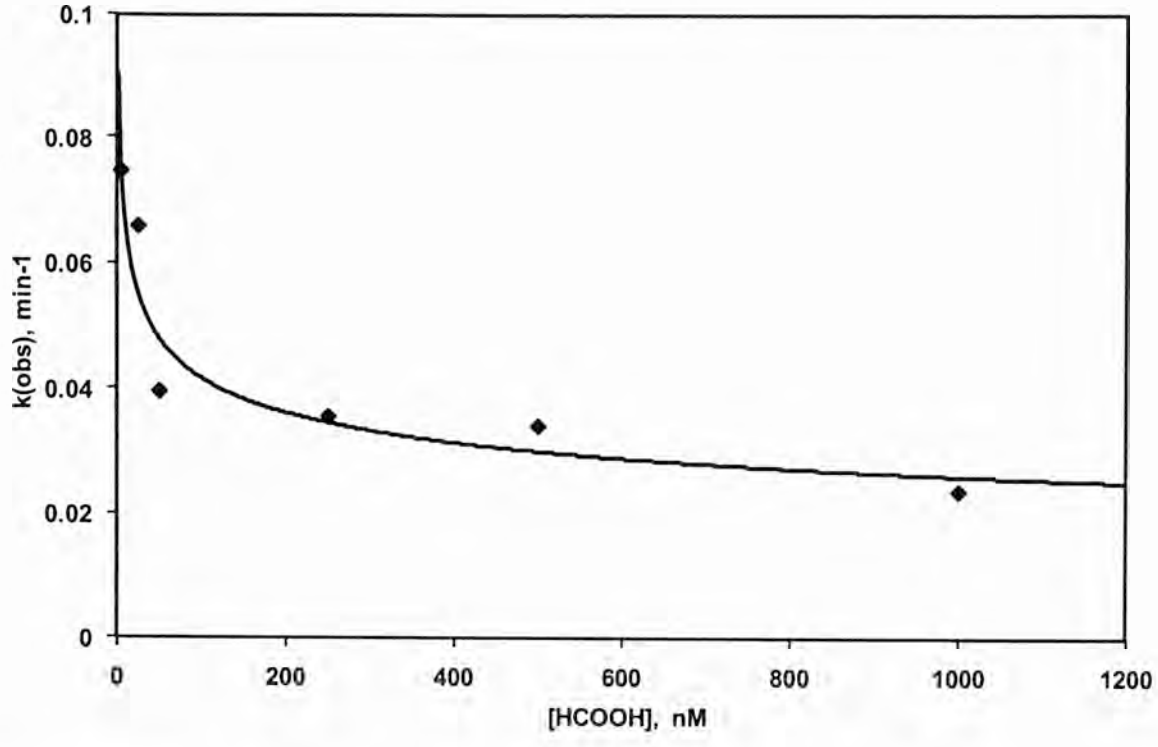

Figure 4.5 Effect of initial concentration of formic acid on sonolytic degradation of formic acid. Conditions: 600 kHz, 30W, pH 3.5, argon saturated solutions, and $[HCOOH]_o$= 200nM

4.3.3.2.3 Effect of initial pH

pH of solution may affect the degradation rate of formic acid by ultrasonic irradiation as a result of two principal effects both of which are related to the pH dependent charge of the dominant species present: (1) the interfacial zone present between the cavitational bubble and bulk solution is negatively charged (Jiang *et al.*, 2002, Singla *et al.*, 2004) which may affect mass transfer rate of negatively charged species through the interface; (2) the speciation of organic compounds may affect the rate constants for reactions with free radicals (Serpone *et al.*, 1992, Tauber *et al.*, 2000, Jiang *et al.*, 2002).

In order to determine the effect of solution pH on formic acid degradation kinetics, experiments at various solution pH were carried out at 600 kHz, 30W(acoustic power), and 200 nM(initial formic acid concentration). The pH was set by addition of 0.1M nitric acid and 0.1 M sodium hydroxide and ranging 2 to 10. The relationship between

initial pH and half life at given pH is shown in Figure 4.6. The pseudo half life initially increases with increase in pH; however reaches a steady value for pH> 3.8.

This observed effect of pH on the pseudo-first order decomposition rate constant (min^{-1}) of formic acid, *k,* can be explained by the variation in the speciation of formic acid with pH. The dominant form of formic acid present in the solution is related to its pK_a value (pK_a = 3.75). At higher pH, (i.e. pH > 3.75), formate ion would be the dominant species, while formic acid would be the main species in the solution at pH values lower than 3.75. The rate constant for the reaction between formic acid/formate ion and hydroxyl radicals is well-established and is described below (Buxton *et al.*, 1988, Duesterberg *et al.*, 2005).

$$HCOOH + OH\bullet \rightarrow HCOO\bullet + H_2O \quad , k_{OH,HCOOH} = 1.3 \times 10^8\ L\ mol^{-1}\ s^{-1} \qquad (11)$$

$$HCOO^- + OH\bullet \rightarrow COO\bullet^- + H_2O \quad , k_{OH,HCOO^-} = 3.2 \times 10^9\ L\ mol^{-1}\ s^{-1} \qquad (12)$$

Based on the rate constant for the hydroxyl radical reaction with formic acid and formate ion, we can calculate a composite rate constant (k_{comp}) at any pH using eq.(13) (Duesterberg *et al.*, 2005, Kwan and Voelker, 2002):

$$k_{comp} = k_{OH,HCOOH}\frac{[HCOOH]}{[HCOOH]_T} + k_{OH,HCOO^-}\frac{[HCOO^-]}{[HCOOH]_T} \qquad (13)$$

where $[HCOOH]_T$ is the total concentration of formic acid ($[HCOOH]_T = [HCOOH] + [HCOO^-]$) and $k_{OH,HCOOH}$ and $k_{OH,HCOO^-}$ are the rate constants of formic acid and formate ion reaction with hydroxyl radicals, respectively.

As shown in eq. 11 and 12, the rate constant for reaction of hydroxyl radical with formate ion is higher than the corresponding rate constant in case of formic acid. Thus, faster degradation kinetics is expected at higher pH where formate ion is the dominant species. This observation is in agreement with our results which shows that the pseudo first order rate constant initially increases with increase in pH before reaching a steady value for pH>3.8. All of the formic acid is present as formate and thus no change in *k* occurs for pH>3.8.

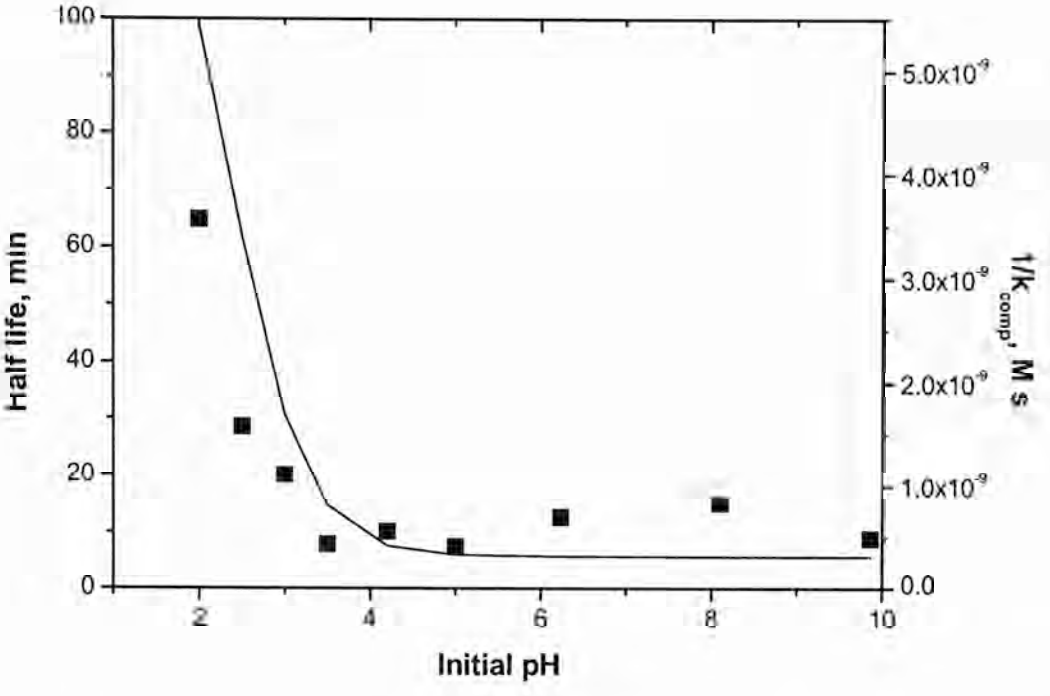

Figure 4.6 Effect of initial pH on rate of formic acid degradation. Conditions: 600 kHz, 30W(acoustic power), argon saturated solution, and $[HCOOH]_0$ = 200 nM. Solid line represents the composite rate constant at given pH and solid squares represent half life (min) at given pH.

4.3.3.2.4 Effect of hydroxyl radical scavenger

In order to confirm that formic acid degradation occurs due to its reaction with hydroxyl radical, we measured the affect of *t*-butanol, a well known hydroxyl radical scavenger (Henglein and Kormann, 1985, Pétrier *et al.*, 1992), on formic acid degradation rate. As shown in Figure 4.7, formic acid degradation was completely inhibited in the presence of 100 μM *t*-butanol at 600 kHz confirming that hydroxyl radicals are the active oxidant of formic acid during ultrasonic irradiation.

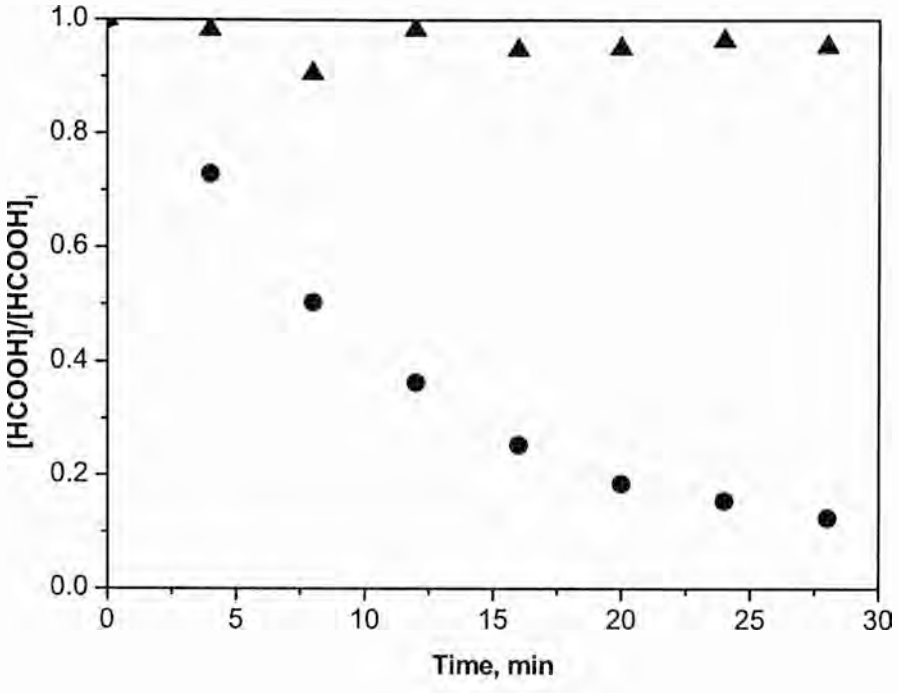

Figure 4.7 Effect of t-butanol on the sonolytic decomposition of formic acid. Conditions: 600 kHz, 30W(acoustic power), pH 3.5, argon saturated solutions, and $[HCOOH]_0 = 200$ nM.

4.3.3.2.5 Reaction mechanism for formic acid degradation

It is interesting to note that formic acid could not be completely decomposed within the experimental duration even though very low concentrations of formic acid (200 nM – 1 μM) were used in this study and the rate constant for reaction of formic acid with hydroxyl radicals is very large (6.5×10^8 M^{-1} s^{-1}, Ross and Ross, 1977). The incomplete degradation of formic acid suggests two possibilities:

1) Formic acid reacts with hydroxyl radicals at the interface; however the diffusion rate of formic acid from the bulk solution is very low and is the rate determining step in formic acid degradation. This explanation is consistent with earlier studies which suggested that hydrophilic compounds are decomposed by hydroxyl radicals at the interface where most of the hydroxyl radicals are present (Adeyuwi, 2001, Jiang *et al.*, 1998).

2) Formic acid degradation occurs in the bulk solution rather than at the bubble interface. As suggested earlier (Goel *et al.*, 2004), only small concentrations of hydroxyl radicals diffuse or move into the bulk solution from the bubble interface, and hence formic acid might react with hydroxyl radicals to a limited extent .

Both these possibilities are consistent with the hydrophilic nature of formic acid with most of the formic acid being present in bulk solution. These explanations are also consistent with earlier studies which suggested that the degradation mechanism depends on the hydrophobicity of the compounds (Henglein and Kormann, 1985). In some studies, the octanol-water partitioning coefficient of the solute was used to predict the extent of partitioning of compounds to the interface and/or inside the bubble (Ayyildiz *et al.*, 2007, Nanzai *et al*, 2008). The octanol-water partition coefficient (Log P) is defined as the ratio of a chemical's concentration in the octanol phase to its concentration in the aqueous phase of an octanol/water binary system. Nanzai *et al.*(2008) found that the octanol-water partition coefficient is the most important parameter determining accumulation of compounds at the gas-liquid interface during ultrasonic degradation. Thus, compounds with higher octanol-water partition coefficients tend to decompose faster than compounds with lower octanol-water partition coefficients (Wu and Ondruschka, 2005).

Reported octanol-water partition coefficients of phenol and formic acid are 1.46 and 0.54 respectively (Lide, 2005) suggesting that phenol will accumulate more readily at the bubble interface than will formic acid. This difference in octonal-water partition coefficients explains two observations:

Firstly, higher accumulation of phenol at the bubble interface (or, possibly, in the bubble) can result in an increased adsorption of energy, leading to a lower water decomposition rate inside the bubble. In addition, accumulation of phenol at the interface can also scavenge hydroxyl radicals in the interface resulting in a reduced hydrogen peroxide formation rate in the presence of phenol (Figure 4.3 (b)). Due to the lower octonal-water partition coefficient of formic acid, accumulation of formic acid at the interface and/or in the bubble is not high enough to scavenge hydroxyl radicals in the interface or affect water decomposition rate in the bubble.

Secondly, phenol competitively inhibits degradation of formic acid (Figure 4.8). Due to the higher hydrophobicity, it is expected that hydroxyl radicals will react with phenol more favourably in the interfacial zone, thereby decreasing formic acid degradation if degradation occurs at the interface. Alternatively, this observation can be explained by the fact that the rate constant for reaction of phenol with hydroxyl radical (6.7×10^9 $M^{-1}s^{-1}$, Buxton *et al.* 1988) is higher than the rate constant for reaction of hydroxyl radical with formic acid (6.5×10^8 $M^{-1}s^{-1}$, Ross and Ross, 1977) at pH 3.5 suggesting that, in the presence of phenol, reaction of hydroxyl radical with formic acid will be out competed.

The effect of phenol addition on formic acid degradation also helps in clarifying the location (interface or bulk solution) of formic acid degradation. If degradation occurs in the bulk solution, due to the (5 times) higher rate constant for reaction of hydroxyl radicals with phenol and the higher concentration of phenol compared to formic acid (by 50-500 times), formic acid degradation should be completely inhibited even at the lowest concentration of phenol used which is not consistent with our observation (Figure 4.8). This result suggests that most of the formic acid is degraded at the interface with diffusion of formic acid from the bulk solution to the interface being the rate limiting step. This conclusion is further supported by observations reported in Figure 4.9. As shown in Figure 4.9, formic acid degradation decreased slightly with increasing concentration of hydrogen peroxide. Due to its hydrophilic nature, most of the added hydrogen peroxide is present in bulk solution and could scavenge hydroxyl radicals diffused from the interface ($H_2O_2(b) + \bullet OH\ (b) \rightarrow HO_2\bullet + H_2O$), thereby decreasing formic acid degradation rates in the bulk solution. Although the rate constant for reaction of hydroxyl radicals with hydrogen peroxide (3.3×10^7 $M^{-1}s^{-1}$, Buxton *et al.* 1988) is around 300 times lower than in case of formic acid, addition of hydrogen peroxide in excess (2500 times) should be enough to inhibit formic acid degradation which is not in agreement with our observation (Figure 4.9); thereby suggesting that only a small portion of formic acid is degraded in the bulk solution.

In summary, the following points should be noted;

1) Hydrogen peroxide is produced as a result of free radical reactions at the interface;
2) Hydrogen peroxide and free radicals would be expected to only be present in the bulk solution as a result of diffusion from the interfacial zone;

3) Most of the formic acid/formate ions ($HCOOH/HCOO^-$) will be present in bulk solution and not at the interface;
4) Formic acid degradation occurs mainly in the interfacial zone; however a small percentage may be degraded in the bulk solution.

The importance of degradation reactions occurring at the bubble interface highlights the need to represent transfer of reactants from bulk to interface and, in some instances, vice versa as shown below:

$$H_2O_2(i) \rightarrow H_2O_2(b)$$
$$\bullet OH(i) \rightarrow \bullet OH(b)$$
$$HCOOH(b) \rightarrow HCOOH(i)$$
$$\bullet OH(i) + HCOOH(i) \rightarrow \text{Products}$$
$$\bullet OH(b) + HCOOH(b) \rightarrow \text{Products}$$

(i) : interface, (b) : bulk solution

Concepts presented qualitatively here will be used in developing a quantitative description of these processes in Chapter 5.

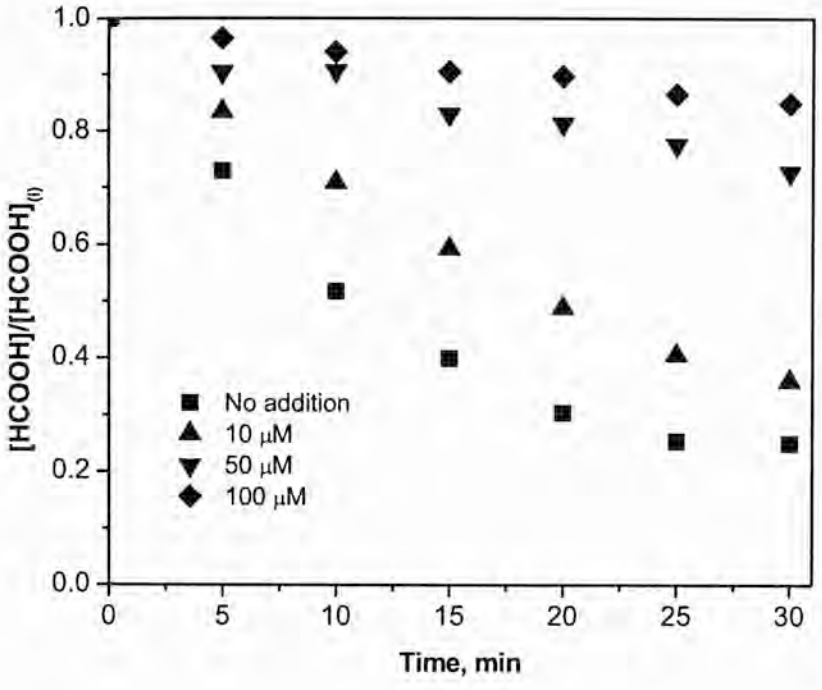

Figure 4.8 Effect of phenol addition on formic acid degradation by ultrasonic irradiation. Conditions : 600 kHz, pH 3.5, argon saturated solution, and $[HCOOH]_0 = 200$ nM.

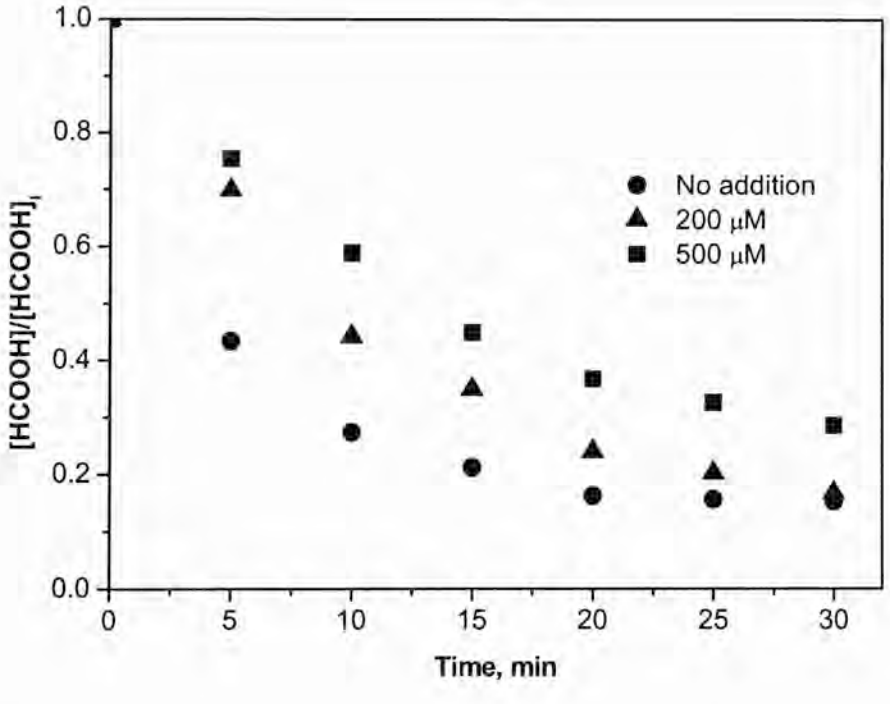

Figure 4.9 Formic acid degradation in the addition of hydrogen peroxide. Condition : 600 kHz, pH 3.5, argon saturated solution, and $[HCOOH]_0 = 200$ nM.

4.3.4 Hydrogen peroxide formation under nitrogen saturated solutions

4.3.4.1 Formation of hydrogen peroxide by ultrasonic irradiation

4.3.4.1.1 Effect of frequency

Results of studies into hydrogen peroxide formation at different frequencies under nitrogen saturated solutions are shown in Figure 4.10. The highest rate of hydrogen peroxide formation (0.472 μM/min) was obtained at 300 kHz while the lowest rate (0.15 μM/min) was obtained at 600 kHz. The variation in the hydrogen peroxide formation rate could be ascribed to the reasons discussed in Section 4.2.2. The bubble collapse times at various frequencies examined under nitrogen saturated solutions are shown in Table 4.5.

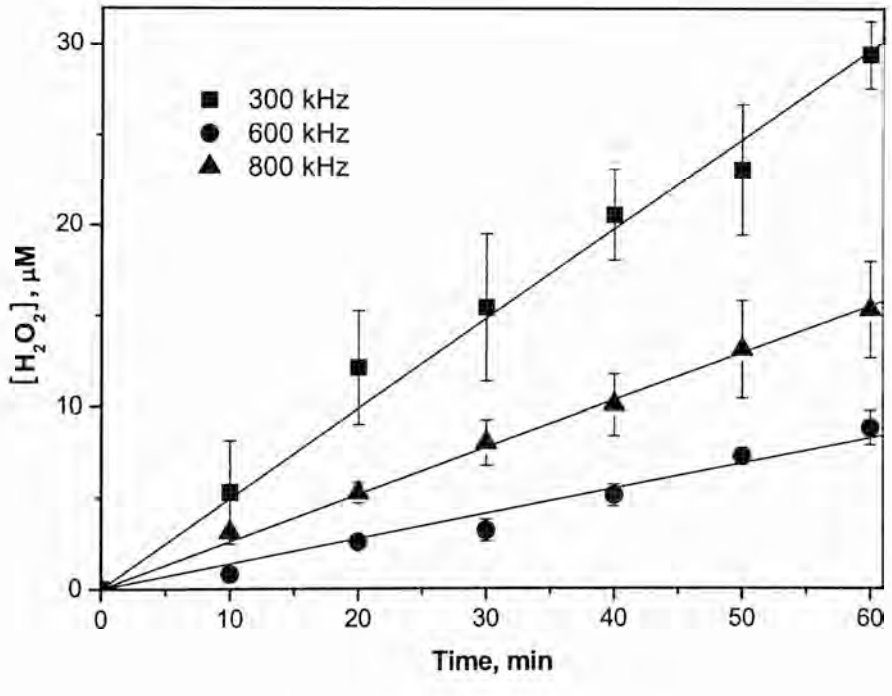

Figure 4.10 Hydrogen peroxide formation at three different frequencies under nitrogen saturated solutions for 30W(acoustic power) and pH 3.5

The hydrogen peroxide production rates obtained under nitrogen saturation are markedly lower than those obtained under argon saturated solutions (see Table 4.1) for all frequencies examined. As discussed earlier, the physical properties of the dissolved gas affects the initiation reaction (i.e., the decomposition of water to yield H• radical and OH• radical). The higher bubble temperature and lower thermal conductivity in the argon system compared to the nitrogen system (Table 4.3) may account for the differences in hydrogen peroxide production observed in the two systems. Nitrate concentration was monitored during sonication but was found to be negligible suggesting that no oxidation of nitrogen occurred in the nitrogen sparged system.

Table 4.5 Properties of bubbles formed on sonication of nitrogen saturated solutions at 25°C using radiation of 300, 600 and 800 kHz.

Freq. (kHz)	Resonance Radius (μm)	Surface area(A) (μm^2)	Vol.(V) (μm^3)	A/V (μm^{-1})	Bubble collapse time (μsec)
300	10.87	1.48×10^3	5.37×10^3	0.28	0.99
600	5.43	3.71×10^2	6.72×10^2	0.55	0.50
800	4.08	2.09×10^2	2.83×10^2	0.74	0.37

4.3.5 Hydrogen peroxide formation and formic acid degradation under oxygen saturated solutions

4.3.5.1 Formation of hydrogen peroxide by ultrasonic irradiation

4.3.5.1.1 Effect of frequency

Hydrogen peroxide formation rates under oxygen saturated solutions at various frequencies examined are shown in Figure 4.11. Hydrogen peroxide generation follows zero order kinetics in oxygen saturated systems similar to that observed in case of argon and nitrogen saturated systems.

Comparison of the hydrogen peroxide generation rates in argon and oxygen systems reveals that the rates are higher in oxygen than under argon at 300 kHz, similar to those found for argon at 600 kHz and slightly less than those found under argon at 800 kHz. These observations can be explained by the following two factors:

1) Variation in the initial sonochemical activity due to differences in physical properties of argon and oxygen;
2) Additional radical reactions occurring in the case of oxygen.

As discussed in Section 4.2.1, the initiation reaction is highest in argon saturated systems at all frequencies. However, the additional hydrogen peroxide generation pathway (i.e., disproportionation of the hydroperoxy radical) in oxygen saturated systems explains the higher (or similar) hydrogen production rates observed in the oxygen system at 300 and 600 kHz. This explanation is consistent with earlier studies (Gong and Hart, 1998, Wakeford *et al.*,1999) in which observations of higher hydrogen peroxide generation rates in the presence of oxygen compared to argon were attributed to the formation and subsequent disproportionation of the hydroperoxyl radical.

Harada and Kumagai (2003) examined the effect of oxygen concentration on hydrogen peroxide formation rate by sonication using radiation of 200 kHz frequency and 200 W power. They observed the highest yield of hydrogen peroxide under a 40% oxgyen-60% argon atmosphere. They ascribed their results to the combined effect of argon with high sonochemical reactivity and the hydroperoxy radical generation in the case of oxygen. This may indeed be the case at lower frequencies but this additional hydrogen peroxide generation pathway may not be important at the higher frequencies where bubble collapse are less violent and bubble lifetimes are shorter resulting in lower hydroperoxy radical generation rates.

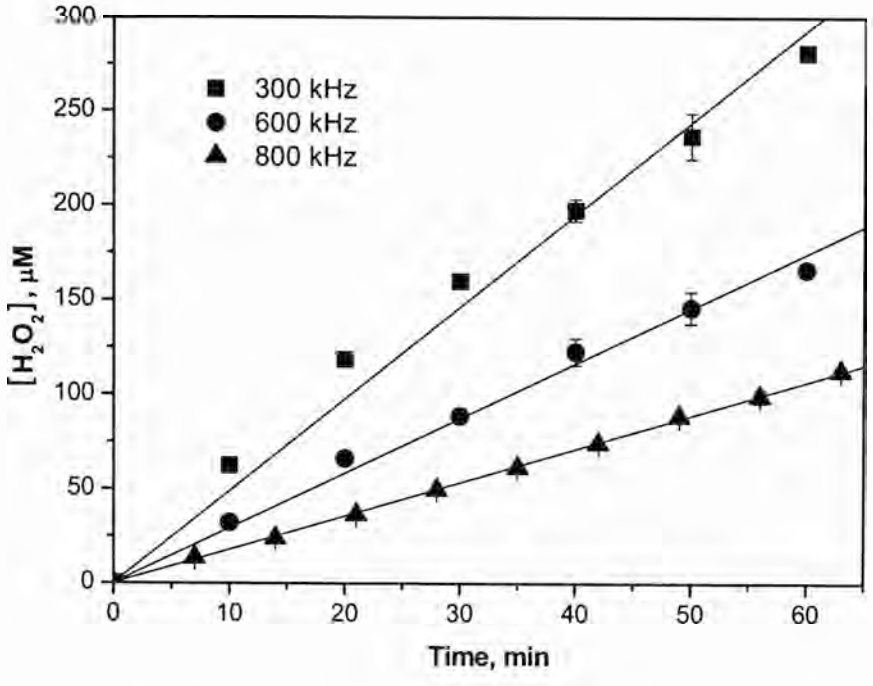

Figure 4.11 Hydrogen peroxide formation at different frequencies under oxygen saturated solutions for 30W (acoustic power) and pH 3.5.

4.3.5.2 Sonolytic degradation of formic acid under oxygen saturated solutions

As seen from results presented in Figure 4.12, sonolytic degradation of formic acid under oxygen saturated solutions followed pseudo-first order kinetics. The pseudo-first order rate constant observed at 300 kHz (0.073 min^{-1}) was higher than that observed at 600 kHz (0.038 min^{-1}) and 800 kHz (0.041 min^{-1}). The observed variation in formic acid degradation at these frequencies is consistent with the effect of frequency on hydrogen peroxide formation. The maximum decomposition rate achieved at low frequency (300 kHz) can be explained by the frequency effect described in section 4.4.2. From our results, it is evident that frequencies of around 300 kHz are optimal for formic acid degradation under oxygen saturated solutions.

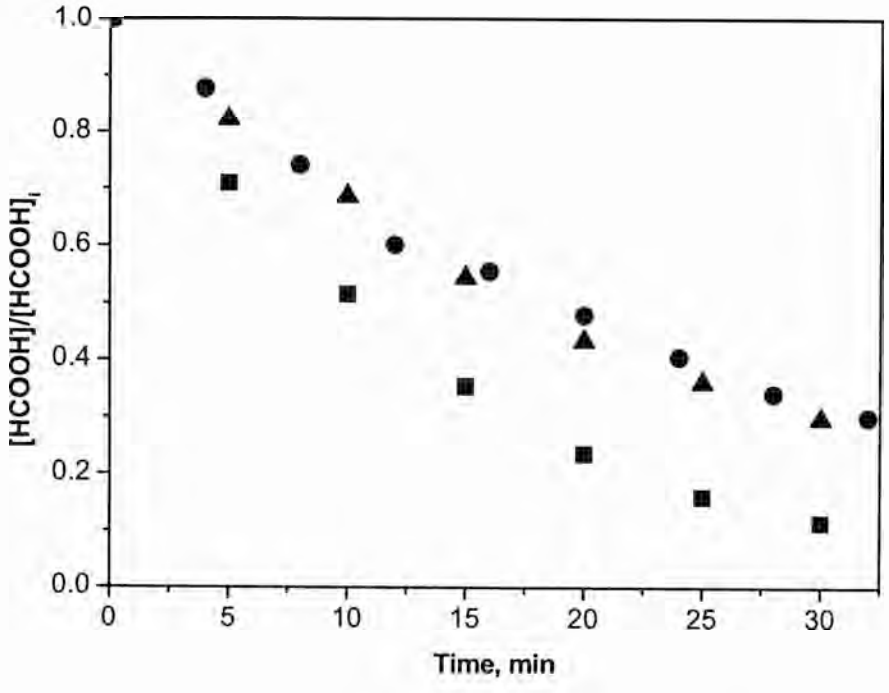

Figure 4.12 Effect of frequency on sonlytic degradation of formic acid under oxygen saturated solutions (▲: 800kHz, ● : 600 kHz, ■ : 300 kHz).

4.3.6 Hydrogen peroxide formation and formic acid degradation under air saturated solutions

4.3.6.1 Formation of hydrogen peroxide by ultrasonic irradiation

4.3.6.1.1 Effect of frequency

The hydrogen peroxide formation rates under air saturated obtained at 300, 600 and 800 kHz are shown in Figure 4.13. The kinetics of hydrogen peroxide formation follows zero order kinetics with the observed rates varying from1.56 μM/min at 800 kHz to 4.31 μM/min at 300 kHz. Comparing all the conditions investigated, the highest hydrogen peroxide formation rate was achieved under air saturated solutions at 300 kHz.

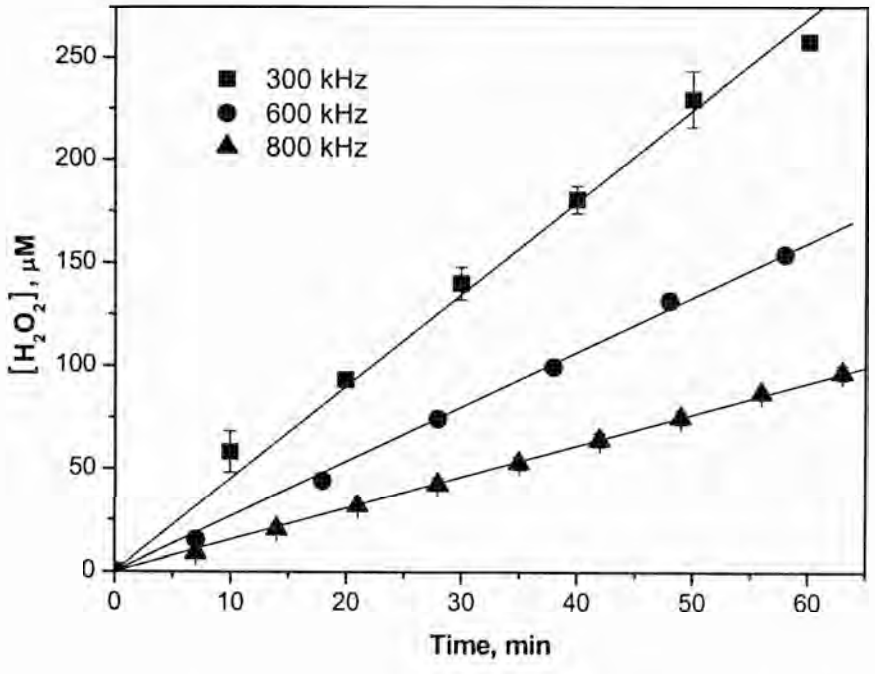

Figure 4.13 Hydrogen peroxide formation at different frequencies under air saturated solutions.

Hydrogen peroxide formation by ultrasonic irradiation under air, argon and oxygen saturated solutions over 90 mins of sonication are shown in Figure 4.14. As shown, nonlinearity occurs after 60 mins under air saturated solution in contrast to the constant generation rate observed in argon and oxygen saturated system.

A variety of additional reactions are to be expected in the presence of air, particularly with regard to the generation of nitrogen-based radicals (Misik and Riesz, 1996, Didenko *et al.*, 1999, Supeno and Kruus, 2000, Nikitenko *et al.*, 2004); i.e.,

$$N_2 + O_2 \rightarrow 2NO \quad (14)$$

$$N_2 + 2O_2 \rightarrow 2NO_2 \quad (15)$$

$$NO + OH\bullet \rightarrow HNO_2 \quad (16)$$

$$NO_2 + OH\bullet \rightarrow HNO_3 \quad (17)$$

$$HNO_2 + H_2O_2 \rightarrow HNO_3 + H_2O \quad (18)$$

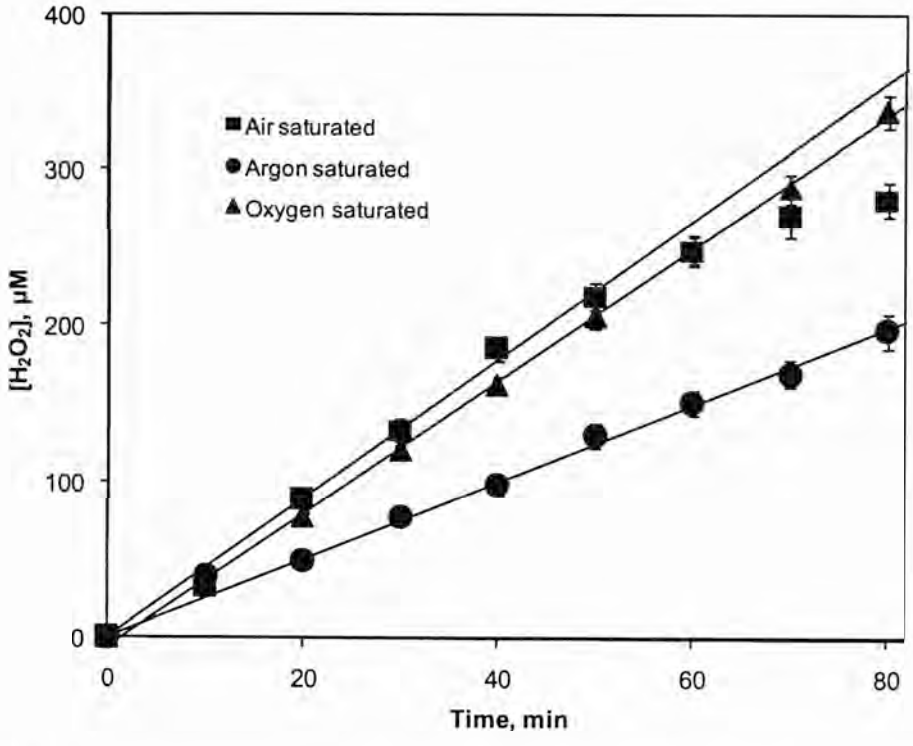

Figure 4.14 Hydrogen peroxide formation for different dissolved gases. Conditions : 300 kHz and pH 3.5.

Nitrogen present in the air may enter the cavitation bubbles and be transformed to oxygenated nitrogen species such as nitrous oxide, nitric oxide and nitrous acid. The latter species may react with hydrogen peroxide that is also formed in the sonolysis process to yield nitrate (reaction 18).

Mead *et al.*(1976) investigated the formation of nitrogen species (nitrate and nitrite) on sonolysis of air saturated aqueous media and obtained initial formation rates of 2.2×10^{-5} M/min for nitrite and 6.0×10^{-6} M/min for nitrate using 447 kHz irradiation. Petrier *et al.* (1999) also investigated the formation of nitrogen containing compounds using 500 kHz ultrasound under air-saturated solutions. Nitrate concentrations were found to increase linearly with time while nitrite concentrations initially increased then decreased after 100 mins.

In all our experiments, a stock solution of 0.1 M nitric acid was used for setting the initial solution pH. As shown in Figure 4.15, any ultrasonically generated nitrate thus appears in addition to the nitrate already present. Studies were also undertaken using a stock solution of 0.1 M hydrochloric acid for setting the initial pH in order to assess the possible interaction between nitrate and H_2O_2 and the processes responsible for nitrate generation. As shown in Figure 4.15, the generation rates of nitrate are almost identical in both electrolytes suggesting that there is little interaction between hydrogen peroxide and nitrate and indicating that generation paths are essentially independent of each other. As nitrate is not formed in the presence of nitrogen alone, it thus appears that both oxygen and nitrogen must be present in significant quantities for nitrate generation to occur.

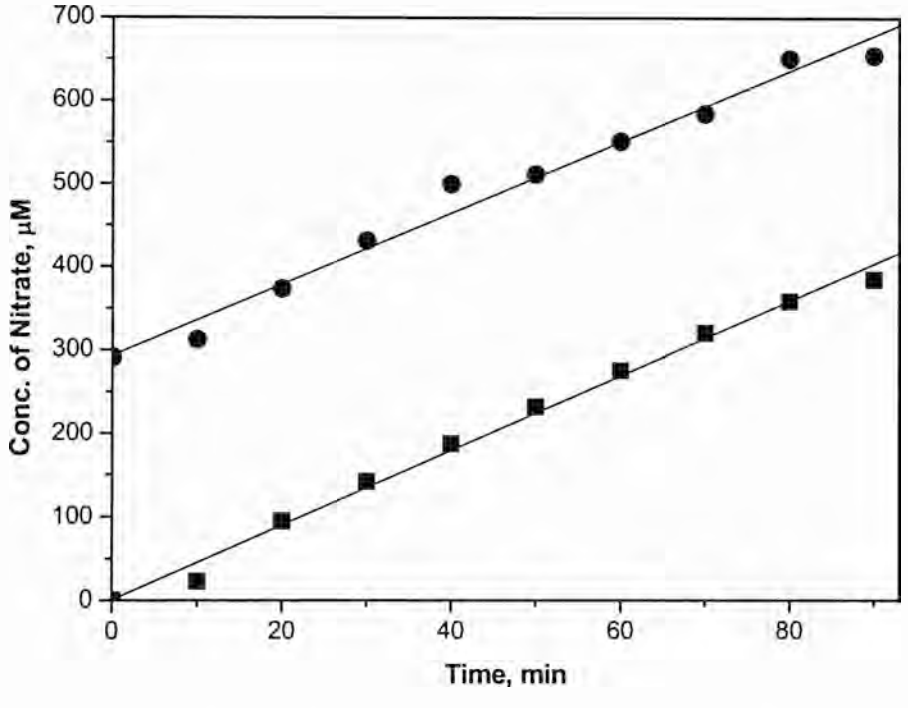

Figure 4.15 Nitrate formation profile with different pH media saturated with air at 300 kHz (■ : pH by hydrochloric acid, ● : pH by nitric acid).

4.3.6.2 Sonolytic degradation under air saturated solutions

Results of studies of formic acid degradation under air saturated solutions are shown in Figure 4.16. In the air saturated system, the formic acid degradation rate is lower than observed in argon and oxygen saturated systems at all frequencies examined. It is also observed that the reaction kinetics do not follow the pseudo first order kinetics in air saturated systems (as previously observed in the other gaseous systems) with the rate of degradation apparently decreasing over time. While the rate constant decreases over time, initial decomposition rate can be determined and are 0.018 min^{-1} at 300 kHz, 0.020 min^{-1} at 600 kHz, 0.017 min^{-1} at 800 kHz. The decreasing rate of formic acid degradation that is observed over time suggests that scavenging of hydroxyl radical by nitrogen species occurs, thereby reducing formic acid degradation rates.

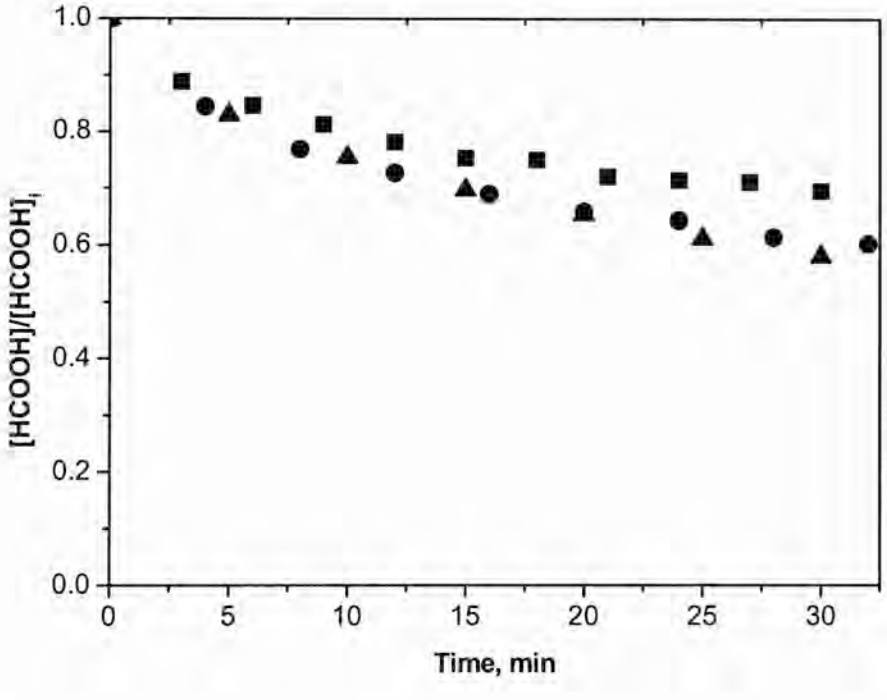

Figure 4.16 Formic acid degradation at three frequencies under air saturated solutions (▲ : 600kHz, ● : 300 kHz, ■ : 800 kHz).

4.4 Conclusions

Hydrogen peroxide formation by ultrasonic irradiation has been investigated at three frequencies (300, 600, and 800 kHz) and in different dissolved gases (argon, oxygen, nitrogen, and air) at an initial pH 3.5. A summary of the rates of hydrogen peroxide production as a function of experimental conditions is shown in Table 4.1. At 600 kHz and 800 kHz, hydrogen peroxide formation rates follow the expected order of effect of physical properties of dissolved gases (Argon > Oxygen > Air > Nitrogen). The maximum hydrogen peroxide formation rate (4.5 μM/min) was achieved under oxygen saturated solution at a frequency of 300 kHz. The pH of the reaction medium did not affect the hydrogen peroxide formation rate.

The mechanism of hydrogen peroxide formation was also examined. Recombination of hydroxyl radicals is the only source for hydrogen peroxide formation in argon and nitrogen saturated systems while, in the presence of oxygen, more hydrogen peroxide production might be expected due to the formation and subsequent recombination of hydroperoxy radicals. The minimal effect of hydrogen peroxide addition on hydrogen peroxide formation rate suggests that the presence of hydrogen peroxide in the bulk solution resulted from diffusion of hydrogen peroxide from bubble interfaces where it was formed by recombination of free radicals. Free radicals (hydroxyl, hydrogen atom, and hydroperoxy radicals) may diffuse to some extent into the bulk solution leading to reactions with organic compound present in the bulk though it is expected that the extent of diffusion will be limited due to the high reactivity of these species.

Formic acid degradation and its degradation mechanism by ultrasonic irradiation was also investigated at three frequencies and dissolved gases. Formic acid degradation followed pseudo-first order kinetics under all conditions examined except in air saturated systems. Optimal frequencies with respect to formic acid degradation were determined to be 300 kHz under oxygen (14.6 nM/min) and 600 kHz under argon (17.4 nM/min). The effect of the initial formic acid concentration was examined at 600 kHz under argon saturated solutions. Rates of formic acid degradation decreased with increase in the initial formic acid concentration. Effects of hydroxyl radical scavengers

(t-butanol and phenol) on formic acid degradation suggest that formic acid degradation by ultrasonic irradiation occurs principally in the interfacial zone.

Chapter 5

Kinetic Modeling of Hydrogen Peroxide Formation and Formic Acid Degradation by Ultrasonic Irradiation

5.1 Introduction

In chapter 4, we discussed the mechanism of hydrogen peroxide generation and formic acid degradation by ultrasonic irradiation under various conditions. In this chapter, a mathematical kinetic model is developed based on the mechanism presented in chapter 4 to describe hydrogen peroxide formation and formic acid degradation on ultrasonic irradiation. Free radical reactions which occur on ultrasonic irradiation are proposed and validated by comparing with the experimental results presented in chapter 4. The mathematical model is used as a vehicle to assess the veracity of possible transformations occurring under a variety of reaction conditions with particular attention given to the effect of the different gases used (i.e. argon, oxygen and nitrogen).

5.2 *Results and Discussion*

5.2.1 Theoretical basis of the mathematical model

The mechanism of hydrogen peroxide formation and formic acid degradation was discussed in detail in chapter 4. In this section, we summarize the important points involved which forms the basis of the mathematical model described in this chapter. These points are as follows:

1) In sonochemistry, the use of hydrophobic and hydrophilic hydroxyl radical scavengers has confirmed the presence of three reaction zones (see Figure 2.2 in Chapter 2): bubble interior, bubble/water interface and bulk solution (Hart and Henglein, 1985, Suslick and Hammerton, 1986). Hydrophobic (volatile) compounds are mainly decomposed by pyrolysis inside the bubble, while hydrophobic (non-volatile) and hydrophilic compounds decay due to their reaction with hydroxyl radicals at the interface and/or bulk solution (Henglein and Kormann, 1985, Petrier et al., 1998).
2) Hydroxyl radicals are produced by decomposition of water in the bubble but rapidly diffuse to the interface. Hydrogen peroxide is formed at the interface by recombination of hydroxyl radicals and subsequently diffuses into the bulk solution. This explanation is consistent with our experimental data which show significant generation of hydrogen peroxide in the bulk solution under all conditions investigated (Table 4.1). Diffusion of a small fraction of hydroxyl radicals from the interface to the bulk solution also occurs.
3) Formic acid degradation takes place principally due to its reaction with hydroxyl radicals at the interface though a portion may be degraded in bulk solution given its

hydrophilic nature. Formic acid degradation at the interface occurs as results of its diffusion from the bulk solution.

4) At a particular frequency, the rate of sonolytic decomposition of water to yield hydrogen and hydroxyl radicals depends on the physical properties of the background gas. As explained in chapter 4, the rate constant for this reaction should be in the order:

$$k_{Ar} > k_{O2} > k_{N2}$$

5) With increase in frequency, the available energy decreases, hence the rate constant for sonolytic decomposition of water decreases with increase in frequency.

6) The diffusion rate constant of radicals (hydroxyl and hydrogen atom) and hydrogen peroxide is proportional to the bubble collapse time. The shorter the bubble collapse time, the faster will be the rate of diffusion of radicals from the interface to the bulk solution.

7) The bubble collapse time decreases with increase in frequency (Tables 4.4 and 4.5); hence the diffusion rate constant of radicals from the interface will increase with increase in frequency for a particular gas.

8) The rate constant for diffusion of free radicals increases with increase in solubility of the gas; hence the diffusion rate of free radicals would be expected to follow the order:

$$k_{Ar} \approx k_{O2} > k_{N2}$$

9) The observation that added hydrogen peroxide did not affect the hydrogen peroxide formation rate suggests that the rate constant for diffusion of hydrogen peroxide from bulk solution to the interface should be small.

A mathematical model that accounts for these issues with regard to hydrogen peroxide formation and formic acid degradation is shown in Tables 5.1 and 5.2. Reaction 1 shows the sonolytic decomposition of water vapour present in the bubble resulting in formation of hydrogen atom and hydroxyl radicals. These decomposition reactions occur in the gas phase. Reaction products such as hydroxyl and hydrogen atom radicals migrate to the interface of the bubble where they subsequently react in the aqueous phase (Zhang *et al.*, 2007). However, hydrogen peroxide formed by the recombination of hydroxyl radicals (and hydroperoxyl radicals in the case where oxygen is present) cannot be stable at the high temperatures and pressures typical of the bubble interior. Thus, we assume that hydrogen peroxide formation occurs in the cooler region where all radical reactions can be considered as a bulk solution reactions with rate constants similar to those reported at ambient temperature and pressure.

At the interface, two reaction mechanisms may be of importance. First, pyrolytic decomposition may occur at the hotter interface close to the bubble interior. This mechanism would be expected to be dominant at the higher concentrations of organics. The average temperature at the interface is reported to be about 800 K (Kotronarou *et al.*, 1991). In this case, temperature would be expected to influence the rate of radical reactions. In this case, all reactions can be considered to occur in the gas phase and, in this case, temperature effects on rate constants can be estimated using the Arrhenius equation. Second, hydroxyl radical reactions may occur at the cooler interface (< 439 K, Kotronarou *et al.*, 1991, Hoffmann *et al.*, 1996) close to the bulk solution. In this region, hydroxyl radicals would be present in aqueous form and may be considered to react with formic acid in aqueous solution. While there may well be a significant temperature gradient at the interface (Adewuyi, 2001), we assume for the purposes of this study that the bulk of the reaction occurs at the outer face of the interface where temperature and pressure is close to that in bulk solution. This simplification is likely to be reasonable for solutes present at low concentrations where the rate of accumulation at the interface is relatively slow.

The hydrogen and hydroxyl radicals so formed quickly diffuse to the interface. Given that the bubble lifetime (< 1 μsec) is very short, we have assumed that the rate for diffusion of the radicals to the interface is very fast. The rate constant for reaction 1

depends on the physical properties of the background gas and the frequency used and was determined based on best-fit model results. Hydrogen gas and hydrogen peroxide are formed by recombination of hydrogen atom and hydroxyl radicals respectively (reactions 2 and 3). Reaction 4 shows the recombination of hydroxyl radicals and hydrogen atoms resulting in the formation of water. Hydrogen atoms also react with hydrogen peroxide and oxygen (if present) to yield hydroxyl radicals (reaction 5) and hydroperoxyl radical respectively (reaction 6). Hydroxyl radicals also react with hydrogen peroxide to yield hydroperoxyl radicals (reaction 7). The hydroperoxyl radicals formed in reaction 6 and 7 may scavenge hydroxyl radicals (reaction 8) and may also produce hydrogen peroxide by recombination (reaction 9). The rate constants for reactions 2-9 used are the same as those reported in the literature. Reactions 10 to 13 represent diffusion of free rascals and hydrogen peroxide from the interface to bulk solution. While the rate constants for these reactions are unknown, they are strongly influenced by the rate of bubble collapse. The higher the rate of bubble collapse, the faster will be the rate of diffusion. Reactions 14-21 represent all free radical reactions that are considered to occur in bulk solution (and are the same as reactions 2-9). Since no affect of added hydrogen peroxide was observed on the hydrogen peroxide formation rate (Figure 4.2 in Chapter 4), the rate of diffusion of hydrogen peroxide from bulk solution to the interface should be small. Hence we have neglected this reaction in the mathematical model.

The degradation of formic acid in bulk solution takes place due to a series of reactions (reactions 22-25) as shown in Table 5.2. The reaction between formic acid/formate and hydroxyl radicals is well established with the reported rate constants varying in the range of 10^8 to 10^9 (Flyunt *et al.*, 2001, Kwan and Voelker, 2002, Duesterberg *et al.*, 2006). Formic acid/formate ion reacts with hydroxyl radicals, resulting in generation of the carboxyl radical, $COO^{\bullet -}$, and water (reaction 22) (Allen, 1961, Buxton and Sellers, 1973, Staehelin and Hoigne, 1985, Flyunt *et al.*, 2001). The rate constant for reaction 22 is a composite value at pH 3.5 and was calculated using equation (13) presented in Chapter 4. In addition to the disproportionation reaction (reaction 23), carboxyl radicals also react with oxygen (reaction 25). As explained in Chapter 4, formic acid/formate is also expected to be degraded principally by hydroxyl radicals at the bubble interface with formic acid present in the interface due to its diffusion from bulk solution (reaction

26). The rate constant for this reaction is determined based on best-fit model results. A similar set of reactions is considered to occur between formic acid and hydroxyl radicals at the interface (reaction 27 to 30) as shown for possible reaction in bulk solution (reactions 22 to 25). The rate constants for reactions 22-25 and 27-30 are the same as those reported in the literature. In the following sections, we discuss the kinetic model for each background gases in detail with the aim of determining the important reactions involved in hydrogen peroxide formation and formic acid degradation.

Table 5.1 Summary of reactions producing free radicals and hydrogen peroxide on ultrasonic irradiation.

No	Reaction	Rate constant ($M^{-1} s^{-1}$)	reference
Reactions occurring in bubble			
1	$H_2O \rightarrow \cdot OH + \cdot H \rightarrow \cdot OH(i) + \cdot H(i)$	Depends on frequency and background gas	In this study
Reactions occurring at interface			
2	$\cdot OH(i) + \cdot OH(i) \rightarrow H_2O_2(i)$	5.2×10^{9}	Buxton *et al.*, 1988
3	$\cdot H(i) + \cdot H(i) \rightarrow H_2$	7.8×10^{9}	Buxton *et al.*, 1988
4	$\cdot OH(i) + \cdot H(i) \rightarrow H_2O$	7.0×10^{9}	Buxton *et al.*, 1988
5	$H_2O_2(i) + \cdot H(i) \rightarrow \cdot OH(i) + H_2O$	9.0×10^{7}	Buxton *et al.*, 1988
6	$O_2 + \cdot H(i) \rightarrow \cdot HO_2(i)$	2.1×10^{10}	Buxton *et al.*, 1988
7	$\cdot OH(i) + H_2O_2(i) \rightarrow \cdot HO_2(i) + H_2O$	3.3×10^{7}	Buxton *et al.*, 1988
8	$\cdot OH(i) + \cdot HO_2(i) \rightarrow H_2O + O_2$	6.6×10^{9}	Buxton *et al.*, 1988
9	$\cdot HO_2(i) + \cdot HO_2(i) \rightarrow H_2O_2 + O_2$	2.3×10^{6}	Kwan and Voelker, 2002
10	$H_2O_2(i) \rightarrow H_2O_2(b)$	Depends on frequency and background gas	This study
11	$\cdot OH(i) \rightarrow \cdot OH(b)$	Depends on frequency and background gas	This study
12	$\cdot H(i) \rightarrow \cdot H(b)$	Depends on frequency and background gas	This study
13	$\cdot HO_2(i) \rightarrow \cdot HO_2(b)$	Depends on frequency and background gas	This study
Reactions occurring in bulk solution			
14	$\cdot OH(b) + \cdot OH(b) \rightarrow H_2O_2(b)$	5.2×10^{9}	Buxton *et al.*, 1988
15	$\cdot H(b) + \cdot H(b) \rightarrow H_2(b)$	7.8×10^{9}	Buxton *et al.*, 1988

16	$\bullet OH(b) + \bullet H(b) \rightarrow H_2O$	7.0×10^{9}	Buxton *et al.*, 1988
17	$\bullet OH(b) + H_2O_2(b) \rightarrow \bullet HO_2(b) + H_2O$	3.3×10^{7}	Buxton *et al.*, 1988
18	$H_2O_2(b) + \bullet H(b) \rightarrow \bullet OH(b) + H_2O$	9.0×10^{7}	Buxton *et al.*, 1988
19	$\bullet HO_2(b) + \bullet HO_2(b) \rightarrow H_2O_2(b) + O_2$	2.3×10^{6}	Kwan and Voelker, 2002
20	$\bullet OH(b) + \bullet HO_2(b) \rightarrow H_2O + O_2$	6.6×10^{9}	Buxton *et al.*, 1988
21	$O_2 + \bullet H(b) \rightarrow \bullet HO_2(b)$	2.1×10^{10}	Buxton *et al.*, 1988

Table 5.2 Reaction showing formic acid degradation by ultrasonic irradiation.

No	Reaction	Rate constant ($M^{-1} s^{-1}$)	reference
Reactions occurring in bulk solution			
22	$HCOOH(b) + \bullet OH(b) \rightarrow COO^{\bullet-}(b) + H_2O + H^+$	1.2×10^{9}	This study
23	$COO^{\bullet-}(b) + COO^{\bullet-}(b) \rightarrow Int(b)$	1.4×10^{9}	Flyunt *et al.*, 2001
24	$Int(b) + H^+ \rightarrow CO_2 + HCOOH(b)$	1.0×10^{7}	Flyunt *et al.*, 2001
25	$COO^{\bullet-}(b) + O_2 + H+ \rightarrow CO_2 + \bullet HO_2(b)$	4.2×10^{9}	Flyunt *et al.*, 2001
26	$HCOOH(b) \rightarrow HCOOH(i)$	Depends on frequency and background gas	In this study
Reactions occurring at interface			
27	$HCOOH(i) + \bullet OH(i) \rightarrow COO^{\bullet-}(i) + H_2O + H^+$	1.2×10^{9}	This study
28	$COO^{\bullet-}(i) + COO^{\bullet-}(i) \rightarrow Int(i)$	1.4×10^{9}	Flyunt *et al.*, 2001
29	$Int(i) + H^+ \rightarrow CO_2 + HCOOH(i)$	1.0×10^{7}	Flyunt *et al.*, 2001
30	$COO^{\bullet-}(i) + O_2 + H+ \rightarrow CO_2 + \bullet HO_2(i)$	4.2×10^{9}	Flyunt *et al.*, 2001

5.2.2 Kinetic modeling of hydrogen peroxide formation and formic acid degradation under argon saturated solutions

The kinetic model with rate constants found to be optimal under argon saturated solutions is shown in Table 5.3. Under argon saturation, the concentration of hydroperoxyl radicals generated via oxidation of hydrogen peroxide by hydroxyl radicals (reaction 7, Table 5.1) is too small to contribute significantly to hydrogen peroxide production. Thus, in the simplified model presented in Table 5.1, we have neglected the reactions involving hydroperoxyl radicals.

Under argon saturated solutions, water decomposition (reaction 1) and diffusion of hydrogen peroxide from the bubble interface to bulk solution (reaction 10) are the dominant reactions controlling hydrogen peroxide formation rate. The rate constants for these two reactions were determined based on best-fit model results.

Formic acid degradation is influenced principally by the water decomposition reaction (reaction 1), diffusion of hydroxyl radicals (reaction 11) from the bubble interface to bulk solution and diffusion of formic acid (reaction 26) from bulk solution to the bubble interface. The rate constant for diffusion of formic acid from bulk solution to the interface was determined based on best-fit model results. As shown in Table 5.3, the rate constant for diffusion of formic acid from bulk solution to the interface is small which is in accordance with its hydrophilic characteristics. Also, slow diffusion of formic acid to the interface is consistent with our experimental results which show no effect of formic acid addition on hydrogen peroxide generation. As shown in Table 5.3, the rate constant for diffusion of formic acid from bulk solution to the interface is affected by frequency. Although the exact reason for this variation is uncertain, it may possibly be due to the impact of frequency on the bubble collapse time. The rate constant for diffusion of hydroxyl radicals from the bubble interface to bulk solution is based on best-fit model results and controls the formic acid degradation occurring in bulk solution. The model results for formic acid degradation are shown in Figure 5.2. The impact of hydrogen atom radical diffusion on hydrogen peroxide formation and formic acid degradation was found to negligible and thus the rate constant for this reaction cannot be determined based on our experimental data.

Table 5.3 Simulated values of rate constants for hydrogen peroxide formation and formic acid degradation under argon saturated solution.

No	Reaction	Rate constant	Reference
1	$H_2O \rightarrow \bullet OH + \bullet H \rightarrow \bullet OH(i) + \bullet H(i)$	300 kHz : 6.2×10^{-7} sec^{-1} 600 kHz : 6.0×10^{-7} sec^{-1} 800 kHz : 1.8×10^{-7} sec^{-1}	This study
2	$\bullet OH(i) + \bullet OH(i) \rightarrow H_2O_2(i)$	5.2×10^{9} M^{-1} s^{-1}	Buxton *et al.*, 1988
3	$\bullet H(i) + \bullet H(i) \rightarrow H_2$	7.8×10^{9} M^{-1} s^{-1}	Buxton *et al.*, 1988
4	$\bullet OH(i) + \bullet H(i) \rightarrow H_2O$	7.0×10^{9} M^{-1} s^{-1}	Buxton *et al.*, 1988

5	$H_2O_2(i) + \bullet H(i) \rightarrow \bullet OH(i) + H_2O$	$9.0\times10^{7}\ M^{-1}\ s^{-1}$	Buxton *et al.*, 1988
7	$\bullet OH(b) + H_2O_2(b) \rightarrow \bullet HO_2(i) + H_2O$	$3.3\times10^{7}\ M^{-1}\ s^{-1}$	Buxton *et al.*, 1988
10	$H_2O_2(i) \rightarrow H_2O_2(b)$	300 kHz : $1.8\times10^{-2}\ sec^{-1}$ 600 kHz : $2.0\times10^{-2}\ sec^{-1}$ 800 kHz : $2.5\times10^{-2}\ sec^{-1}$	This study
11	$\bullet OH(i) \rightarrow \bullet OH(b)$	300 kHz : $2.0\times10^{-3}\ sec^{-1}$ 600 kHz : $1.6\times10^{-2}\ sec^{-1}$ 800 kHz : $1.7\times10^{-2}\ sec^{-1}$	This study
14	$\bullet OH(b) + \bullet OH(b) \rightarrow H_2O_2(b)$	$5.2\times10^{9}\ M^{-1}\ s^{-1}$	Buxton *et al.*, 1988
15	$\bullet H(b) + \bullet H(b) \rightarrow H_2(b)$	$7.8\times10^{9}\ M^{-1}\ s^{-1}$	Buxton *et al.*, 1988
16	$\bullet OH(b) + \bullet H(b) \rightarrow H_2O$	$7.0\times10^{9}\ M^{-1}\ s^{-1}$	Buxton *et al.*, 1988
17	$\bullet OH(b) + H_2O_2(b) \rightarrow \bullet HO_2(b) + H_2O$	$3.3\times10^{7}\ M^{-1}\ s^{-1}$	Buxton *et al.*, 1988
18	$H_2O_2(b) + \bullet H(b) \rightarrow \bullet OH(b) + H_2O$	$9.0\times10^{7}\ M^{-1}\ s^{-1}$	Buxton *et al.*, 1988
22	$HCOOH(b) + \bullet OH(b) \rightarrow COO\bullet^{-}(b) + H_2O$	$1.2\times10^{9}\ M^{-1}\ s^{-1}$	Duesterberg *et al.*, 2006
23	$COO\bullet^{-}(b) + COO\bullet^{-}(b) \rightarrow int(b)$	$1.4\times10^{9}\ M^{-1}\ s^{-1}$	Flyunt *et al.*, 2001
24	$Int(b) + H^{+} \rightarrow CO_2 + HCOOH(b)$	$1.0\times10^{7}\ M^{-1}\ s^{-1}$	Flyunt *et al.*, 2001
26	$HCOOH(b) \rightarrow HCOOH(i)$	300 kHz : $8.1\times10^{-4}\ sec^{-1}$ 600 kHz : $7.8\times10^{-4}\ sec^{-1}$ 800 kHz : $3.8\times10^{-4}\ sec^{-1}$	This study
27	$HCOOH(i) + \bullet OH(i) \rightarrow COO\bullet^{-} + H_2O + H^{+}$	$1.2\times10^{9}\ M^{-1}\ s^{-1}$	Duesterberg *et al.*, 2006
28	$COO\bullet^{-} + COO\bullet^{-} \rightarrow int$	$1.4\times10^{9}\ M^{-1}\ s^{-1}$	Flyunt *et al.*, 2001
29	$int + H^{+} \rightarrow CO_2 + HCOOH(i)$	$1.0\times10^{7}\ M^{-1}\ s^{-1}$	Flyunt *et al.*, 2001

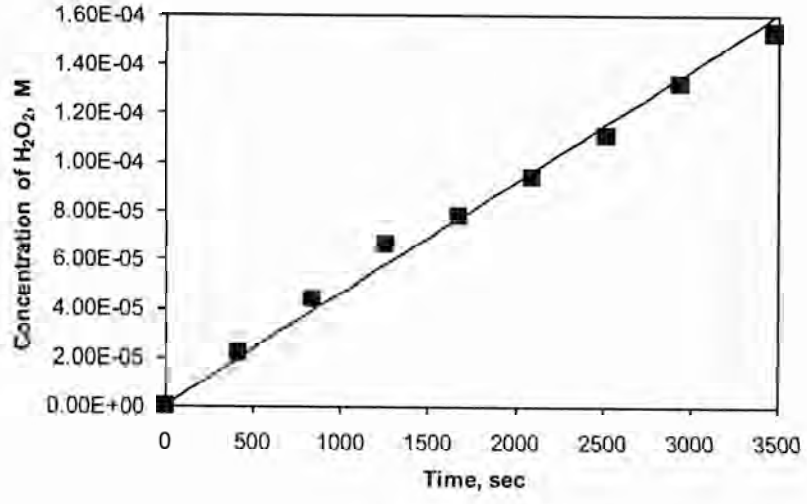

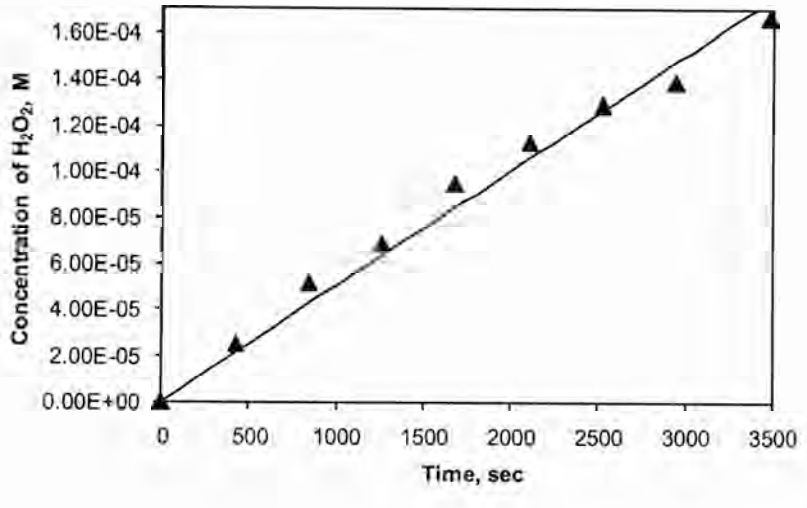

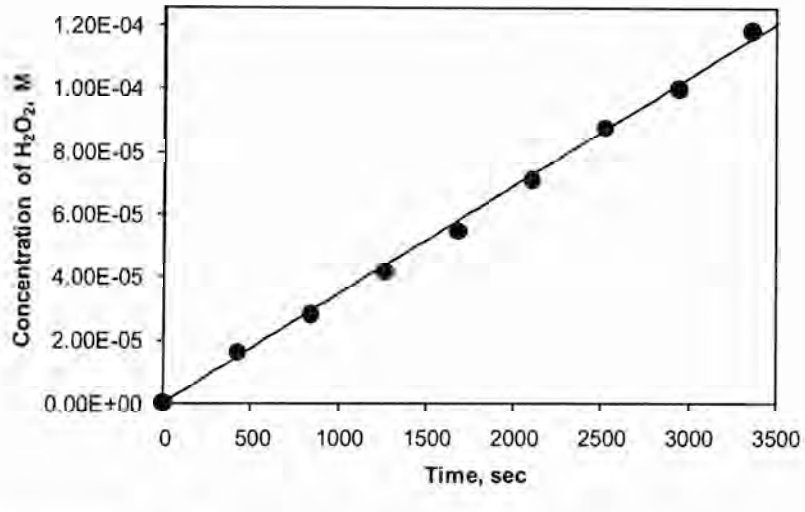

Figure 5.1 Hydrogen peroxide formation under argon saturated solutions. Closed points and solid line represent the experimental and model data respectively (■: 300 kHz, ▲: 600 kHz, ●: 800 kHz).

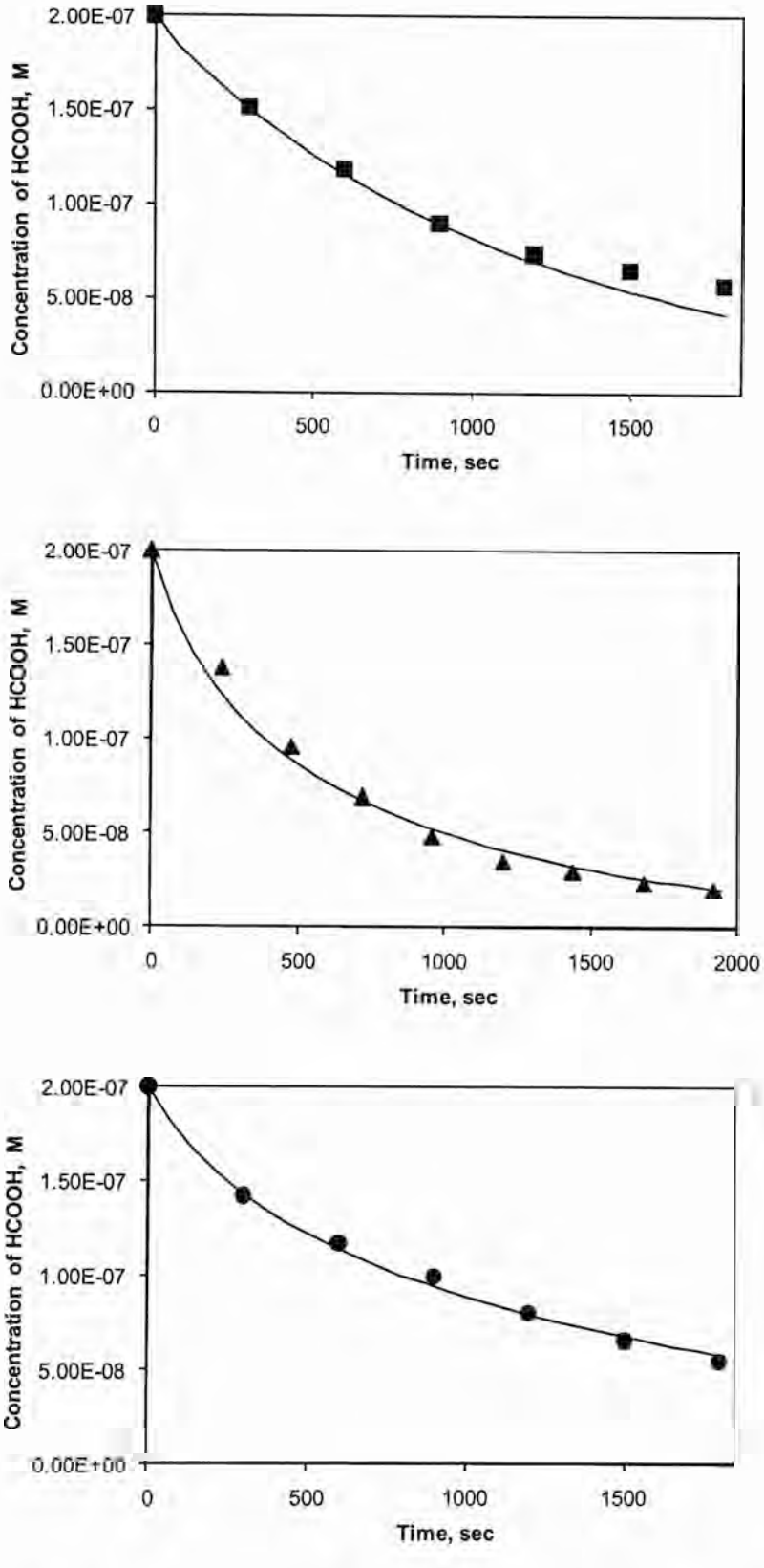

Figure 5.2 Formic acid degradation under argon saturated solutions. Closed points and solid line represent the experimental and model results respectively (■: 300 kHz, ▲: 600 kHz, ● : 800 kHz).

The model also predicts the affect of hydrogen peroxide addition on formic acid degradation observed under argon saturated solutions as shown in Figure 5.3. If formic acid degradation occurs in the bulk solution only, the effect of hydrogen peroxide addition on formic acid degradation should be significant due to scavenging of hydroxyl radicals by added hydrogen peroxide. Both experimental and model results however show that the impact on formic acid degradation is small thereby suggesting that most of the formic acid is degraded at the interface.

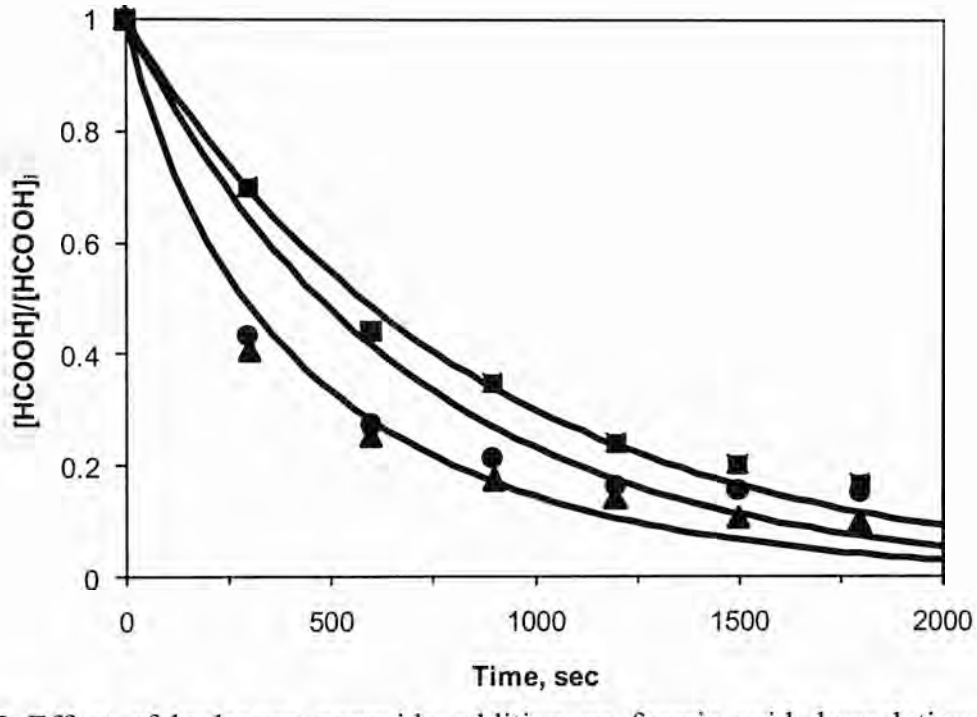

Figure 5.3 Effect of hydrogen peroxide addition on formic acid degradation. Closed points and solid lines represent the experimental and model results respectively. Conditions : 600 kHz, 30W, pH 3.5, argon saturated solutions, and 200nM of HCOOH (■: 500 μM of H_2O_2, ● : 200 μM of H_2O_2 ▲: No addition).

As seen from Figure 5.4, the proposed model also adequately describes the effect of initial concentration of formic acid on its degradation kinetics.

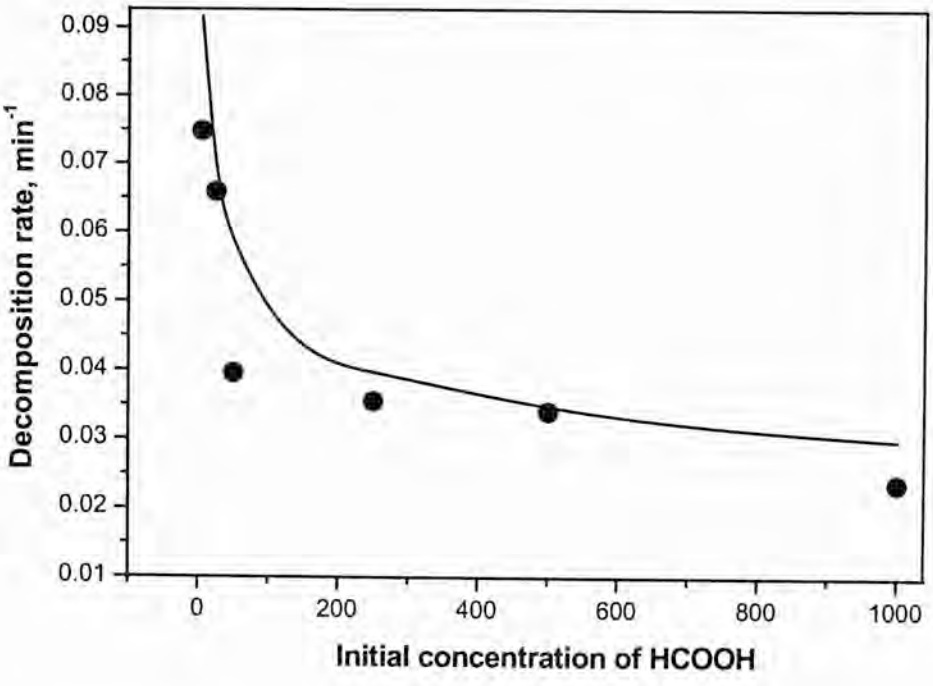

Figure 5.4. Effect on initial concentration of formic acid on formic acid degradation rate. Closed points and solid line represent observed and model predicted decomposition rates respectively.

5.2.3 Kinetic modeling of hydrogen peroxide formation and formic acid degradation under oxygen saturated solutions

Under oxygenated solutions, hydrogen atom radicals react with oxygen to produce hydroperoxyl radicals (reaction 9) (Buxton *et al.*, 1988) at the interface. The hydroperoxyl radicals so formed may disproportionate to form hydrogen peroxide (reaction 9) but may also react with hydroxyl radicals to produce oxygen and water thereby lowering the rate of hydrogen peroxide formation (reaction 8) (Pétrier *et al.*, 1992b). Hydroperoxyl radical-related reactions in the bulk solution are also included (reactions 19, 20, and 21) in the kinetic model under oxygen saturated solution. Recombination of hydroxperoxyl radicals is an additional pathway for hydrogen peroxide formation at the interface as well as in the bulk solution. Also, in the presence of oxygen, carboxyl radicals produced by hydroxylation of formic acid (reactions 25 and 30) are scavenged, yielding carbon dioxide and hydroperoxyl radicals (Flyunt *et al.*, 2001).

Under oxygen saturated solutions, the water decomposition reaction (reaction 1) and diffusion of hydrogen peroxide from the bubble interface to bulk solution are the main reactions controlling hydrogen peroxide formation. The rate constants for both these

reactions are determined based on best-fit model results. The rate constant for reaction 1 was lower under oxygen saturation than in the case of argon saturation which is consistent with the fact that more critical conditions (higher temperature and pressure) exist in the bubble under argon saturated solutions. The reactions used to describe hydrogen peroxide formation and formic acid degradation under oxygen saturated solutions are shown in Tables 5.1 and 5.2. Comparing with the results under oxygen free solutions (i.e., argon or nitrogen saturation), hydroperoxyl radicals appear to play a role in hydrogen peroxide formation. Formic acid degradation is mainly controlled by i) diffusion of formic acid from bulk solution to the bubble interface, and ii) hydroxyl radical diffusion from the interface to the bulk solution. Values of rate constants determined from best fits to the experimental data for hydrogen peroxide formation and formic acid degradation are summarised in Table 5.4. The model fits to experimentally measured hydrogen peroxide and formic acid concentrations as a function of sonolysis time are shown in Figures 5.5 and 5.6 respectively.

Table 5.4: Simulated values of rate constants for reactions under oxygen saturated solutions.

No	Reaction	Rate constants (sec^{-1})
1	$H_2O \rightarrow \bullet OH + \bullet H$	300 kHz : 1.8×10^{-7} 600 kHz : 9.0×10^{-8} 800 kHz : 4.5×10^{-8}
10	$H_2O_2 \rightarrow H_2O_2(b)$	300 kHz : 1.38×10^{-2} 600 kHz : 1.44×10^{-2} 800 kHz : 1.65×10^{-2}
11	$\bullet OH \rightarrow \bullet OH(b)$	300 kHz : 1.0×10^{-2} 600 kHz : 1.6×10^{-2} 800 kHz : 4.0×10^{-2}
14	$\bullet HO_2 \rightarrow \bullet HO_2(b)$	300 kHz : 1.0×10^{-2} 600 kHz : 2.0×10^{-2} 800 kHz : 3.0×10^{-2}
26	$HCOOH(b) \rightarrow HCOOH$	300 kHz : 1.2×10^{-3} 600 kHz : 6.5×10^{-4} 800 kHz : 6.2×10^{-4}

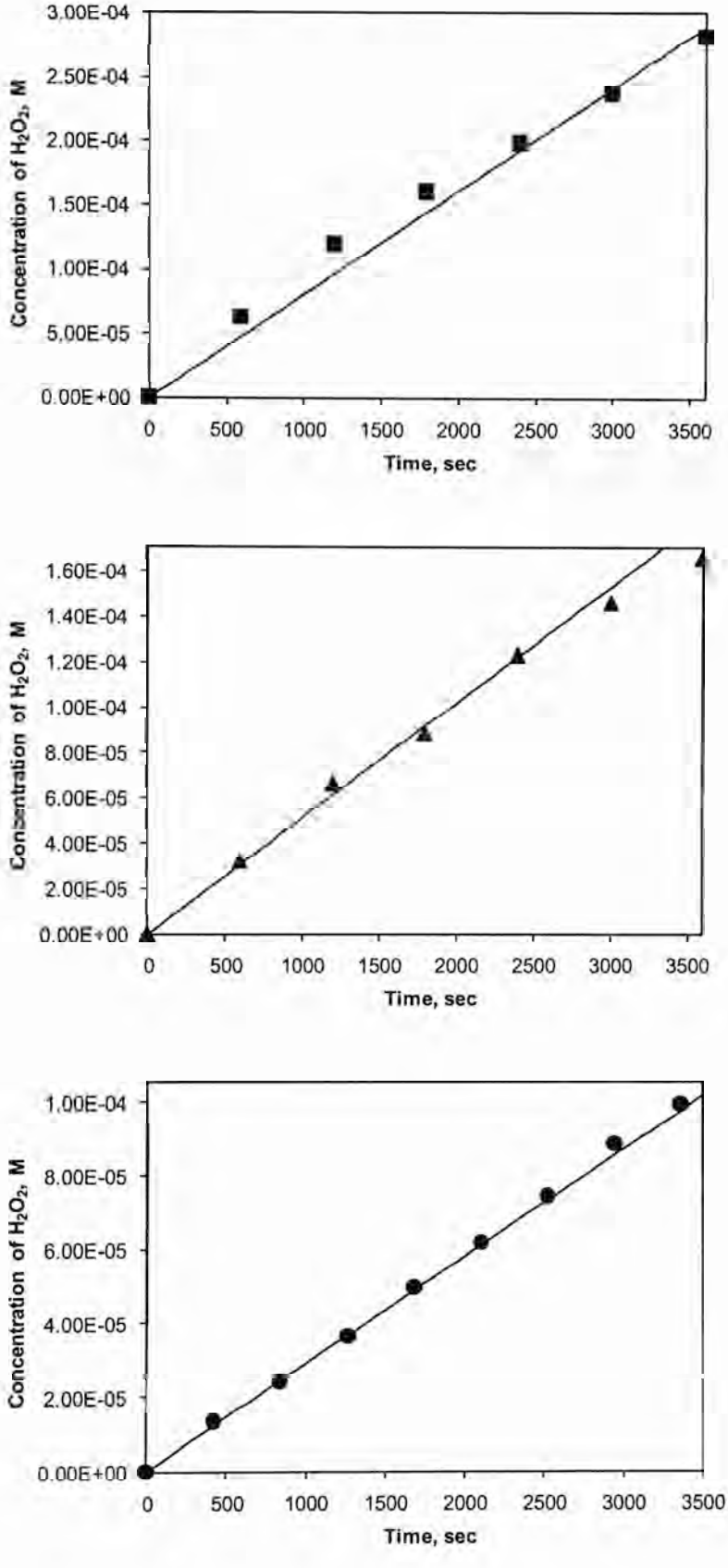

Figure 5.5 Hydrogen peroxide formation under oxygen saturated solutions. Closed point and solid line represent the experimental and model results respectively (■ : 300 kHz, ▲: 600 kHz, ● : 800 kHz).

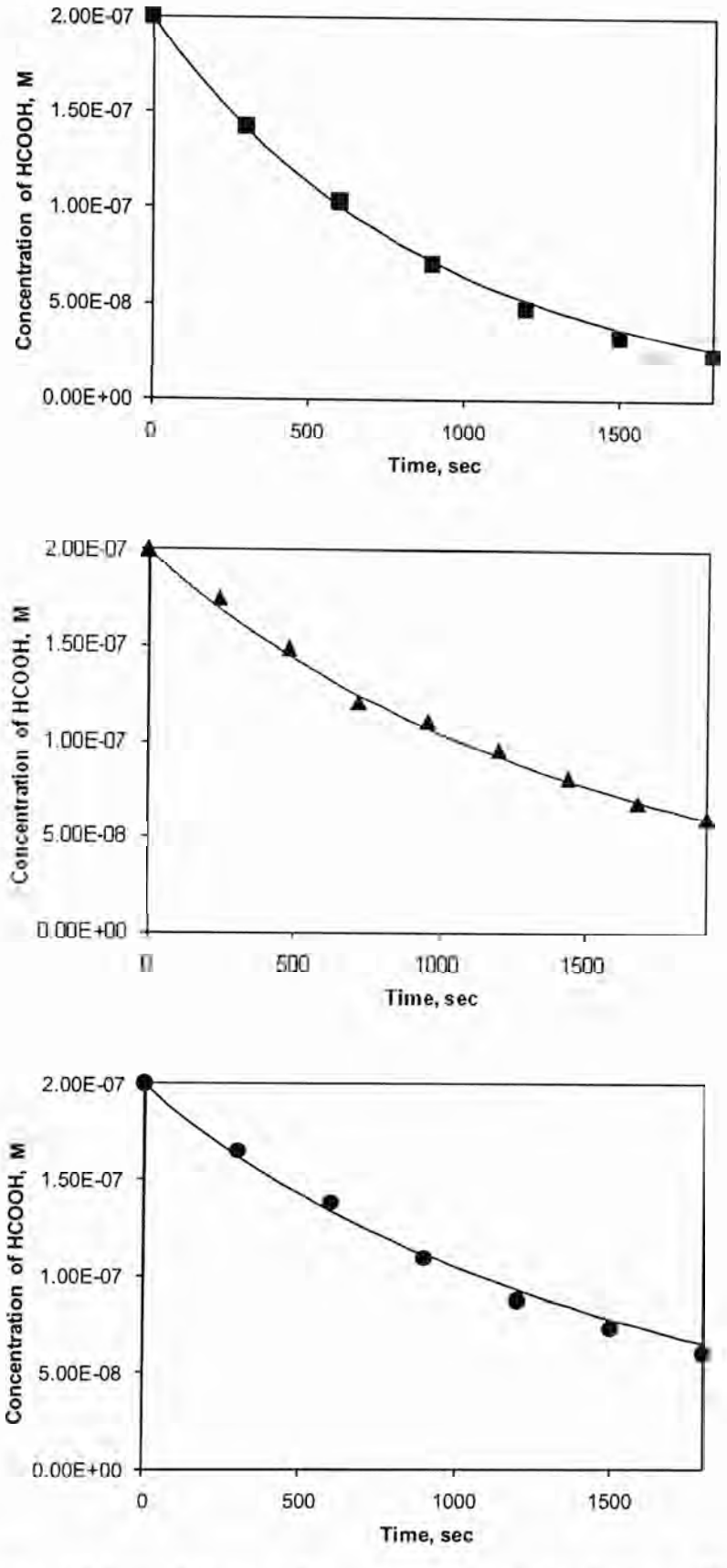

Figure 5.6 Formic acid degradation under oxygen saturated solutions. Closed points and solid lines represent the experimental and model data respectively (■: 300 kHz, ▲: 600 kHz, ● : 800 kHz).

5.2.4 Model prediction of hydrogen peroxide formation by ultrasonic irradiation under nitrogen saturated solutions

The reactions involved in hydrogen peroxide production under nitrogen saturated solutions are assumed to be the same as those used in the case of argon. It should be noted however that, under nitrogen saturated solutions, nitrogen species may be produced in the bubble by pyrolytic decomposition (Wakeford *et al*, 1994, Supeno and Kruus, 2000). For simplicity, however, reactions involving nitrogen species have been ignored. In other words, the rate constant for the water decomposition reaction represents an apparent value including the forward reaction resulting in production of hydroxyl and hydrogen atom radical and other reactions scavenging these radicals. Simulated values of rate constants used to describe hydrogen peroxide formation under nitrogen saturated solutions are shown in Table 5.5 and model predictions are depicted in Figure 5.7. Under nitrogen saturated solutions, the water decomposition reaction and diffusion of hydrogen peroxide from the bubble interface to bulk solution are the main reactions controlling hydrogen peroxide formation rate. The model-predicted rate constant for the water decomposition reaction under nitrogen saturation is lower than is the case for argon and oxygen. This variation occurs for two main reasons:

1) Differences in the physical properties of the gas such as specific heat ratio, solubility, and thermal conductivity results in less critical condition inside the bubble under nitrogen saturated solutions; and
2) Scavenging of hydroxyl and hydrogen atom radical by nitrogen species such as nitric oxide and nitrous oxide produced by pyrolysis inside the bubble causes decrease in the overall production rate of hydroxyl and hydrogen atom radicals.

Table 5.5 Simulated values of rate constants for hydrogen peroxide generation under nitrogen saturated solutions.

NO.	Reaction	Rate constants (sec^{-1})
1	$H_2O \rightarrow \bullet OH + \bullet H$	300 kHz : 2.97×10^{-8} 600 kHz : 2.2×10^{-9} 800 kHz : 2.0×10^{-9}
11	$H_2O_2 \rightarrow H_2O_2(b)$	300 kHz : 1.5×10^{-2} 600 kHz : 1.6×10^{-2} 800 kHz : 3.4×10^{-2}

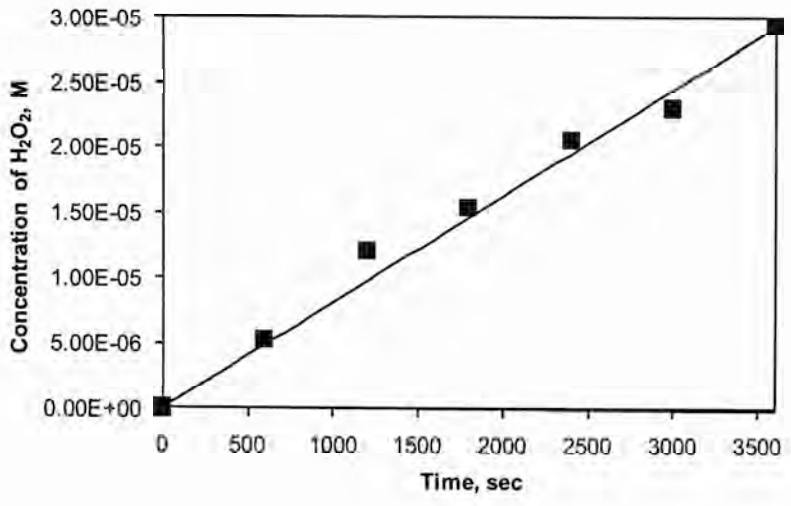

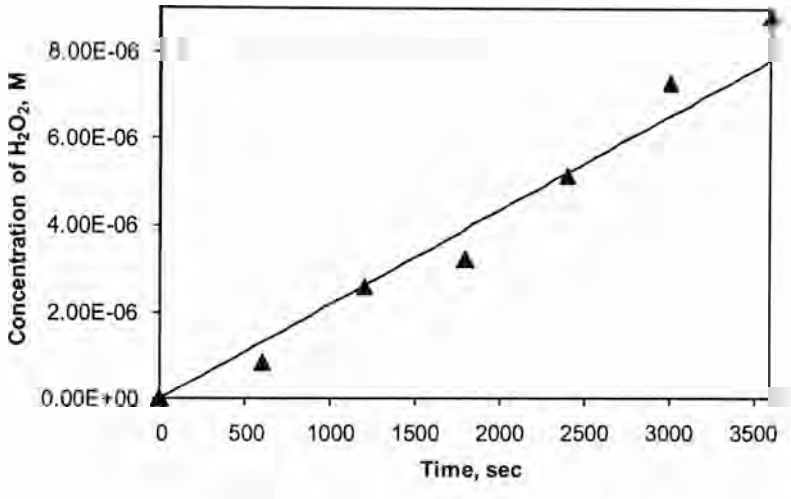

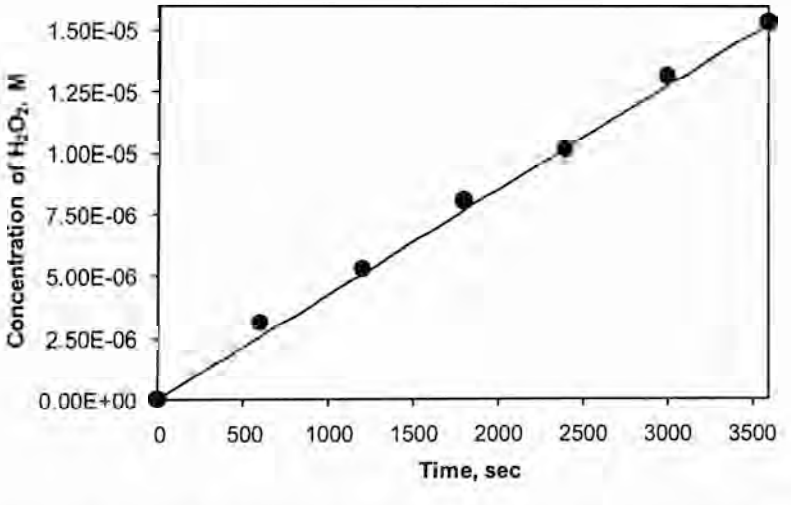

Figure 5.7 Hydrogen peroxide formation under nitrogen saturated solutions. Closed points and solid line represent the experimental and model data respectively (■ : 300 kHz, ▲: 600 kHz, ● : 800 kHz).

5.2.5 Sensitivity studies

The set of reactions presented in Tables 5.1 and 5.2 are adequate in describing the data obtained however it should be recognized that these reactions represent a considerable simplification of the complete reaction set likely to be operating with many additional side reactions, intermediates, and by-products potentially present. However, the proposed mathematical model adequately describes concentration profiles for both hydrogen peroxide and formic acid observed for all conditions investigated in this study. It should be noted that the purpose of the mathematical modeling is not to show the complete reaction set, but rather to identify the most important reactions controlling hydrogen peroxide formation and formic acid degradation by ultrasonic irradiation under the conditions of interest here.

Sensitivity analysis was used to determine the most important reactions controlling hydrogen peroxide formation and formic acid degradation on ultrasonic irradiation and was undertaken by calculation of normalized sensitivity coefficients (NSCs) and by principal component analysis (PCA).

NSCs are a quantitative measure of the change in concentration of a particular species at a particular time in response to perturbations in each rate constant (Savage, 2000). NSCs are a matrix of signed numbers. While numbers with large negative values indicate that reactions act as sinks, numbers with large positive values identify reactions that represent major sources for each species. The magnitude of the NSCs then gives an indication of which reactions act as major sources and sinks of a particular species of interest at any given time. Sensitivity calculations were carried out at 10 equal time intervals during the experimental period for each frequency and background gas used in this study.

As the model presented was based on best fit to the measured species, sensitivity analysis was limited to hydrogen peroxide and formic acid only. The NSC matrices were produced by the kinetic modeling software program Kintecus V3.7 (Ianni, 2006) using the reactions and rate constants listed in Tables 5.1 and 5.2.

While NSCs provide an indication of the system response to perturbations in one rate constant at a time, they do not explain interactions between reactions (Vajda *et al.*, 1985). In order to investigate these interactions, principal component analysis (PCA) proposed by Vajda *et al.* (1985) was carried out on the NSC matrices. In PCA, only component $\psi(k)$ whose normalised eigenvalues (λ / λ_{Tot}) contribute more than 0.1% to the system response were considered and, within those, only components whose eigenvector coefficients had an absolute value greater than 0.2 were considered to have a significant contribution. PCA was conducted by using NSCs calculated for species whose concentrations were measured experimentally.

From the analysis of the log of the sum of squared NSCs over the entire reaction time for those species measured experimentally, a comparative means for comparing the influence of various reactions on the species concentration profiles can be obtained. Reactions with small values of the log of the sum of squared NSCs have little influence on the species as perturbations in their rate constants have little effect on the species' concentration during the reactions.

The value of the sum of NSCs under argon saturated solutions is shown in Figure 5.8. Reactions for NSC analysis are selected from Table 5.3. Diffusion of hydrogen peroxide (reaction 10) is the dominant reaction controlling the formation of hydrogen peroxide. This is also supported by the results of PCA shown in Table 5.6 with the largest eigenvalues corresponding to eigenvectors whose component is reaction 10. The results also show that the water decomposition reaction (reaction 1) and interfacial free radical reactions are important.

Figure 5.9 shows the results of log of sum of squares of NSCs for formic acid degradation under argon at 600 kHz. As shown, diffusion of hydroxyl radicals (reaction 11), hydrogen peroxide (reaction 10) and formic acid (reaction 26) from the bubble interface to bulk solution are the main reactions controlling formic acid degradation Also hydroxyl radical inhibition resulting from hydrogen peroxide formation (reaction 17) is important as result of its effect on the concentration of hydroxyl radicals. In the PCA results shown in Table 5.7, those reactions are seen to possess the largest eigenvalue. The calculated value of the NSCs does not vary substantially with frequency.

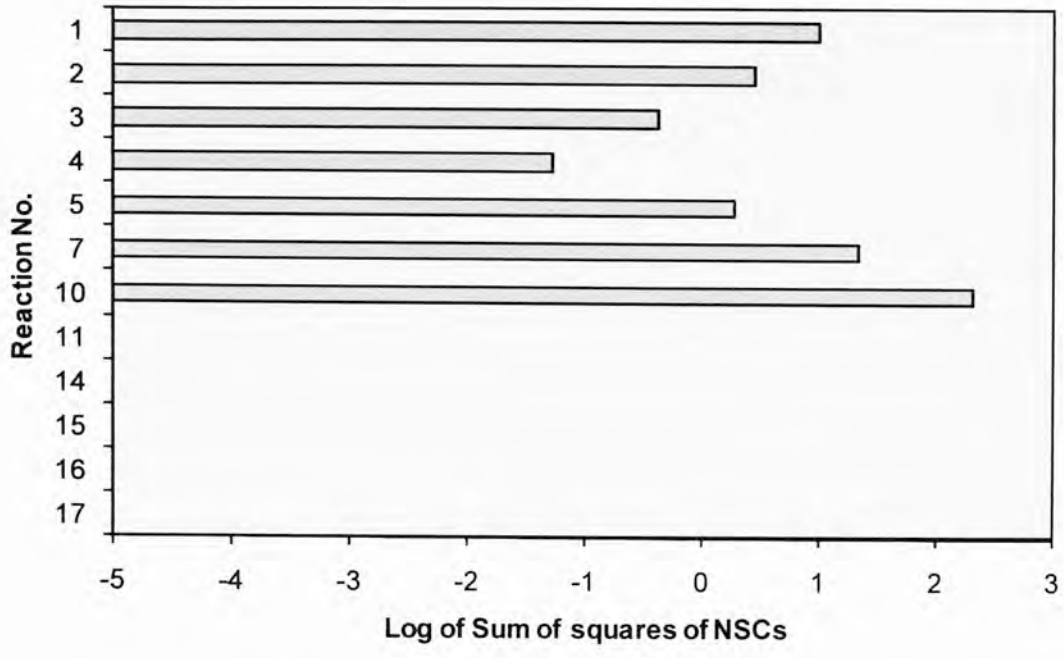

Figure 5.8 Log of sum of squares of the NSCs of reactions involved in hydrogen peroxide formation at 600 kHz under argon saturated solutions.

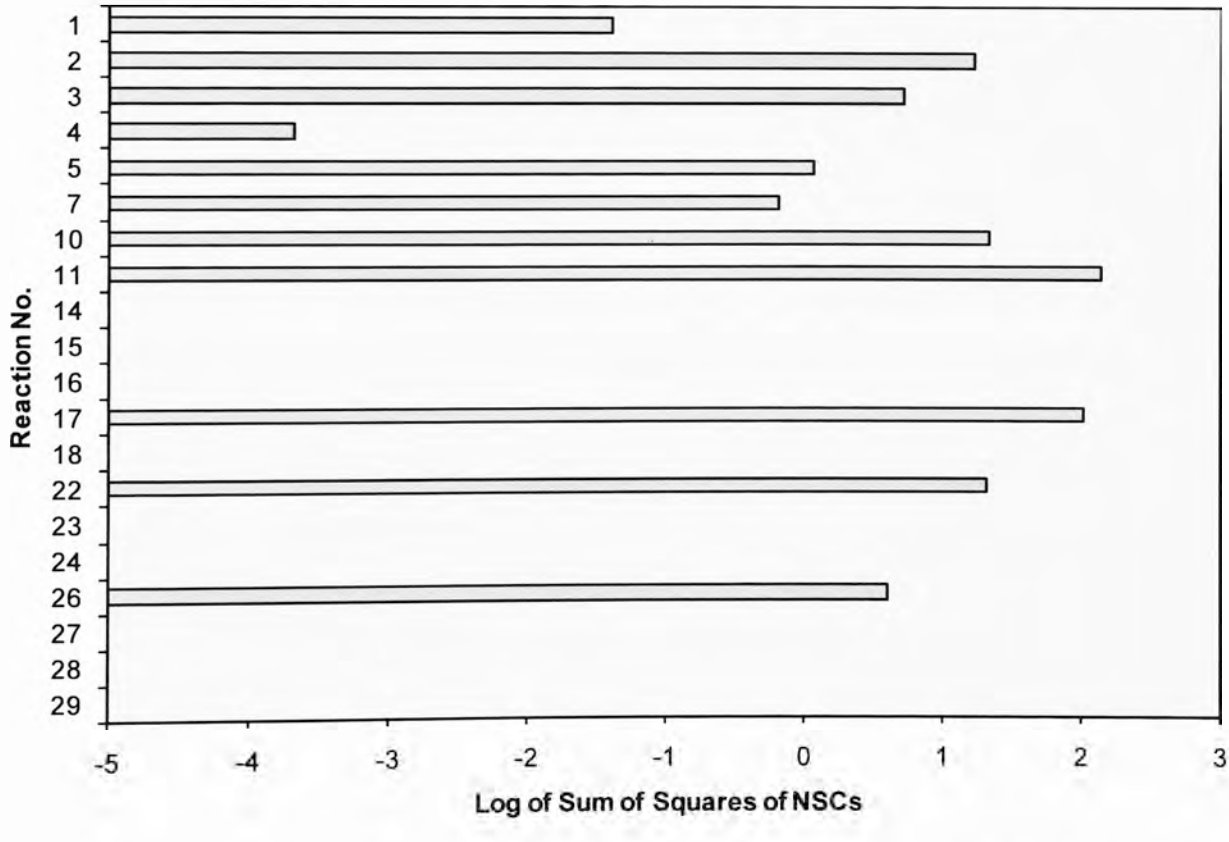

Figure 5.9 Log of sum of squares of NSCs for reactions involved in formic acid degradation at 600 kHz under argon saturated solutions.

Table 5.6 PCA results for hydrogen peroxide formation under argon at 600 kHz.

Eigenvalue	Eigenvector for selected reactions (reaction no.(eigenvector))
57.22	10(0.85), 2(0.60), 1(0.55), 11(0.53), 7(0.52), 5(0.50), 17(0.49), 3(0.32)
40.26	1(0.92), 11(0.47), 4(0.30), 2(0.22)
11.88	11(0.68), 7(0.61), 10(0.37), 1(0.23)
5.12	17(0.48), 10(0.39), 7(0.33), 2(0.32), 5(0.21)
2.06	3(0.89), 7(0.37), 1(0.21)
1.74	2(0.62), 11(0.45), 7(0.39), 5(0.35), 3(0.29)

Table 5.7 PCA results for formic acid degradation under argon at 600 kHz.

Eigenvalue	Eigenvector for each reactions (reaction no.(eigenvector))
142.67	11(0.75), 17(0.63), 2(0.53), 10(0.49), 3(0.30), 22(0.28), 5(0.27), 7(0.24), 1(0.23)
54.90	1(0.90), 10(0.37), 4(0.29), 11(0.26), 5(0.24), 7(0.24)
29.43	3(0.57), 17(0.56), 11(0.30), 2(0.25), 10(0.24)
19.02	11(0.55), 26(0.37), 1(0.33), 7(0.32), 10(0.28), 27(0.26), 22(0.25), 24(0.24)
13.81	29(0.79), 26(-0.75), 7(-0.75), 10(-0.51), 24(0.44), 27(0.40), 1(-0.37), 11(0.34), 22(-0.30)
11.12	27(-0.34)
9.94	29(-0.84), 24(-0.71), 22(0.40), 7(0.27)
6.92	22(-0.53), 24(-0.44), 3(0.41), 7(0.29), 26(-0.24)
4.30	22(-0.30), 10(-0.27), 7(0.21), 17(-0.20)
3.20	23(-0.76), 28(0.57), 26(0.36), 10(-0.32), 29(-0.27), 7(0.25), 27(-0.22)
2.87	28(-0.68), 23(-0.44)

Log sum of squares of the NSCs for hydrogen peroxide generation under oxygen saturated solutions are shown in Figure 5.10. Under oxygen saturated solutions, reactions related to hydroperoxyl radicals at the interface (reactions 7, 8 and 9) and diffusion of hydrogen peroxide (reaction 10) from the bubble interface to bulk solution

have a major impact on hydrogen peroxide formation. Also, the initiation reaction (reaction 1) and the reaction describing the recombination of hydroxyl radicals (reaction 2) are critical for hydrogen peroxide generation. In the presence of oxygen, recombination of both hydroxyl and hydroperoxyl radicals are the major sources of hydrogen peroxide. As shown in Table 5.8, PCA results show the four largest eigenvalues (together accounting for more than 99.99% of the system response) correspond to eigenvectors whose component are reaction 1, 2, 7, 8, 9 and 10. Sensitivity analysis of reactions accounting for formic acid degradation (see Figure 5.11) show that formic acid degradation is controlled by the diffusion of formic acid (reaction 26) and hydroxyl radical (reaction 11) from bubble interfaces to bulk solution.

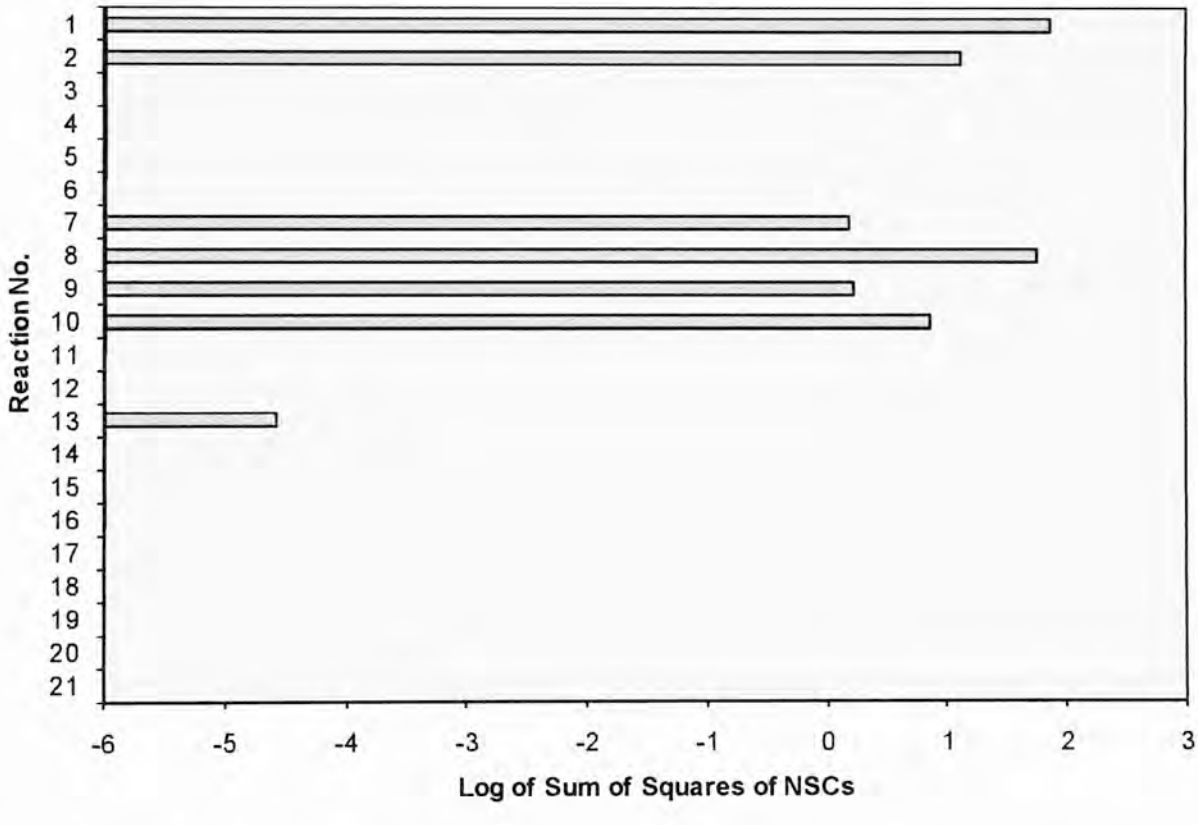

Figure 5.10 Log of sum of squares of NSCs for reactions involved in hydrogen peroxide formation at 300 kHz under oxygen saturated solutions.

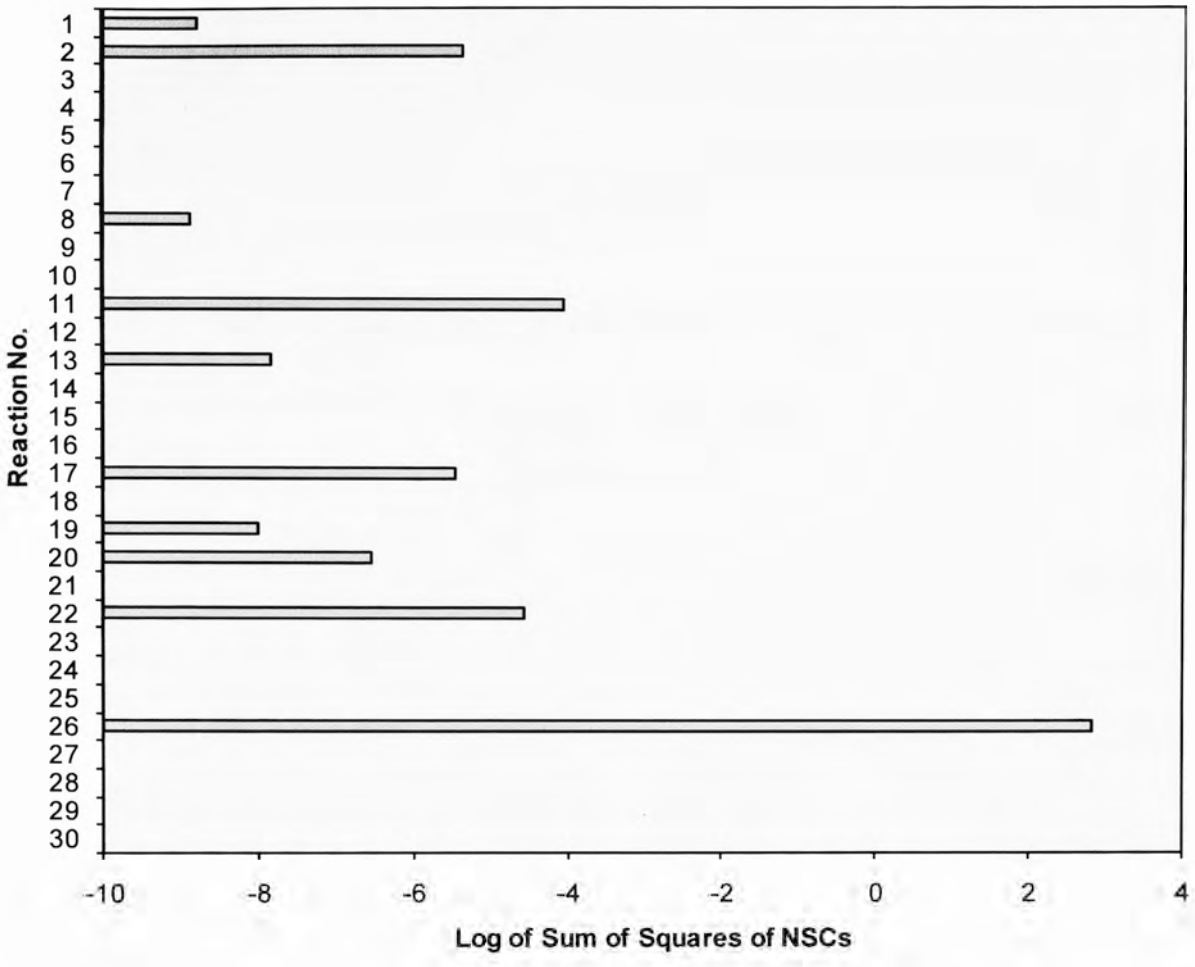

Figure 5.11 Log of sum of squares of NSCs for reactions involved in formic acid degradation at 300 kHz under oxygen saturated solutions.

Table 5.8 PCA results for hydrogen peroxide formation under oxygen saturated solutions at 600 kHz.

Eigenvalue	Eigenvector for selected reactions (reaction no.(eigenvector))
271.49	1(0.75), 6(0.66), 21(0.39), 12(0.39)
53.67	21(0.82), 12(0.82), 1(0.70), 8(0.63), 2(0.48), 3(0.35), 15(0.33), 11(0.23), 7(0.20)
36.80	6(0.26), 8(0.26), 2(0.23)
16.35	11(1.00), 17(0.89), 8(0.62), 6(0.36), 10(0.32), 1(0.30), 2(0.27), 9(0.21), 20(0.21)
7.40	13(0.58), 9(0.37), 19(0.35), 7(0.29), 10(0.28)
6.09	10(1.00), 13(0.35), 2(0.27)
2.52	9(0.78), 7(0.78), 13(0.70), 8(0.43), 17(0.33), 20(0.30), 1(0.27), 19(0.26), 2(0.25), 3(-0.24)
1.89	15(0.86), 3(0.47)
1.85	19(0.52), 20(0.44), 17(0.36), 2(0.28)

1.61	3(0.69), 15(0.40), 12(0.23), 21(0.23)
1.41	2(0.49), 11(0.23)

Table 5.9 PCA results for formic acid degradation under oxygen saturated solutions at 600 kHz.

Eigenvalue	Eigenvector for each reactions (reaction no.(eigenvector))
269.14	1(0.75), 6(-0.66), 21(0.39), 12(0.39)
78.60	26(1.00), 11(-0.64), 2(0.52), 25(-0.51), 17(-0.47), 30(0.38), 22(-0.38), 8(0.35), 1(-0.22), 21(-0.21), 12(-0.20)
54.24	30(0.82), 21(0.48), 12(0.48), 1(-0.43), 8(-0.38), 29(0.34), 28(0.34), 26(-0.28), 2(-0.26), 3(0.21)
51.48	30(0.83), 21(0.48), 12(0.48), 1(0.40), 26(-0.39), 28(-0.34), 29(-0.34), 8(-0.29), 3(0.24), 25(-0.24), 11(0.21)
39.86	26(0.37), 11(-0.25), 2(0.21)
32.07	8(0.57), 6(-0.46), 11(0.37), 3(-0.28), 25(-0.27), 9(0.22), 21(0.20), 12(0.20)
11.94	27(0.66), 10(-0.32), 2(-0.31)
7.70	25(-1.00), 22(0.92), 10(0.61), 17(0.54), 11(-0.54)
6.48	13(0.36), 10(-0.32), 19(-0.31), 9(0.27), 22(0.23), 27(-0.21), 7(0.20)
5.86	10(-0.64), 13(-0.42), 19(0.33), 23(-0.30), 27(-0.29), 7(0.27), 9(-0.23)
4.44	17(0.68), 10(0.49), 22(-0.48), 24(0.36), 23(0.36), 25(-0.35), 27(-0.24)
3.02	29(0.73), 28(0.73), 30(-0.60)
2.41	9(-0.57), 7(0.52), 13(0.49), 19(0.43), 8(-0.28)
1.89	15(-0.77), 3(0.42)
1.60	3(0.76), 15(-0.44), 12(-0.25), 21(-0.25), 6(0.21)
1.28	2(0.89), 27(-0.45), 11(-0.38), 8(-0.27)
0.59	24(-0.55), 23(-0.55), 17(-0.38), 20(0.24), 11(0.21)

5.3 Conclusions

In this chapter, a kinetic model is developed which describes hydrogen peroxide formation and formic acid degradation on ultrasonic irradiation. The model provides excellent fits to our experimental data under all conditions investigated. The model also identifies the important reactions controlling hydrogen peroxide formation and formic acid degradation. Hydrogen peroxide formation is shown to be controlled by recombination of hydroxyl radicals and, in the presence of oxygen, hydroperoxyl radicals. Under all conditions investigated, the water decomposition reaction and diffusion of hydrogen peroxide from the bubble interface to the bulk solution are the key reactions controlling hydrogen peroxide formation.

The model shows that reaction of formic acid with hydroxyl radicals at both the interface and in the bulk solution are key to its degradation. The rate of formic acid degradation is controlled by diffusion of formic acid from bulk solution to bubble interfaces. Slow diffusion rate of formic acid from bulk solution to bubble interfaces explains the slow decomposition rate of formic acid observed experimentally. This result also supports the observation of no effect of formic acid addition on hydrogen peroxide formation.

Chapter 6

Effect of Fe(II) Addition on Formic Acid Degradation by Ultrasonic Irradiation

6.1 Introduction

Extensive research has been undertaken in the past to improve the efficiency of sonochemical reactions, considering that a significant portion of the energy used in producing radical species is not effectively converted into an optimum yield of the desired products (Olson and Barbier, 1994, Hua *et al*, 1995). As discussed earlier, hydrogen peroxide is formed by recombination of hydroxyl radicals and hydroxperoxyl radicals; i.e.

$$\bullet OH + \bullet OH \rightarrow H_2O_2 \quad (1)$$

$$\bullet HO_2 + \bullet HO_2 \rightarrow H_2O_2 \quad (2)$$

However, hydrogen peroxide production and its subsequent reaction with hydroxyl radical (eq. 3) limits the steady-state concentration of hydroxyl radicals which do have high reactivity towards target organic compounds; i.e.,

$$H_2O_2 + \bullet OH \rightarrow \bullet HO_2 + H_2O \quad (3)$$

Indeed, the production of hydroxyl radicals needs to be increased if more effective degradation of target compounds is to be achieved. Many researchers have concentrated on ways to improve the efficiency of sonochemical degradation of organic compounds by increasing the production of reactive radicals (Dutta *et al.*, 2002, Beckett and Hua, 2003, Yim *et al.*, 2003, Ioan *et al*, 2007). One possible pathway to increase hydroxyl radical production is to use ferrous iron which reacts with hydrogen peroxide to produce hydroxyl radicals; i.e.,

$$Fe(II) + H_2O_2 \rightarrow Fe(III) + OH\bullet \qquad (4)$$

The increased yield of hydroxyl radical in the presence of ferrous iron may lead to increased sonochemical degradation (Bucket and Hua, 2000, Joseph *et al*, 2000, Neppolian *et al*, 2002, Yim *et al*, 2002,). However, the concentration of hydroxyl radicals in the presence of ferrous iron may also be limited by the rapid oxidation of ferrous iron by hydroxyl radicals; i.e.,

$$Fe(II) + OH\bullet + H^+ \rightarrow Fe(III) + H_2O \qquad (5)$$

Thus, it is expected that there will be an optimum ferrous iron concentration where maximum hydroxyl radical production and hence maximum degradation of organic compound occurs.

In this chapter, the effect of ferrous iron addition on formic acid degradation by ultrasonic irradiation is investigated. Experimental results for hydrogen peroxide formation and formic acid degradation by ultrasonic irradiation were presented in Chapter 4 and a model that satisfactorily described the results obtained was presented in Chapter 5. This mathematical model is extended in this chapter by combination with Fenton reactions enabling description of the effect of ferrous iron addition on hydrogen peroxide formation and formic acid degradation.

6.2 Materials and Methods

Sonolytic radiation of 300 kHz frequency was used for formic acid degradation in the presence of Fe(II). A 10 mM ferrous iron (Fe(II)) stock solution was prepared from ferrous sulphate ($Fe_2SO_4 \cdot 7H2O$, Ajax Chemicals) in 2mM HCl. Fe(II) concentrations ranging from 10 to 500 μM of Fe(II) are used in the experiments described here. The initial pH of solution was set at 3.5 by addition of an appropriate amount of 0.1N nitric acid and no further control was applied. 200 nM of C^{14} labeled formic acid was used as the target substrate. The Fe(II) concentration was measured spectrophotometrically using 1,10-phenanthroline as the complexing agent (Fortune and Mellon, 1938) as described in detail in Chapter 3.4.6. Hydrogen peroxide concentration was measured spectrophotochemically as described in Chapter 3.4.3.2.

6.3 Results and Discussion

6.3.1 Effect of Fe(II) addition on formic acid degradation

Figures 6.1 and 6.2 show the effect of Fe(II) addition on formic acid degradation by ultrasonic irradiation of pH 3.5 solutions under argon and oxygen saturated solutions, respectively. In both cases, Fe(II) addition clearly affects the rate of formic acid degradation by ultrasonic irradiation with an initial increase at low Fe(II) concentrations followed by a reduction in degradation rate. The maximum rate of formic acid degradation was observed at Fe(II) concentrations of 100 μM and 30 μM under argon and oxygen saturated solutions respectively.

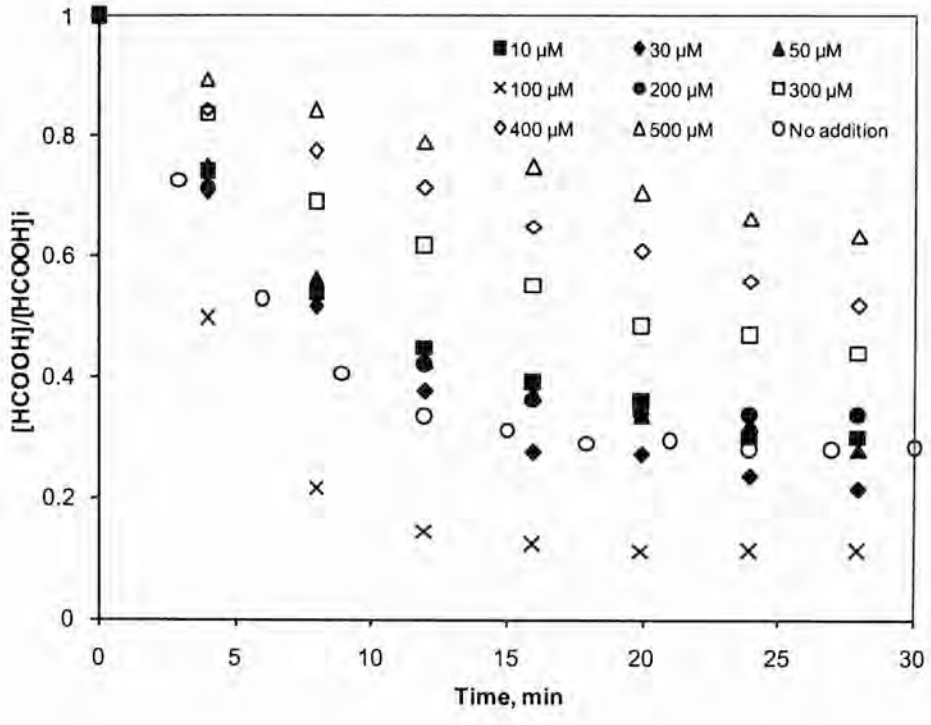

Figure 6.1 Effect of Fe(II) addition on degradation of 200 nM formic acid by 300 kHz ultrasonic irradiation of a pH 3.5 solution saturated with argon.

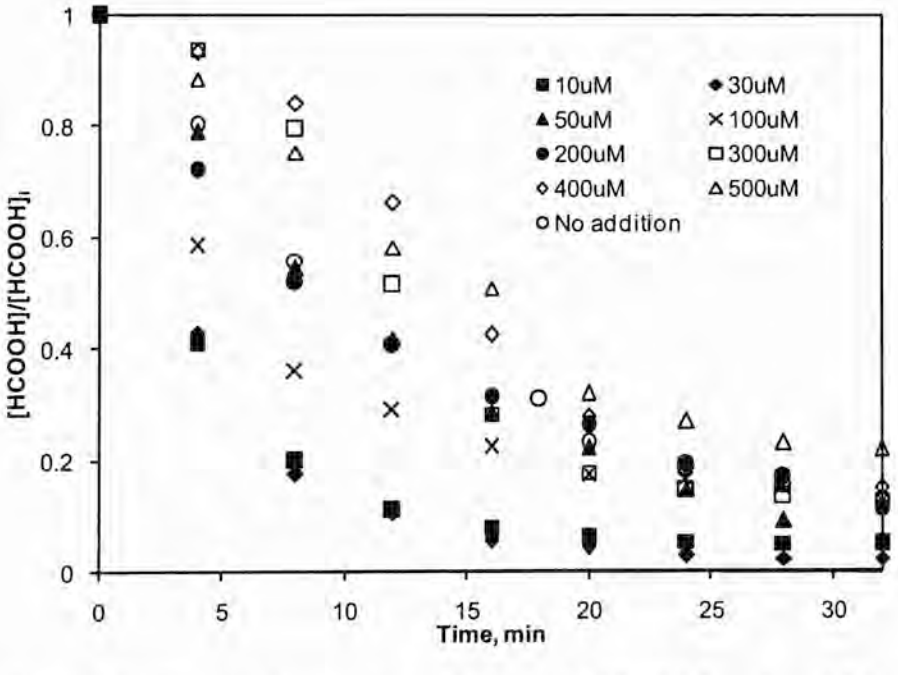

Figure 6.2 Effect of Fe(II) addition on degradation of 200 nM formic acid by 300 kHz ultrasonic irradiation of a pH 3.5 solution saturated with oxygen.

As seen in Figures 6.3 and 6.4, formic acid decay generally initially exhibits first order decay though at the higher Fe(II) concentrations under oxygen saturated solutions, some departure from pseudo first order is observed at later times. Initial pseudo first order rate constants were determined from linear fits to the data at early times.

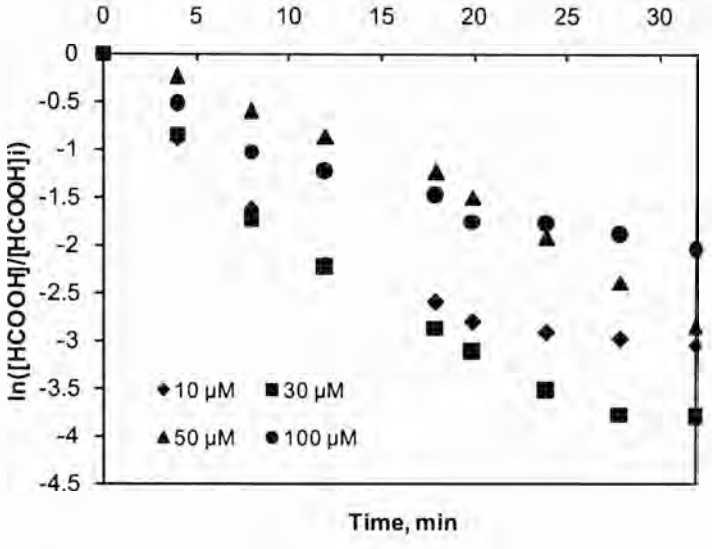

Figure 6.3 Pseudo first order kinetic analysis of formic acid degradation at the lower concentration range of Fe(II) (10 µM – 100 µM) under oxygen saturated solutions.

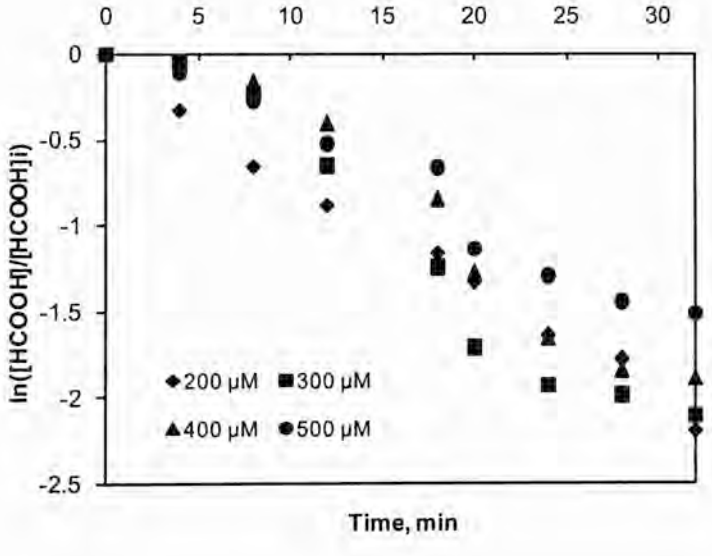

Figure 6.4 Pseudo first order kinetics of formic acid degradation at higher concentration range of Fe(II) (200 µM - 500 µM) under oxygen saturated solutions.

Figure 6.5 shows the effect of Fe(II) addition under air saturated solutions. In this case, the effect of Fe(II) addition is substantially less dramatic than is the case under argon or oxygen saturated solutions with only a slight increase in degradation rate in the presence of 100 μM Fe(II). As noted in Chapter 4, it appears that hydroxyl radical scavenging by nitrogen species leaves little scope for degradation of formic acid and any enhancement in hydroxyl radical generation resulting from Fe(II) addition does little to increase formic acid degradation.

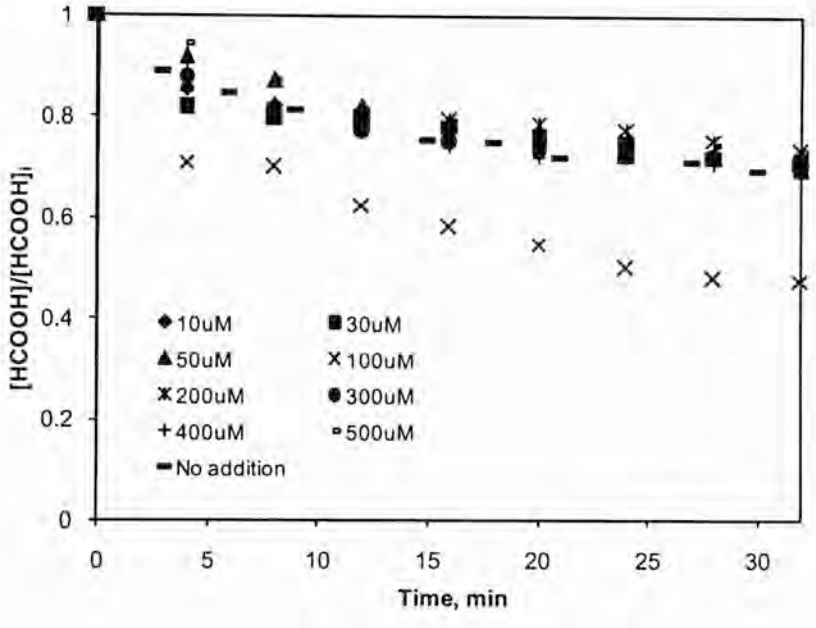

Figure 6.5 Degradation of formic acid (200 nM) at various Fe(II) concentrations on 300 kHz sonolysis of pH 3.5 air saturated solutions.

Initial pseudo-first order degradation rate constants as a function of Fe(II) concentration in the presence of different background gases are shown in Figure 6.6. The rate constants for formic acid degradation initially increase with increasing initial concentration of Fe(II) for solutions saturated with argon and oxygen but, as noted above, peak at 100 μM and 30 μM [Fe(II)] respectively, and then exhibit a slow decrease in degradation rate as [Fe(II)] increases further. The oxygen saturated system is clearly more responsive to Fe(II) addition than is the argon saturated system with the pseudo first order degradation rate increasing from 0.09 min^{-1} to 0.19 min^{-1} for only a 30 μM Fe(II) addition in the O_2 case compared to an increase from 0.04 min^{-1} to 0.12 min^{-1} for a 100 μM Fe(II) addition in the argon case. The decrease in formic acid

degradation rate at the higher Fe(II) presumably occurs (as suggested in the Introduction) because of the increasing competition for hydroxyl radicals between Fe(II) and formic acid. This issue will be examined further in the modelling section presented in Section 6.3.3.

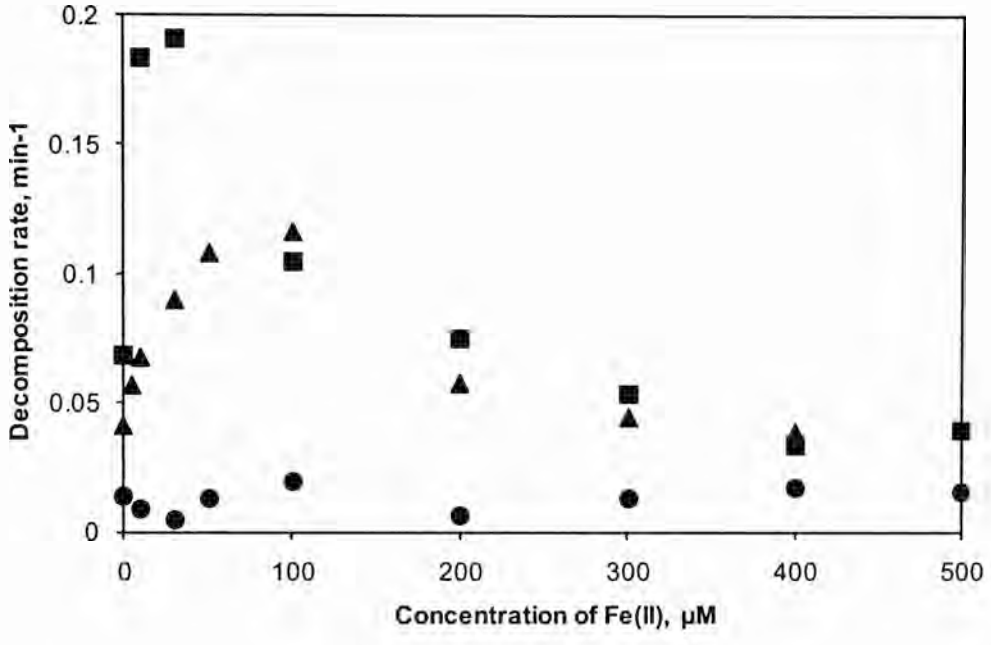

Figure 6.6 Comparison of the effect of Fe(II) addition on formic acid decomposition rate constant for different dissolved gases (▲ argon, ■ oxygen, ● air).

6.3.2 Effect of Fe(II) addition on hydrogen peroxide formation

To investigate the effect of Fe(II) addition in more detail, we also measured the extent of hydrogen peroxide generation in the presence of Fe(II) under argon saturated solutions. Results are presented in Figure 6.7 with extent of hydrogen peroxide formation decreasing with increasing concentration of Fe(II). This effect is presumably observed because of the reaction of Fe(II) with H_2O_2. This explanation is supported by an observed decrease in ferrous iron concentration over time as is shown in Figure 6.8. Model reactions for hydrogen peroxide formation in the presence of Fe(II) are summarised in Table 6.1.

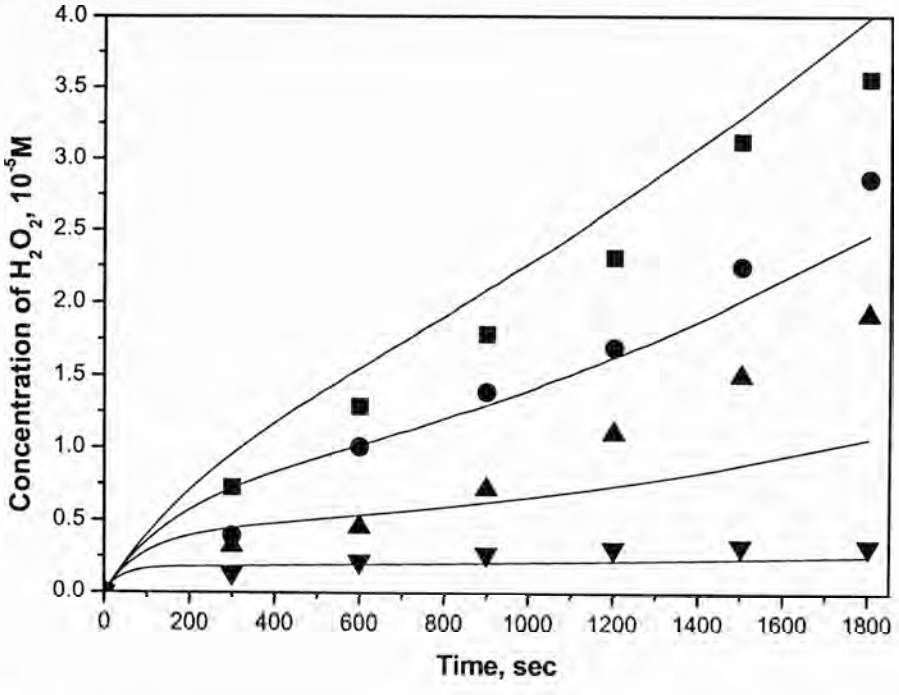

Figure 6.7 Hydrogen peroxide formation by ultrasonic irradiation in presence of Fe(II) at 300 kHz under argon saturated solutions. Closed symbol represent the experimental result and solid line represents the model fit. ■: [Fe(II)] = 50 μM ● : [Fe(II)] = 100 μM ▲ : [Fe(II)] = 200 μM ▼ : [Fe(II)] = 500 μM.

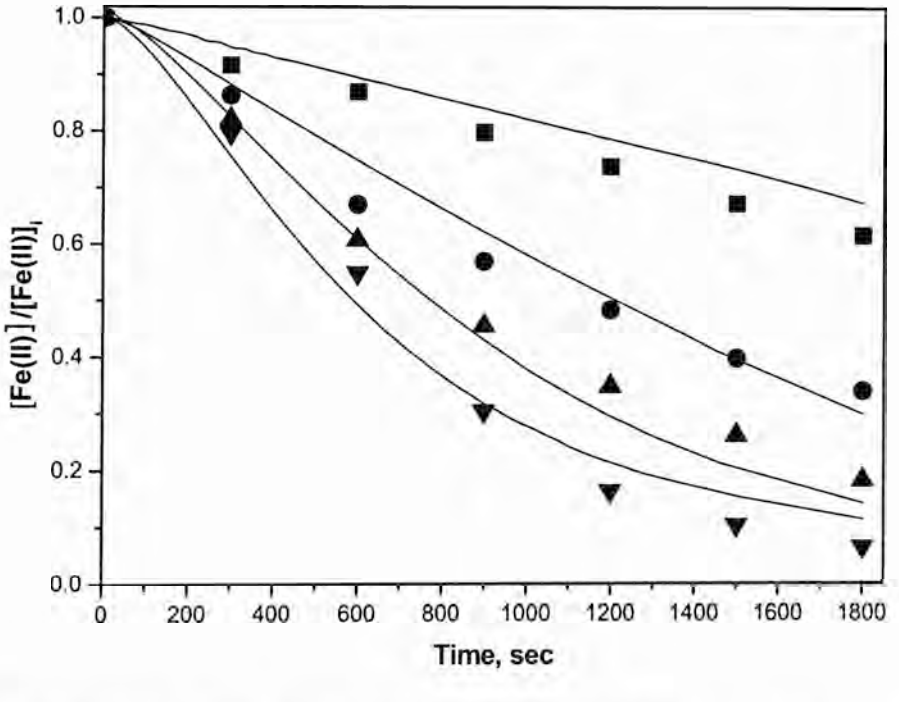

Figure 6.8 Variation in Fe(II) concentration over time on ultrasonic irradiation of argon saturated solutions at 300 kHz and for different concentrations of added FeII. Closed symbol represents experimental result and solid line represents model fit. ■: [Fe(II)] = 50 μM ● : [Fe(II)] = 100 μM ▲ : [Fe(II)] = 200 μM ▼ : [Fe(II)] = 500 μM.

6.3.3 Kinetic model for hydrogen peroxide formation and formic acid degradation in the presence of Fe(II)

In this section, we examine the ability of a simple combination of the model for description of the sonolytic breakdown of formic acid with a previously reported model for the Fenton-mediated breakdown of the same compound (Duesterberg *et al.*, 2005). Key reactions for both the sonolytic breakdown and Fenton-mediated breakdown of formic acid under anoxic conditions are presented in Table 6.1 and 6.2. As seen in Figure 6.9, use of these equations together with previously reported rate constants for each reaction provides a description of the effect of [Fe(II)] that is similar to the observed trend but which slightly over-predicts the effect of added Fe(II) at low Fe(II) concentrations.

As shown in Figure 6.7 and 6.8, the mathematical model satisfactorily describes the hydrogen peroxide formation and decrease in Fe(II) concentration at all added Fe(II) concentrations examined in this study. These results support the assumption that the Fenton reactions occur in the bulk solution and confirm the major surmised effects that interaction of added Fe(II) with sonolytically generated H_2O_2 that disperses into bulk solution produces additional hydroxyl radicals that act to enhance the degradation of formic acid in bulk solution. The impact of high Fe(II) concentrations of added Fe(II) in inhibiting the enhancement observed at low Fe(II) doses is principally a result of competition between formic acid and Fe(II) for hydroxyl radicals generated in bulk solution by the Fenton process.

While a number of factors could account for the slight difference between modelled and observed effect of Fe(II) addition on formic acid degradation rate, two are particularly worth addressing. Firstly, while solution pH was initially set at 3.5, there was no attempt to control the pH over the course of sonolysis and there was invariably an increase (up to about 4.5) over the course of the approximately 30 minute sonolyis experiments. Provided iron precipitation does not occur, the effect of increasing pH is to increase the ability of added iron to promote Fenton-mediated formic acid degradation. This occurs both because of the increased redox cycling of iron that occurs as a result of the more facile reduction of Fe(III) by superoxide radical anion compared to its

protonated form, the hydroperoxyl radical (pKa = 4.8), and because of the higher rate of hydroxyl radical attack on the formate anion than the protonated formic acid (pKa = 3.75).

Table 6.1 Reactions for hydrogen peroxide formation and Fenton reactions

No	Reaction	Rate constant	Reference
Reaction in the bubble			
1	$H_2O \rightarrow \cdot OH + \cdot H \rightarrow \cdot OH(i) + \cdot H(i)$	6.2×10^{-7} s^{-1}	In this study
Reactions at the interface			
2	$\cdot OH(i) + \cdot OH(i) \rightarrow H_2O_2(i)$	5.2×10^{9} M^{-1} s^{-1}	Buxton *et al.*, 1988
3	$\cdot H(i) + \cdot H(i) \rightarrow H_2$	7.8×10^{9} M^{-1} s^{-1}	Buxton *et al.*, 1988
4	$\cdot OH(i) + \cdot H(i) \rightarrow H_2O$	7.0×10^{9} M^{-1} s^{-1}	Buxton *et al.*, 1988
5	$H_2O_2(i) + \cdot H(i) \rightarrow \cdot OH(i) + H_2O$	9.0×10^{7} M^{-1} s^{-1}	Buxton *et al.*, 1988
6	$\cdot OH(i) + H_2O_2(i) \rightarrow \cdot HO_2(i) + H_2O$	3.3×10^{7} M^{-1} s^{-1}	Buxton *et al.*, 1988
7	$H_2O_2(i) \rightarrow H_2O_2(b)$	1.8×10^{-2} s^{-1}	In this study
Reactions in the bulk solution			
8	$\cdot OH(b) + \cdot OH(b) \rightarrow H_2O_2(b)$	5.2×10^{9} M^{-1} s^{-1}	Buxton *et al.*, 1988
9	$\cdot H(b) + \cdot H(b) \rightarrow H_2(b)$	7.8×10^{9} M^{-1} s^{-1}	Buxton *et al.*, 1988
10	$\cdot OH(b) + \cdot H(b) \rightarrow H_2O$	7.0×10^{9} M^{-1} s^{-1}	Buxton *et al.*, 1988
11	$\cdot OH(b) + H_2O_2(b) \rightarrow \cdot HO_2(b) + H_2O$	3.3×10^{7} M^{-1} s^{-1}	Buxton *et al.*, 1988
12	$H_2O_2(b) + \cdot H(b) \rightarrow \cdot OH(b) + H_2O$	9.0×10^{7} M^{-1} s^{-1}	Buxton *et al.*, 1988
13	$Fe(II) + H_2O_2(b) \rightarrow Fe(III) + OH(b) + OH^-$	51 M^{-1} s^{-1}	Walling, 1975
14	$Fe(III) + H_2O_2(b) \rightarrow Fe(II) + HO_2(b) + H^+$	2.0×10^{-3} M^{-1} s^{-1}	Kwan and Voelker, 2002
15	$Fe(III) + HO_2(b) \rightarrow Fe(II) + H^+ + O_2$	7.82×10^{5} M^{-1} s^{-1}	Kwan and Voelker, 2002
16	$Fe(II) + HO_2(b) \rightarrow Fe(III) + H_2O_2(b)$	1.34×10^{6} M^{-1} s^{-1}	Kwan and Voelker, 2002
17	$Fe(II) + OH(b) \rightarrow Fe(III) + OH^-$	3.20×10^{8} M^{-1} s^{-1}	Kwan and Voelker, 2002

Table 6.2 Reaction showing formic acid degradation by ultrasonic irradiation.

No	Reaction	Rate constant (M^{-1} s^{-1})	reference
Reactions occurring in bulk solution			
18	HCOOH(b) + •OH(b) → $COO^{\bullet-}$(b) + H_2O + H^+	1.2×10^9	In this study
19	$COO^{\bullet-}$(b) + $COO^{\bullet-}$(b) → Int(b)	1.4×10^9	Flyunt *et al.*, 2001
20	Int(b) + H^+ → CO_2 + HCOOH(b)	1.0×10^7	Flyunt *et al.*, 2001
21	HCOOH(b) → HCOOH(i)	8.1×10^{-4}	In this study
Reactions occurring at interface			
22	HCOOH(i) + •OH(i) → $COO^{\bullet-}$ (i) + H_2O + H^+	1.2×10^9	In this study
23	$COO^{\bullet-}$(i) + $COO^{\bullet-}$(i) → Int(i)	1.4×10^9	Flyunt *et al.*, 2001
24	Int(i) + H^+ → CO_2 + HCOOH(i)	1.0×10^7	Flyunt *et al.*, 2001

The presence of oxygen influences both the sonolytic production of hydroxyl radicals as well as hydrogen peroxide and, potentially, the extent of iron redox cycling in the Fenton-mediated degradation of formic acid as a result of the ability of carboxyl radicals to reduce oxygen to superoxide (which, in turn, leads to enhanced redox cycling of iron (Duesterberg *et al.*, 2005)). The additional reaction that must be considered is shown below together with the previously reported rate constant. As can be seen from Figure 6.10, excellent agreement between predicted and observed effects of Fe(II) addition on rate constant for formic acid degradation is observed.

		Rate constant (M^{-1} s^{-1})	reference
25	$COO^{\bullet-}$(b) + O_2 + H+ → CO_2 + $\bullet HO_2$(b)	4.2×10^9	Flyunt *et al.*, 2001

As observed in Chapter 4, a higher hydrogen peroxide formation rate under oxygen saturated solutions (i.e., 4.5 μM/min) than under argon saturated solutions (i.e., 2.6 μM/min) was obtained. Thus, a higher rate of hydroxyl radical production can be expected in the presence compared to the absence of oxygen through the reaction of hydrogen peroxide with added Fe(II). Oxygen is likely to play an important role in redox cycle of iron species as well as hydrogen peroxide formation. Whether formic acid is present or not, superoxide radical can always be formed by the reaction of oxygen with hydroxyl radicals by ultrasonic irradiation in the presence of oxygen. The

species can reduce the Fe(III) leading to higher Fe(II) concentration and thus more hydroxyl radical concentration.

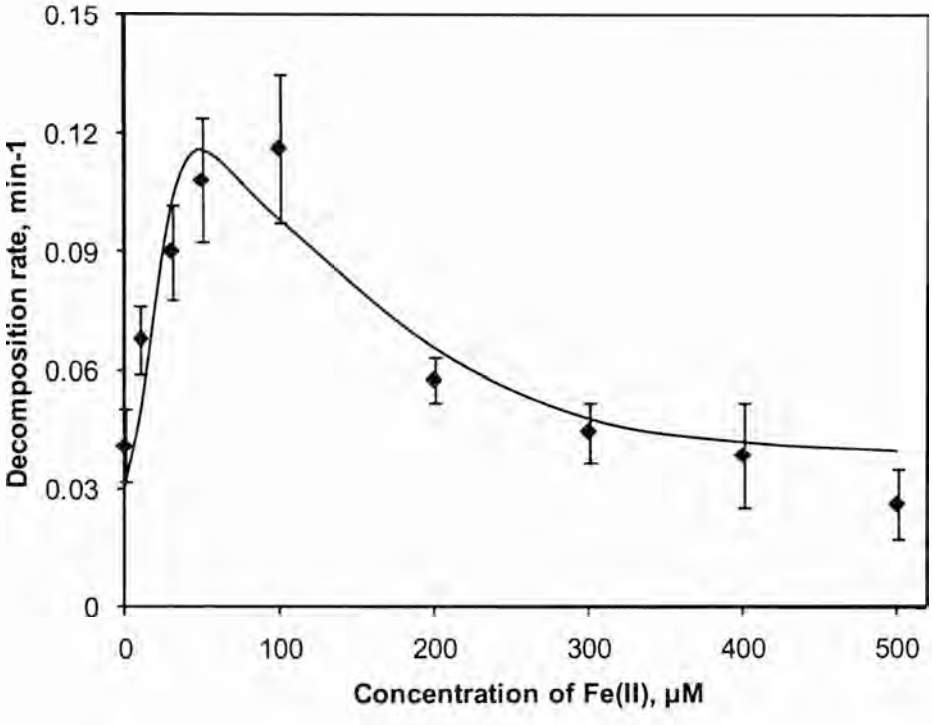

Figure 6.9 Effect of added Fe(II) concentration on initial pseudo-first order decay rate constant of formic acid(200 nM) under argon saturated solutions at 300 kHz. Symbols represent the experimental data while the solid line represents the model predicted results.

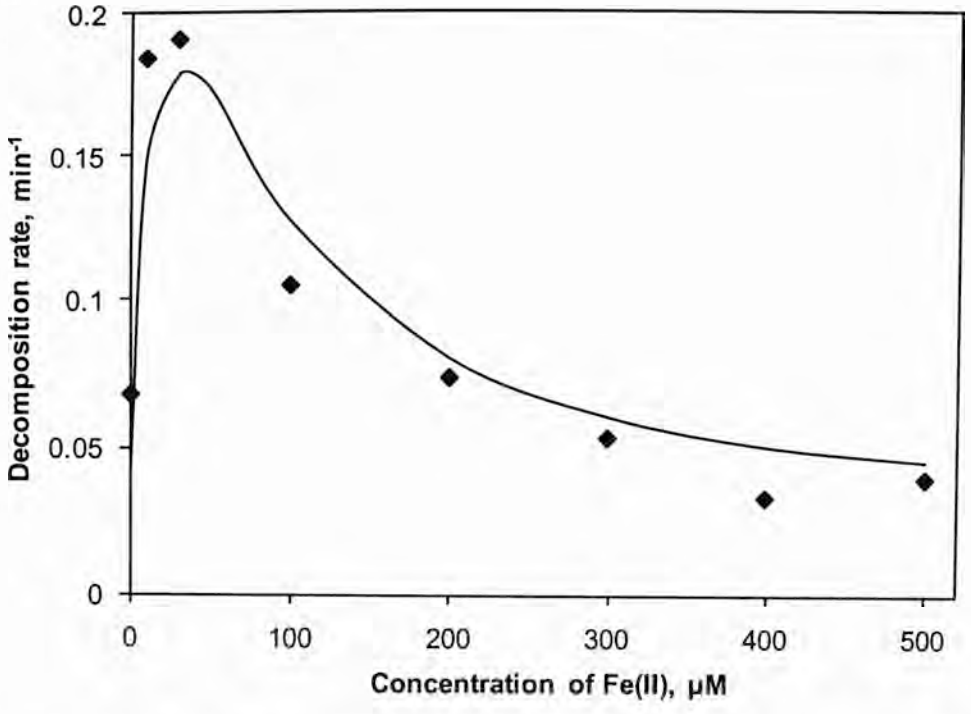

Figure 6.10 Effect of added Fe(II) concentration on initial pseudo-first order decay rate constant of formic acid(200 nM) under oxygen saturated solutions at 300 kHz. Symbols represent the experimental data while the solid line represents the model predicted results.

6.4 Conclusions

In this chapter, the effect of ferrous iron addition on formic acid degradation and hydrogen peroxide production by ultrasonic irradiation is investigated. Ferrous iron addition increased formic acid degradation by approximately 3 fold in the presence of 30 µM ferrous iron under oxygen saturated solutions and 100 µM ferrous iron under argon saturated solutions. However, the effect of ferrous iron addition on formic acid degradation was minor under air saturated solutions, possibly as result of hydroxyl radical scavenging by nitrogen species.

To investigate the reaction scheme and the mechanisms, ferrous iron and hydrogen peroxide concentrations were also monitored over time in the presence of ultrasonic irradiation. The mathematical model developed here based on the model proposed in chapter 5 can predict ferrous iron and hydrogen peroxide concentrations observed on ultrasonic irradiation under argon saturated solutions. These results support the conclusion that hydrogen peroxide reaction with ferrous iron occurs in bulk solution. Formation of hydrogen peroxide formation by ultrasonic irradiation was observed to

initiate the Fenton reaction on addition of Fe(II). Based on the reaction of hydrogen peroxide with Fe(II) in the bulk solution, the effect of initial concentration of Fe(II) on the rate constant for formic acid degradation is adequately described under both argon and oxygen saturated solutions. Model predictions showed that higher rates of generation of hydroxyl radicals enhanced the rate of formic acid degradation under both conditions. The model presented suggested that higher rate constants for formic acid degradation in the presence of oxygen could be accounted for due to i) enhancement of the extent of iron redox cycling as a result of the hydroperoxyl radical-mediated reduction of Fe(III) and ii) the presence of higher hydrogen peroxide concentrations. It should be noted that model reactions in this study were simplified by neglecting the possible effect of pH variation on the reactions and their rate constants. Despite this (and other simplifications), the kinetic model proposed here provides insight into the reaction mechanism associated with iron-catalysed hydroxyl mediated degradation of formic acid and provides an excellent description of the data obtained.

Chapter 7

Implication of Findings to Other Contaminants; Optimisation of Phenol Degradation by Ultrasonic Irradiation

7.1 Introduction

Ultrasonic irradiation (or sonolyis) is a so-called advanced oxidation processes but, unlike other AOPs, contaminant degradation can occur by two different mechanisms, namely, pyrolysis by thermolytic decomposition in the bubble and free radical (especially hydroxyl radical) reaction at the interface and/or in the bulk solution. The results of investigations into the kinetics and mechanism of reactions leading to hydrogen peroxide formation and formic acid degradation on ultrasonic irradiation have been presented in previous chapters. In this chapter, results of application of ultrasonic irradiation to degradation of a contaminant of different hydrophobicity to formic acid are presented and assessed in light of the approach that has been successfully used to describe hydrogen peroxide generation and formic acid degradation. Phenol was chosen as the target compound since it is a common anthropogenic contaminant of well defined characteristics. Phenol is one of the most abundant pollutants in industrial wastewater and is also formed as an intermediate product in the industrial synthesis of many products. The mechanism of degradation of phenol by hydroxyl radical attack is well established (Serpone *et al.*, 1992, Berlan *et al.*, 1994, Petrier *et al.*, 1994, Rivas *et al.*, 1998, Emery *et al.*, 2003) And this understanding together with insights into sonolytic processes described in earlier chapters is used to interpret the results presented in this chapter on the sonolytic degradation of phenol.

7.2 Materials and Methods

All chemicals used in the experiments were reagent grade and used as received. Aqueous media were prepared and used by dissolving the chemicals in pure water obtained from a Milli-Q plus Millipore system. Stock solutions (100 mM) of phenol and byproducts (hydroquinone, benzoquinone, and catechol) were stored in the dark. The experimental procedure used here is the same as that described in Chapter 4. Both hydrogen peroxide formation and phenol degradation was observed at two frequencies (300 and 600 kHz) since high hydrogen peroxide generation and formic acid degradation rates were observed at these frequencies (see Chapter 4). The initial solution pH was set either using nitric acid or phosphoric acid. Three different dissolved gases (air, argon and oxygen) were used to determine their effect on sonolytic degradation of phenol. The experimental solution was sparged with the dissolved gas for at least 15 mins to attain saturation concentration in the solution prior to ultrasonic irradiation. The concentration of phenol and its by-products were determined by HPLC as described in Chapter 3.4.4. The hydrogen peroxide concentration was measured using the spectrophotometric method described in Chapter 3.4.3.1.

7.3 Results and discussions

7.3.1 Sonochemical degradation of phenol

The kinetics of sonolytic degradation of phenol was measured for two frequencies (300 and 600 kHz) and three dissolved gases (air, argon and oxygen). Phenol degradation followed pseudo-first-order kinetics at both frequencies as shown in Figure 7.1 to 7.3. The initial pseudo first order rate constants for phenol degradation determined under various conditions are summarised in Figure 7.4. As shown, the initial pseudo first order rate constants of phenol degradation are higher under oxygen and air saturated solutions than under argon saturated solutions at 300 kHz. Also, the initial pseudo first order rate constants of phenol degradation were higher at 600 kHz at all initial concentration of phenol examined except 400 μM. The initial pseudo first order rate constant is also dependent on initial phenol concentration with the rate constant increasing with decrease in initial concentration of the phenol. A decrease in rate

constants at higher organic concentration is consistent with other studies (Petrier *et al.*, 1994, Kotronarou *et al.*, 1991) as well the results of formic acid degradation rate described in Chapter 4 (see Fig 4.4).

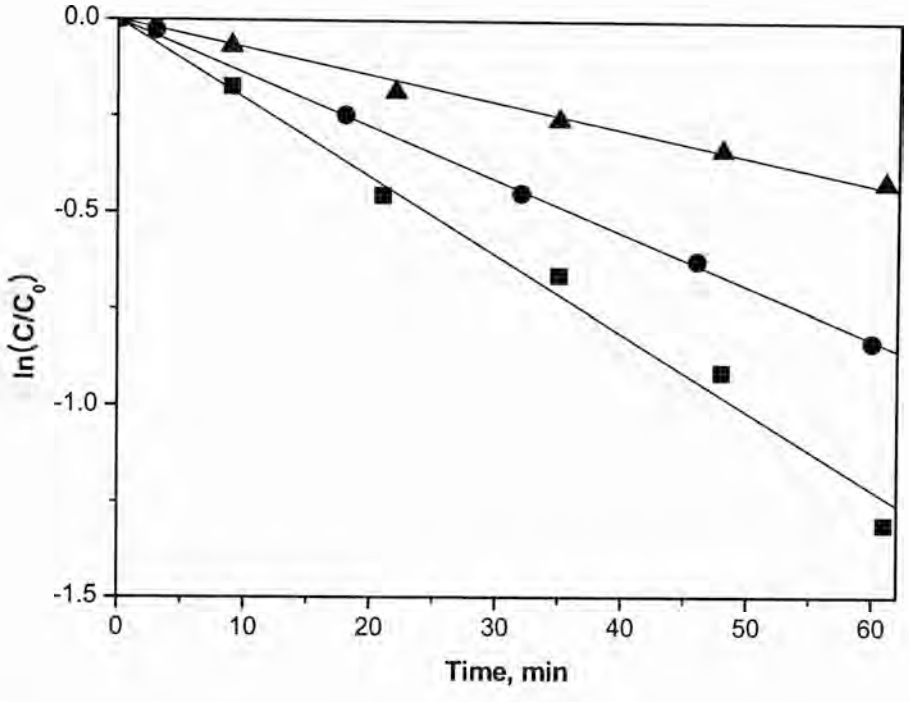

Figure 7.1 Phenol concentration change under argon saturated solutions at 300 kHz (■: 100 μM, ● : 200 μM, ▲ : 400 μM).

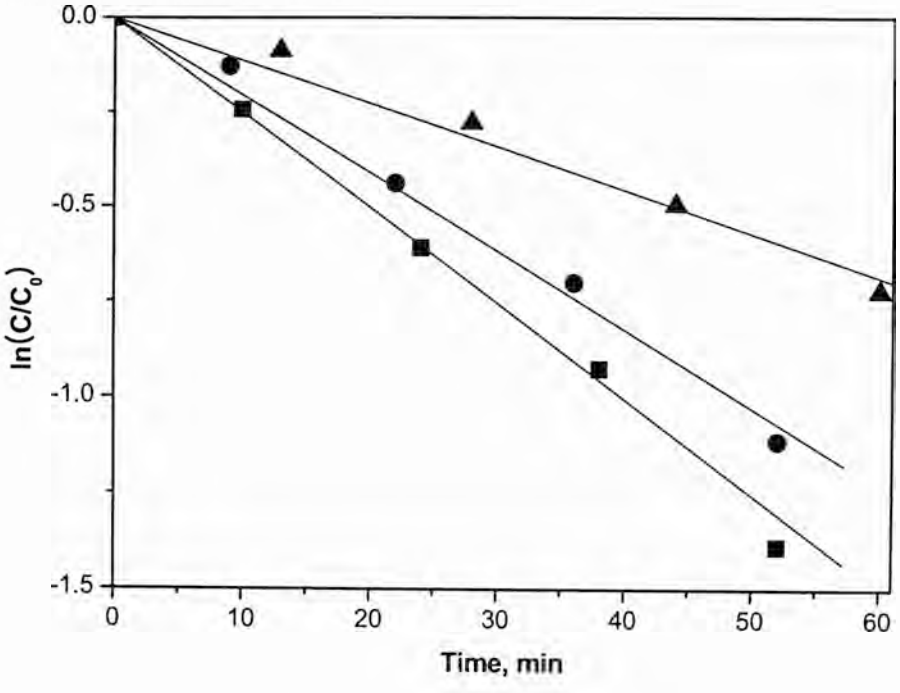

Figure 7.2 Phenol concentration changes under oxygen saturated solutions at 300 kHz (■: 100 μM, ● : 200 μM, ▲ : 400 μM).

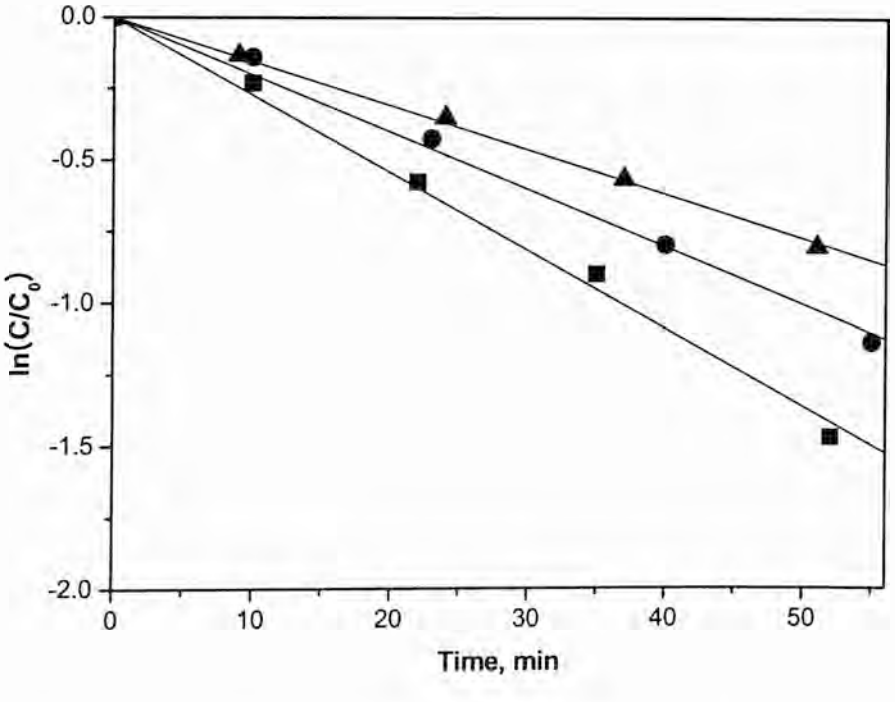

Figure 7.3 Phenol concentration changes under air saturated solutions at 300 kHz (■ : 100 μM, ● : 200 μM, ▲ : 400 μM).

The maximum pseudo-first order rate constant is achieved at 600 kHz under argon saturated solutions. This observation contradicts our earlier result which showed that the rate of hydrogen peroxide formation under oxygen and air saturated solutions is similar to that in case of argon at 600 kHz (See Table 4.1 in Chapter 4). However, this contradiction can be explained by the difference in hydrogen peroxide production pathways in the presence of argon and oxygen. Under argon saturated solutions, hydrogen peroxide is formed only by recombination of hydroxyl radicals ($\bullet OH + \bullet OH \rightarrow H_2O_2$) while in the case of oxygen and air, recombination of hydroperoxyl radicals ($\bullet HO_2 + \bullet HO_2 \rightarrow H_2O_2 + O_2$) also results in hydrogen peroxide formation. Under oxygen and air saturated solutions, hydroperoxyl radicals scavenge hydroxyl radicals available for phenol degradation ($\bullet OH + \bullet HO_2 \rightarrow H_2O + O_2$), thereby decreasing the phenol degradation rate.

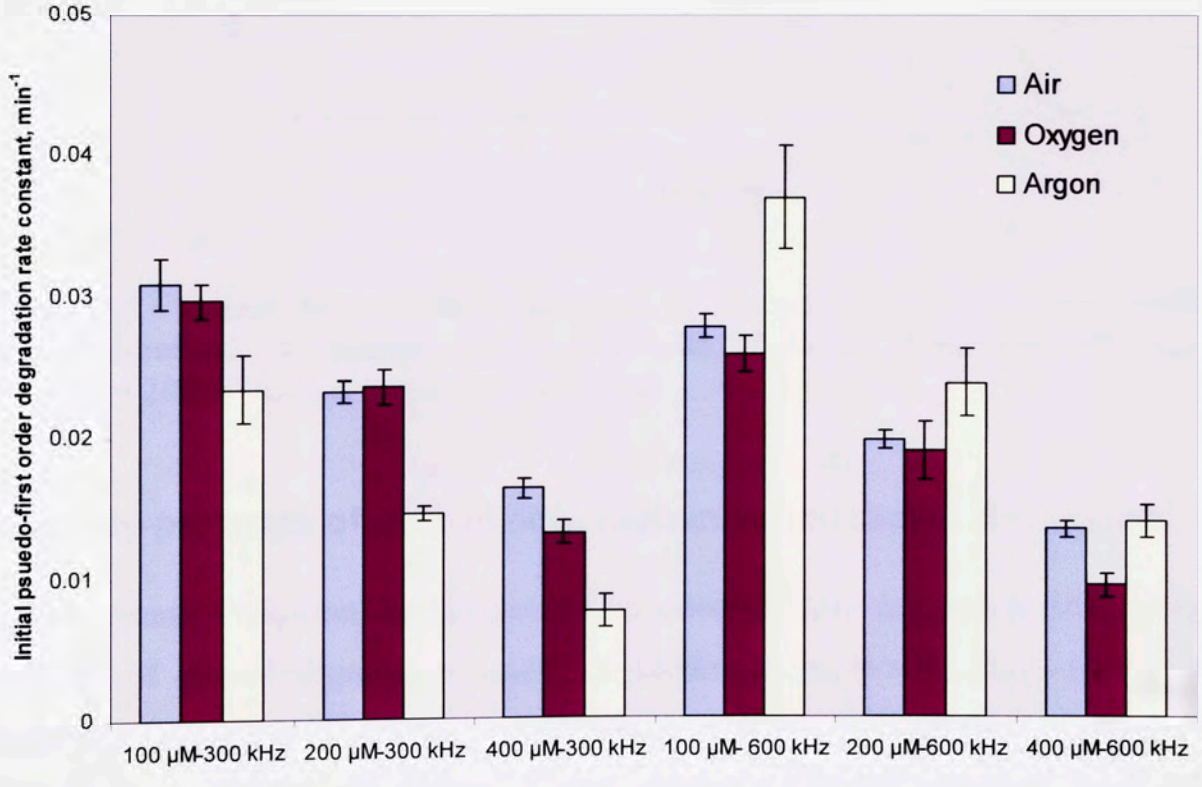

Figure 7.4 Summary of degradation rate of phenol by ultrasonic irradiation under different dissolved gases and frequencies.

Sonolytic degradation of phenol was completely inhibited by the addition of 1 % (*v/v*) *t*-butanol, a hydroxyl radical scavenger (Figure 7.5). This observation confirms that phenol degradation occurs due to its interaction with hydroxyl radical in the concentration range examined here. However it is to be noted that pyrolytic degradation may occur at higher concentrations of phenol (Serpone *et al.*, 1994, Petrier *et al.*, 1994, Rong *et al.*, 2002).

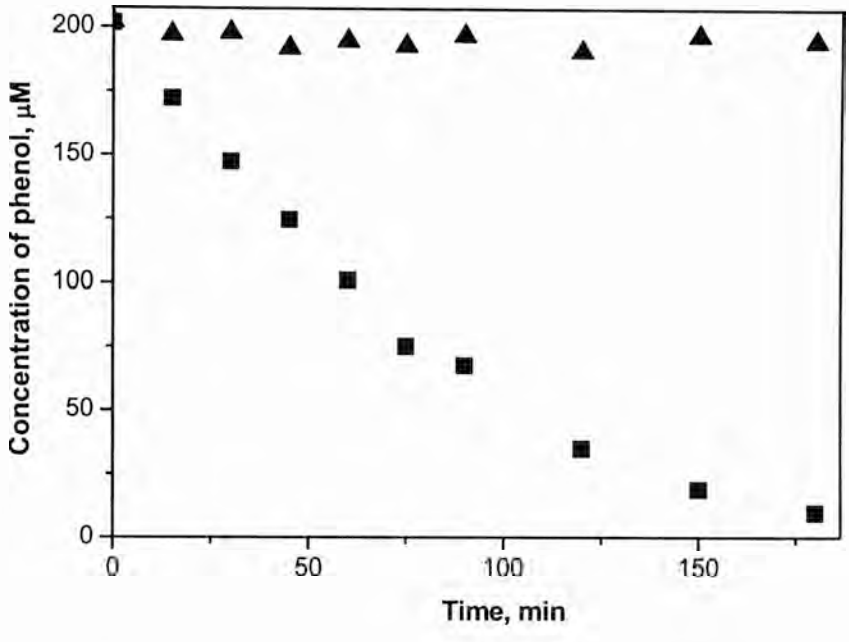

Figure 7.5 Phenol degradation in presence of *t*-butanol (■: phenol concentration without *t*-butanol, ▲: phenol concentration with *t*-butanol). Conditions: 600 kHz, [phenol] = 200µM and argon saturated solutions.

7.3.2 By-products of phenol degradation by ultrasonic irradiation

On ultrasound irradiation, hydroquinone and catechol were detected as primary by-products of phenol degradation under all conditions examined. These results are consistent with earlier published results (Serpone *et al.*, 1992, Petrier *et al.*, 1994, Timothy *et al.*, 2006). The highly reactive hydroxyl radicals and hydrogen atoms produced on ultrasonic irradiation can activate the phenol aromatic ring. It is well known that this effect is felt most strongly at the *ortho* and *para* positions. This fact is confirmed by our results which showed formation of hydroquinone and catechol but resorcinol was not detected.

As shown in Figures 7.6-7.8, the yield of by-products was different for different background gases. Catechol and hydroquinone were the dominant species for all background gases used in this study. While under argon saturated solution, the concentration of catechol is slightly higher than hydroquinone, the concentrations of hydroquinone and catechol formed are similar under oxygen saturated solutions.

Benzoquinone formation was detected only under air saturated solutions (Figure 7.8). The benzoquinone detected under air saturated solutions should be *p*-benzoquinone which is the dehydrated form of hydroquinone. *Ortho*-benzoquinone, which can be derived from catechol degradation, is fairly unstable and can easily cleave to form aliphatic compounds. Benzoquinone and dihydroxybenzenes are in redox equilibrium with the possibility of transformation between these species during sampling and HPLC analysis (Scheck and Frimmel, 1995). Also, *o*-benzoquinone standards were not available commercially which prevented us from confirming its formation by HPLC analysis. *p*-benzoquinone can rapidly react with hydrogen atom radical resulting in formation of hydroquinone (Serpone *et al.*, 1992) and hence higher yield of hydrogen atom radicals under oxygen and argon saturated solutions (see Chapter 4) can explain the lack of formation of hydroquinone under these conditions. Also, it is to be noted that the final pH was lower than the initial pH only under air saturated solutions which could be explained by the production of simple acids such as maleic or formic acid from degradation of quinones. The production of *p*-benzoquinone as an intermediate is also affected by the solution pH. It has previously been reported that no benzoquinone formation was detected above pH 3.5 (Serpone *et al.*, 1992). Under air saturated solutions, the concentration of catechol is much higher than that of other intermediates.

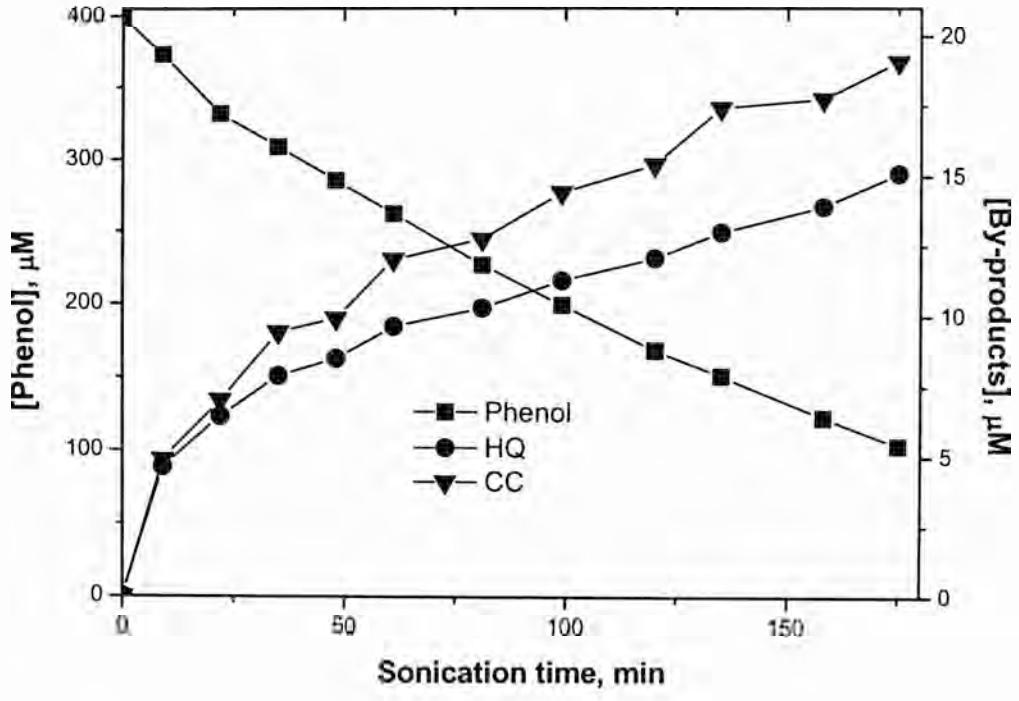

Figure 7.6 By-product formation on sonolytic degradation of phenol under argon saturated solutions. Experimental conditions: Phenol concentration = 400 µM, Frequency = 600 kHz, pH 3.5.

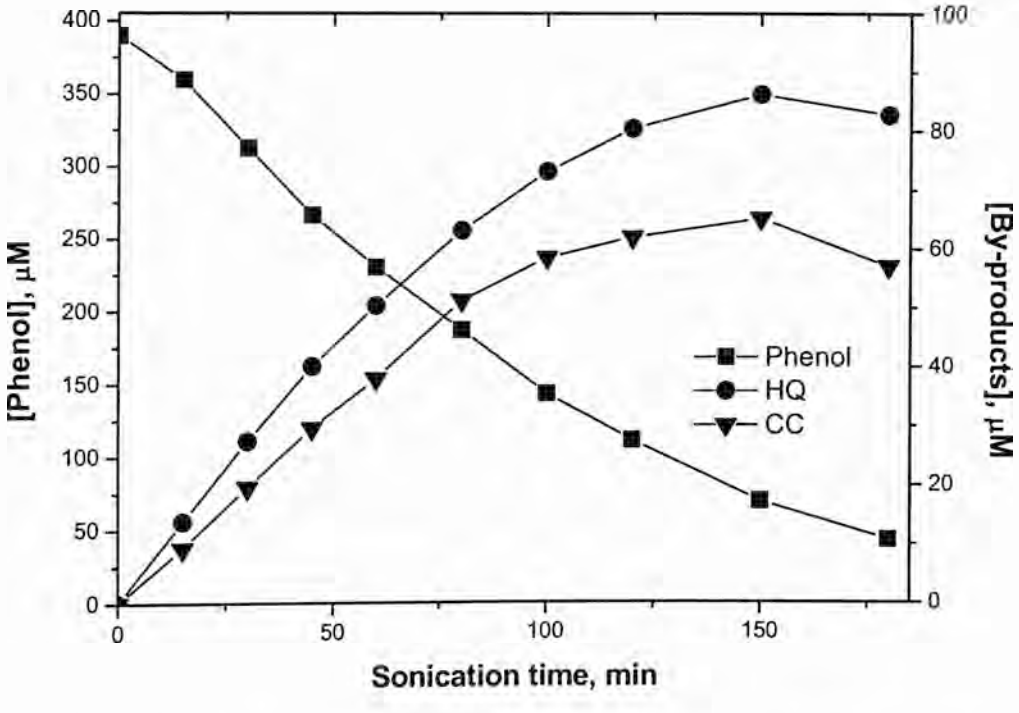

Figure 7.7 By-product formation on sonolytic degradation of phenol under oxygen saturated solutions. Experimental conditions: Phenol concentration = 400 µM, Frequency = 600 kHz, pH 3.5.

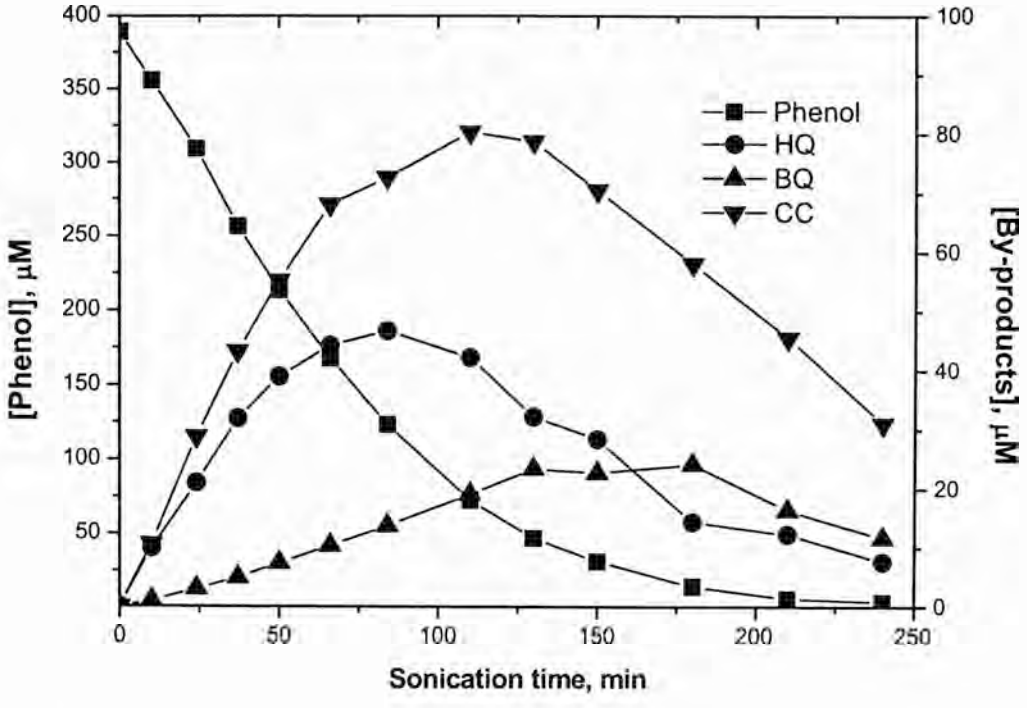

Figure 7.8 By-product formation on sonolytic degradation of phenol under air saturated solutions. Experimental conditions: Phenol concentration = 400 μM, Frequency = 600 kHz, pH 3.5.

7.3.3 Effect of initial phenol concentration

Experiments with different initial concentrations of phenol (20-1000 μM) were carried out at 300 kHz under air saturated solutions. Degradation of aqueous phenol solutions by ultrasonic irradiation exhibits pseudo-first-order reaction kinetics at all concentrations examined as shown in Figure 7.9. The pseudo-first order rate constants were calculated accordingly using the integrated form of the related rate equation:

$$\frac{C}{C_0} = e^{-kt} \qquad (1)$$

where C and C_0 are concentrations of phenol at time t and zero respectively, and k is the pseudo first order degradation rate constant. The variation in observed pseudo first order rate constant (k_{obs}) with respect to initial phenol concentration is presented in Figure 7.9. As shown, the pseudo-first-order rate constant of phenol degradation is dependent on initial phenol concentration with the rate constant decreasing with increasing initial

concentration of phenol. While complete degradation was achieved for 20μM of phenol in less than 60 min, only 20% was degraded over 60 mins in presence of 1000 μM phenol. The pseudo-first order rate constant decreased from 0.0623 min^{-1} for initial phenol concentration of 20 μM to a value of 0.0092 min^{-1} for initial phenol concentration of 1000 μM.

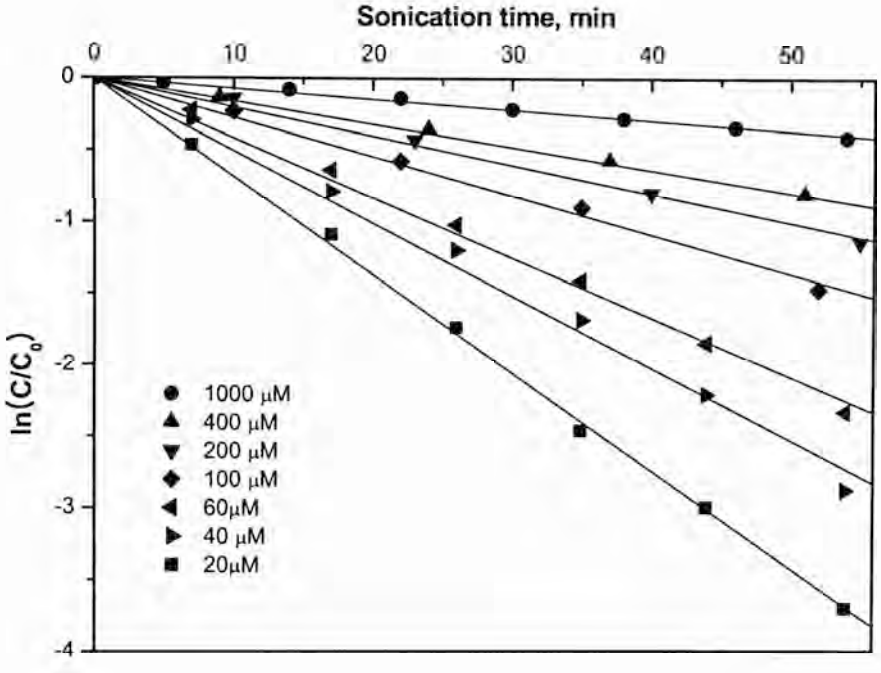

Figure 7.9 Degradation of phenol shown as $\ln(C/C_0)$ versus time at 300 kHz with 30 W (acoustic power) at pH 3.5. C represents the concentration of phenol at time t and C_0 represents the initial concentration of phenol.

The observed initial rate of decomposition is depicted in Figure 7.10 as the plot of $1/k_{obs}$ versus phenol concentration showing two distinct regimes:

For regime 1, at low concentration of phenol (< 100 μM),

$1/k_{obs} = 12.417 + 0.1923\ C_0$

For regime 2, at higher concentration of phenol (> 100 μM),

$1/k_{obs} = 25.843 + 0.0836\ C_0$

where, C_0 is the initial concentration of phenol.

Results that the rate constant for degradation of organic compounds by sonication decreases with increasing concentration of organic compound are consistent with findings of Serpone *et al.* (1994). They investigated 4-chlorophenol (4-CP) degradation by ultrasonic irradiation (frequency 20 kHz, power 50 W) in air saturated aqueous medium at relatively low initial 4-CP concentration (18.2 – 394 μM). They showed that at higher concentrations of 4-CP, the sonochemical degradation show saturation-type kinetics reminiscent of Langmuirian behaviour in solid/gas systems. They suggest that hydroxyl radical reaction with 4-chlorophenols takes place in the solution bulk at low concentrations, while at the higher concentrations the reactions occur predominantly at the interface.

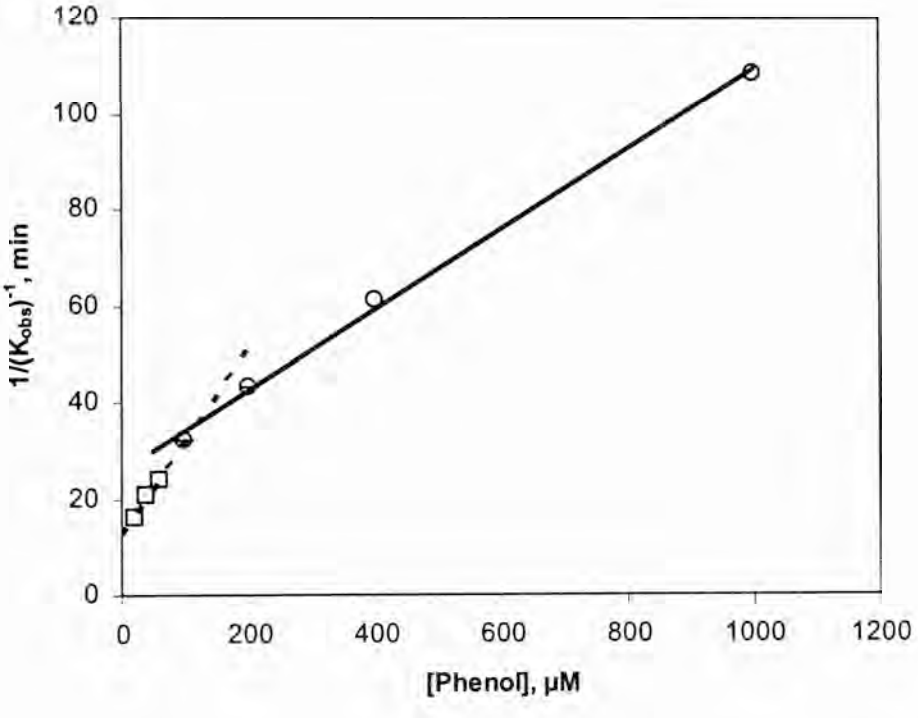

Figure 7.10 Effect of initial phenol concentration on sonochemical degradation of phenol.

7.3.4 Effect of pH on sonochemical degradation of phenol

The interfacial zone surrounding cavitational bubbles is negatively charged and hydrophobic(Serpone *et al.*, 1992, Tauber *et al.*, 2000). Hence neutral species of

hydrophilic compounds can more easily diffuse to, and accumulate at, the hydrophobic liquid-gas bubble interface suggesting that pH (which will influence the speciation of organic compounds if they possess acid/base properties) may affect the degradation rate of organic compounds. Many researchers (Kotronarou *et al.*, 1991, Okouchi *et al.*, 1992, Ku *et al.*, 1997) have observed that the degradation rate of target organic compounds by ultrasonic irradiation decreases with an increase in solution pH, while others (Wu *et al.*, 1992) showed that organic compounds degraded more rapidly at higher pH. The sonolytic degradation of phenol was examined at different pH values to determine the effect of pH on its degradation kinetics. The initial pH was adjusted by addition of appropriate volumes of 10 mM NaOH stock solution to 10 mM phosphate buffer. The experimental results of phenol degradation at three different pH values at 300 kHz under air saturated solution are summarized in Table 7.1. The profile of phenol degradation and by-products evolution overtime are shown in Figure 7.11 to 7.13.

Table 7.1 Effect of initial pH on phenol degradation rate by ultrasonic irradiation. Conditions : 300 kHz, air saturated solution and $[phenol]_o$ = 200 μM.

Initial pH	Pseudo-first order degradation rate constant (min^{-1})
pH 3.5	0.0190
pH 5.5	0.0176
pH 7.5	0.0182
pH 3.5 *	0.0226

* : phosphate buffer was not used ; initial pH was set by nitric acid

As shown in Table 7.1, pseudo-first order degradation rate constants were not significantly affected over the range of pH values used in this study. This observation can be explained by the fact that the protonated and uncharged form of phenol (pK_a = 9.99) is the dominant specie for pH ≤ 9, therefore, the rate constant of phenol degradation on sonication would be expected (as is observed) to be similar in the pH range of 3-8 examined here. This explanation is consistent with the results of an earlier study (Singla *et al.*, 2004) which showed that degradation of benzoic acid was favoured

at solution pH < pK_a of benzoic acid. At pH < pKa, benzoic acid was degraded both inside the bubble by pyrolysis and at the interface by the hydroxyl radical. At pH > pK_a, benzoic acid degradation occured due to its reaction with hydroxyl radicals only due to the low diffusivity of the deprotonated form of benzoic acid across the gas liquid interface.

As shown in Table 7.1, the initial pseudo first order degradation rate constant of phenol is higher in the absence of the phosphate buffer. This could be due to scavenging of hydroxyl radicals by phosphate species (Schmidt *et al.*, 1995, Howard and Meylan, 1997) as shown by the reactions below.

$$OH\bullet + PO_4^{3-} \rightarrow \text{product}, \qquad k < 1.0\times10^7\ M^1\ s^{-1} \qquad (2)$$

$$OH\bullet + HPO_4^{2-} \rightarrow \text{product}, \qquad k = 1.5\times10^5\ M^{-1}\ s^{-1} \qquad (3)$$

$$OH\bullet + H_2PO_4^- \rightarrow HO^- + H_2PO_4\bullet, \qquad k = 2.0\times10^4\ l\ M^{-1}\ s^{-1} \qquad (4)$$

$$OH\bullet + H_3PO_4 \rightarrow H_2O + H_2PO_4\bullet, \qquad k = 2.7\times10^6\ M^{-1}\ s^{-1} \qquad (5)$$

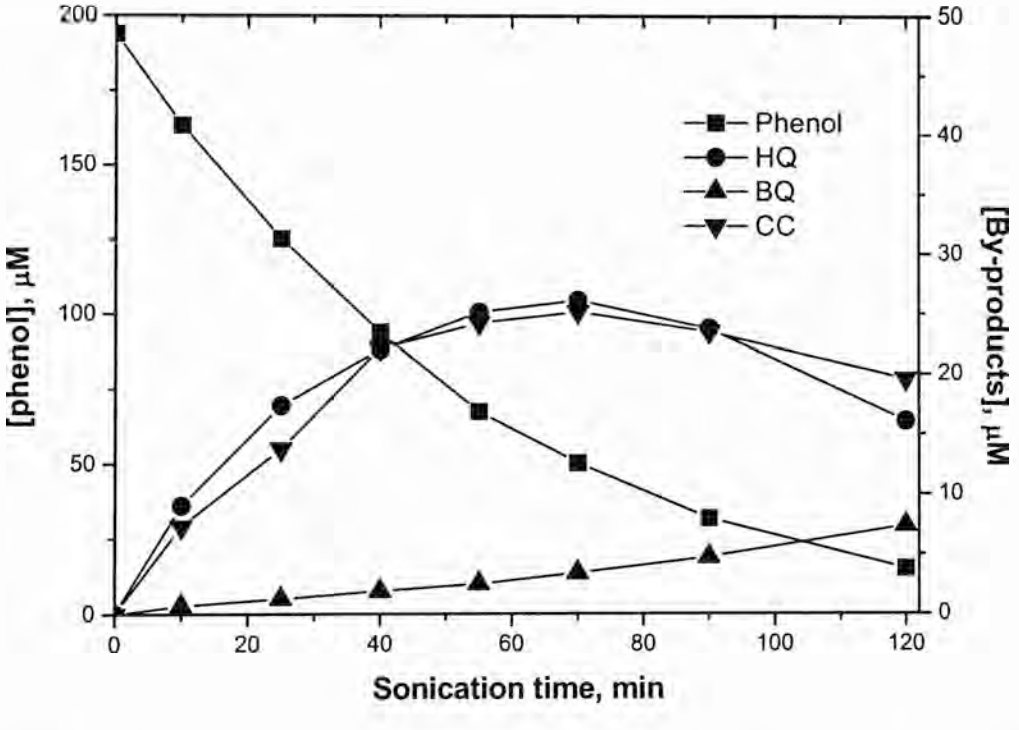

Figure 7.11 Sonolytic degradation of phenol at pH 3.5. Conditions: 300 kHz, 30 W(acoustic power), air saturated solutions (HQ: hydroquinone, BQ: benzoquinone, CC: catechol).

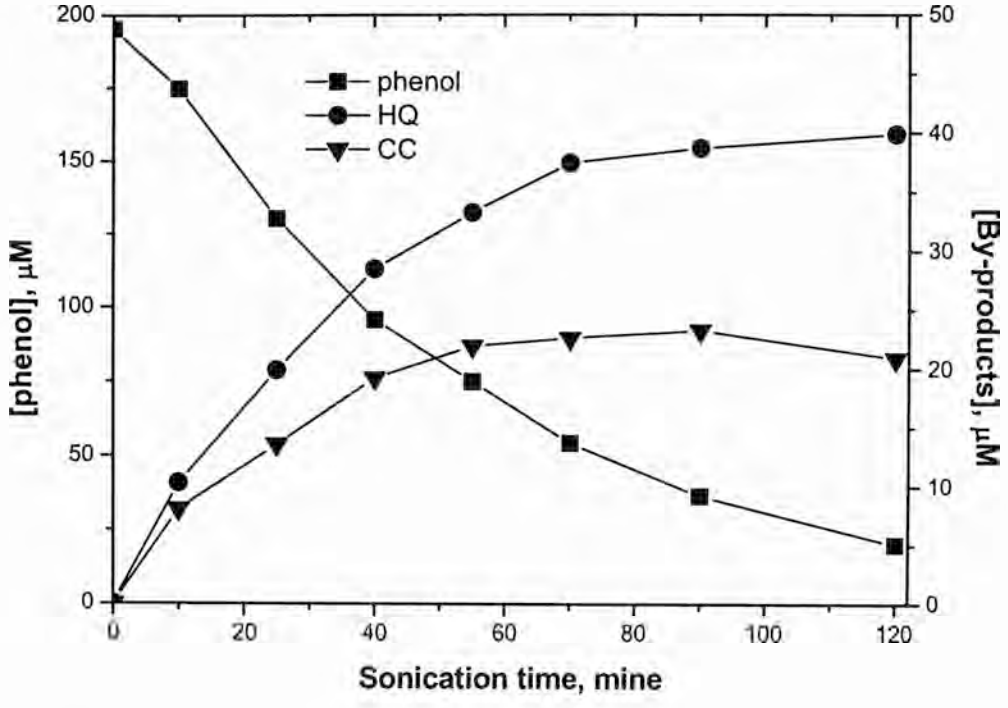

Figure 7.12 Sonolytic degradation of phenol at pH 5.5. Conditions: 300 kHz, 30 W(acoustic power), air saturated solution (HQ : hydroquinone, CC : catechol).

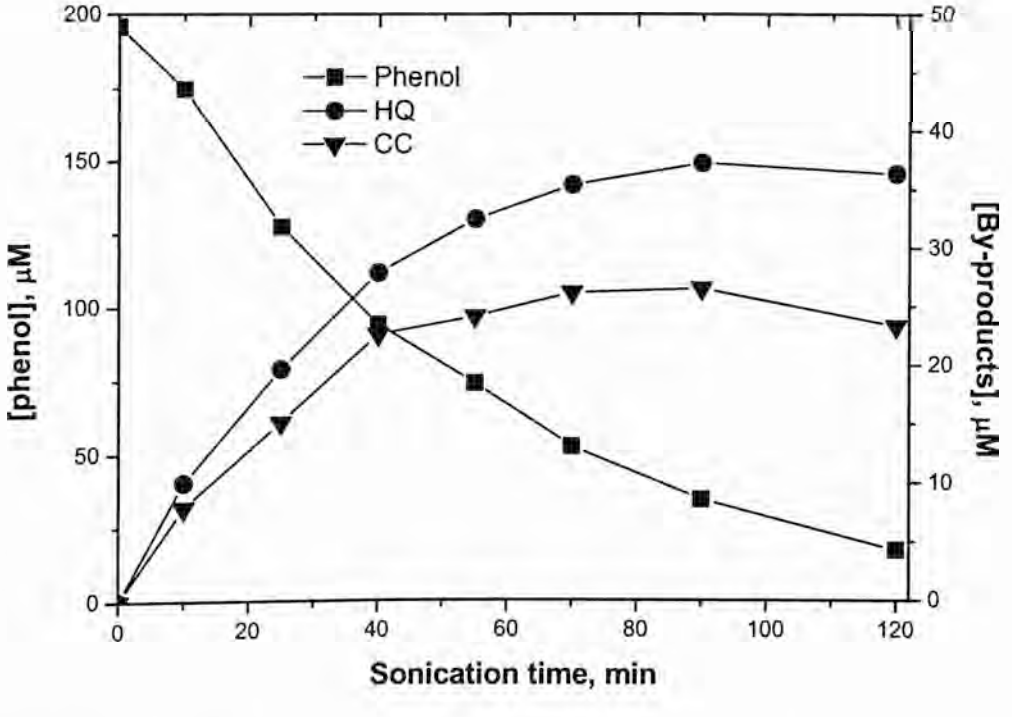

Figure 7.13 Sonolytic degradation of phenol at pH 7.5. Conditions: 300 kHz, 30 W(acoustic power), air saturated solution (HQ: hydroquinone, CC: catechol).

Hydroquinone (HQ) and catechol (CC) were detected as primary by-products in all cases except at pH 3.5. In addition to HQ and CC, benzoquinone (BQ) was also detected at pH 3.5 (see Figure 7.11) even though similar pseudo first order phenol degradation rate constants were observed at all pH values. As shown in Table 7.2, the yield of catechol is similar at all pHs examined; however the concentration of hydroquinone at initial pH 3.5 was 50% less than other conditions suggesting that hydroquinone easily decomposes to form benzoquinone under acidic conditions.

Table 7.2 Effect of pH on the concentration of hydroquinone and catechol produced on sonolysis after 2 hours ($[phenol]_0$ = 200 μM). Condition : 300 kHz, 30W, air saturated solutions.

Initial pH	[Hydroquinone], μM	[Catechol], μM	The ratio of hydroquinone/Catechol
3.5	16.11	19.6	0.82
5.5	39.91	20.89	1.91
7.5	36.36	23.34	1.56

7.3.5 Effect of acoustic power on phenol degradation

When acoustic power increases, it simultaneously increases the amplitude of vibration, the maximum radius of the bubble as well as its collapse time thereby affecting free radical generation. The effect of acoustic power on hydrogen peroxide formation and phenol degradation was investigated at 300 kHz under air saturated solutions. As shown in Figure 7.14, hydrogen peroxide formation and phenol degradation rate increased with increasing acoustic power. These results are consistent with the earlier reports (Gutierrez and Henglein, 1990, Entezari *et al.*, 1997) which showed that as the power increases, the reaction rate increases to a maximum and then decreases with continued increase in power. However, it should be noted that the optimum acoustic power is also dependent on the frequency applied (Whillock and Harvey, 1997b).

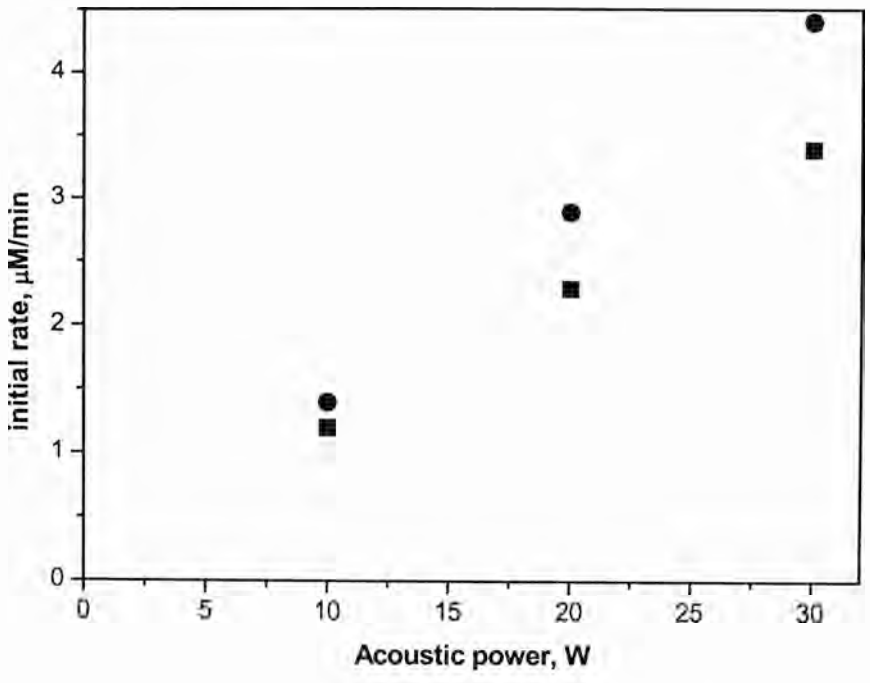

Figure 7.14 Effect of acoustic power on phenol degradation rate and hydrogen peroxide formation rate (● : hydrogen peroxide formation rate, ■ : phenol decomposition rate). Conditions: 300 kHz, pH 3.5, air saturated solution.

7.3.6 Effect of Fe(II) addition on phenol degradation

7.3.6.1 Effect of initial Fe(II) concentration

As shown in Chapter 6, ferrous iron addition can increase generation of hydroxyl radicals by Fenton's reaction :

$$Fe(II) + H_2O_2 \rightarrow Fe(III) + OH\bullet + OH^- \quad (6)$$

The sonolytic degradation of phenol in the presence of Fe(II) was performed under air-saturated solutions at pH 3.5. As shown in Table 7.3, the pseudo-first order degradation rate constant of phenol by ultrasonic irradiation significantly increased in the presence of Fe(II) presumably due to increased yield of hydroxyl radicals through the Fenton reaction (Joseph *et al.*, 2000, Jiang and Waite, 2003). A maximum increase in the measured pseudo-first order degradation rate constant was observed in the presence of 300 μM Fe(II). However, the rate constants slowly decreased with the

increased in Fe(II) to higher concentration due to the scavenging of hydroxyl radicals by the added Fe(II).

Table 7.3 Pseudo-first order degradation rate constant of phenol in the presence of Fe(II).

Concentration of Fe(II)	Psuedo-first order degradation rate constants, min^{-1}	$t_{(1/2)}$, min
0	0.0226	30.67
100	0.0334	20.75
300	0.0371	18.68
500	0.0363	19.09
700	0.0346	20.03
1000	0.0339	20.45

Conditions: 300 kHz, 30 W(acoustic power), pH 3.5, phenol concentration 200 μM, air saturated solutions.

7.3.7 Mathematical modelling of phenol degradation kinetics

The kinetics of phenol degradation was modelled by combining the mathematical model for hydroxyl radical generation (proposed in Chapter 5) with the reactions of hydroxyl radicals with phenol and its by-products as shown in Table 7.4. Mathematical model results were obtained and compared to experimental data collected at 300 kHz for 200 μM of initial phenol concentration under argon saturated solutions (see Figure 7.15). Free radical reactions and their rate constants shown in Table 7.4 are the same as those used in Chapter 5 to model the hydrogen peroxide formation at 300 kHz under argon saturated solutions. Reactions for phenol degradation due to its interaction with hydroxyl radicals are shown in Table 7.5. As in the case of formic acid degradation, we have assumed that phenol slowly diffuses into the interface and phenol degradation occurs both in the bulk solution as well as at the interface. Phenol is decomposed by hydroxyl radicals leading to formation of hydroquinone (reactions 14 and 26) and catechol (reactions 15 and 27) as primary intermediates (Timothy et al., 2006). Hydroquinone and catechol can be further degraded by hydroxyl radicals to produce p-

benzoquinone and o-benzoquinone respectively (reactions 16, 17, 25 and 26). Further oxidation of benzoquinone by hydroxyl radicals produces unsaturated carboxylic acids (reactions 18 and 27) such as muconic snd maleic acids (Berlan *et al*, 1994, Timothy *et al.*, 2006). The diffusion rate constants for phenol and its intermediates were determined based on best fit model results. The diffusion rate constant of benzoquinone cannot be determined because benzoquinone formation was not detected under argon saturated solutions. As shown in Figure 7.15, the model results show a good fit to phenol degradation and its by-product formation under argon saturated solutions.

The model also provides a good fit to phenol degradation rates under oxygen and air saturated solutions with appropriate changes to rate constants for the initiation reaction and diffusion reaction of radical and organic compounds. However, the model over-predicts the hydroquinone and catechol formation rate over time under these conditions. This is probably due to some missing sink reactions for hydroquinone and catechol which are not included in the model for e.g. comproportionation reaction of hydroquinone (HQ) (eq 7) resulting in formation of semiquinone radicals (SQ) which in turn oxidize to benzoquinone(BQ) in the presence of oxygen (eq 8) (Chen and Pignatello, 1997); i.e.

$$HQ + BQ \rightarrow \bullet SQ + \bullet SQ \quad (7)$$

$$SQ + O_2 \rightarrow BQ + \bullet HO_2 \quad (8)$$

Furthermore, the hydroperoxy radical (formed under air and oxygen saturated solutions) can also oxidize hydroquinone and catechol (Bieleski *et al* , 1985).

Table 7.4 Model reactions for phenol degradation under argon saturated solutions at 300 kHz.

No	Reaction	Rate constant	Reference
Reaction in the bubble			
1	$H_2O \rightarrow \bullet OH + \bullet H \rightarrow \bullet OH(i) + \bullet H(i)$	6.2×10^{-7} s^{-1}	In this study
Reactions at the interface			
2	$\bullet OH(i) + \bullet OH(i) \rightarrow H_2O_2(i)$	5.2×10^{9} M^{-1} s^{-1}	Buxton *et al.*, 1988

3	$\bullet H(i) + \bullet H(i) \rightarrow H_2$	$7.8\times10^{9}\ M^{-1}\ s^{-1}$	Buxton *et al.*, 1988
4	$\bullet OH(i) + \bullet H(i) \rightarrow H_2O$	$7.0\times10^{9}\ M^{-1}\ s^{-1}$	Buxton *et al.*, 1988
5	$H_2O_2(i) + \bullet H(i) \rightarrow \bullet OH(i) + H_2O$	$9.0\times10^{7}\ M^{-1}\ s^{-1}$	Buxton *et al.*, 1988
6	$\bullet OH(i) + H_2O_2(i) \rightarrow \bullet HO_2(i) + H_2O$	$3.3\times10^{7}\ M^{-1}\ s^{-1}$	Buxton *et al.*, 1988
7	$\bullet OH(i) \rightarrow \bullet OH(b)$	$1.8\times10^{-2}\ s^{-1}$	In this study
8	$H_2O_2(i) \rightarrow H_2O_2(b)$	$2.0\times10^{-3}\ s^{-1}$	In this study
Reactions in the bulk solution			
9	$\bullet OH(b) + \bullet OH(b) \rightarrow H_2O_2(b)$	$5.2\times10^{9}\ M^{-1}\ s^{-1}$	Buxton *et al.*, 1988
10	$\bullet H(b) + \bullet H(b) \rightarrow H_2(b)$	$7.8\times10^{9}\ M^{-1}\ s^{-1}$	Buxton *et al.*, 1988
11	$\bullet OH(b) + \bullet H(b) \rightarrow H_2O$	$7.0\times10^{9}\ M^{-1}\ s^{-1}$	Buxton *et al.*, 1988
12	$\bullet OH(b) + H_2O_2(b) \rightarrow \bullet HO_2(b) + H_2O$	$3.3\times10^{7}\ M^{-1}\ s^{-1}$	Buxton *et al.*, 1988
13	$H_2O_2(b) + \bullet H(b) \rightarrow \bullet OH(b) + H_2O$	$9.0\times10^{7}\ M^{-1}\ s^{-1}$	Buxton *et al.*, 1988

Table 7.5 Reactions showing phenol degradation by ultrasonic irradiation.

No	Reaction	Rate constant	reference
Reactions occurring at interface			
14	Phenol(i) + •OH(i) → Hydroquinone(i)	$3.0\times10^{8}\ M^{-1}\ s^{-1}$	Walling, 1975
15	Phenol(i) + •OH(i) → Catechol(i)	$7.3\times10^{9}\ M^{-1}\ s^{-1}$	Walling, 1975
16	Hydroquinone(i) + •OH(i) →p-Benzoquinone(i)	$5.2\times10^{9}\ M^{-1}\ s^{-1}$	Buxton *et al.*, 1988
17	Catechol(i) + •OH(i) → o-Benzoquinone(i)	$1.1\times10^{10}\ M^{-1}\ s^{-1}$	Buxton *et al.*, 1988
18	p-Benzoquinone(i) + •OH(i) → acid(i)	$8.3\times10^{9}\ M^{-1}\ s^{-1}$	Buxton *et al.*, 1988
19	o-Benzoquinone(i) + •OH(i) → acid(i)	$8.3\times10^{9}\ M^{-1}\ s^{-1}$	Buxton *et al.*, 1988
20	Hydroquinone(i) → Hydroquinone(b)	$12\ s^{-1}$	In this study
21	Catechol(i) →Catechol(b)	$34\ s^{-1}$	In this study
22	p-Benzoquinone(i) → p-Benzoquinone(b)	ND	
23	o-Benzoquinone(i) → o-Benzoquinone(b)	ND	
24	acid(i) → acid(b)	$2\ s^{-1}$	In this study
Reactions occurring in the bulk solution			
25	Phenol(b) → Phenol(i)	$2.6\times10^{-4}\ s^{-1}$	In this study
26	Phenol(b) + •OH(b) → Hydroquinone(b)	$3.0\times10^{8}\ M^{-1}\ s^{-1}$	Walling, 1975
27	Phenol(b) + •OH(b) → Catechol(b)	$7.3\times10^{9}\ M^{-1}\ s^{-1}$	Walling, 1975
28	Hydroquinone(b) + •OH(b) → Benzoquinone(b)	$5.2\times10^{9}\ M^{-1}\ s^{-1}$	Buxton *et al.*, 1988
29	Catechol(b) + •OH(b) → Benzoquinone(b)	$1.1\times10^{10}\ M^{-1}\ s^{-1}$	Buxton *et al.*, 1988
30	Benzoquinone(i) + •OH(i) → acid(i)	$8.3\times10^{9}\ M^{-1}\ s^{-1}$	Buxton *et al.*, 1988

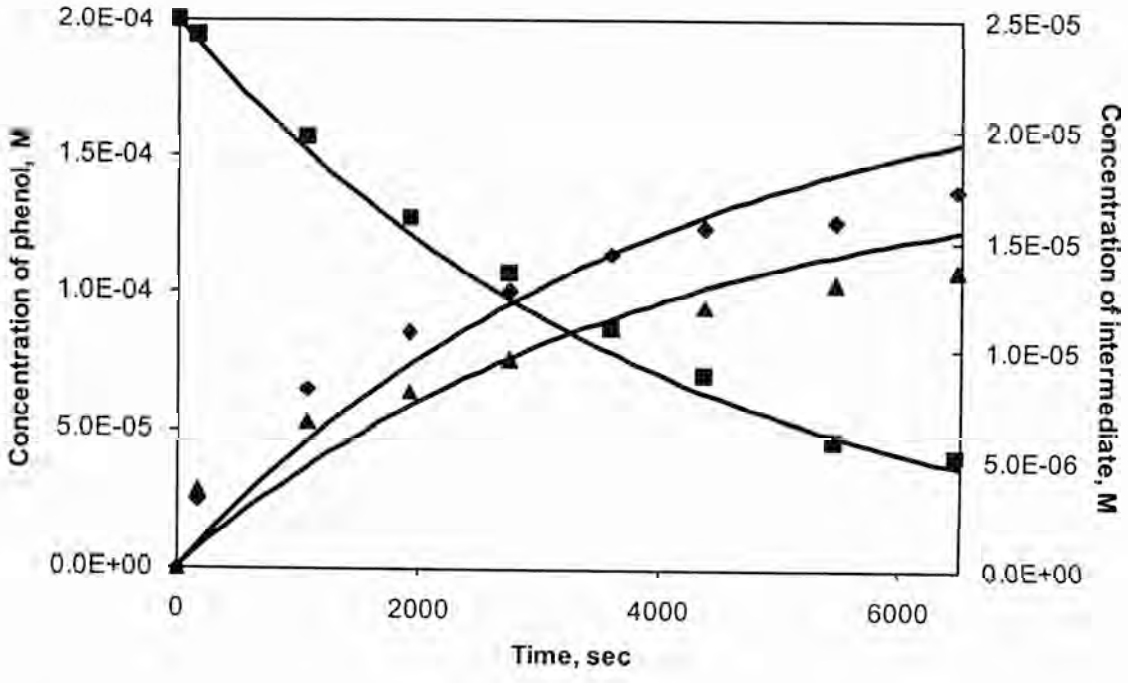

Figure 7.15 Observed and predicted profile of phenol degradation and intermediates formation by ultrasonic irradiation. Conditions : 300 kHz, 30 W(acoustic power), pH 3.5, 200 μM of phenol, and argon saturated. Solid line and closed symbol represent observed and predicted profile of phenol and intermediates (■ : phenol, ▲ : hydroquinone ● : catechol)

The effect of initial concentration of phenol on phenol degradation kinetics may be examined using the proposed model. As noted earlier, the first order rate constant for phenol degradation decreases in a biphasic manner with increase in pohenol concentration with a transition at about 100 μM phenol from rapid reduction in rate constant with increase in phenol concentration for $[phenol]_o$ < 100 μM to a slower reduction for $[phenol]_o$ > 100 μM (see Figure 7.10). Simulation using the proposed model does show a reduction in degradation rate constant with increasing initial concentration of phenol with this change occurring because of increasing back diffusion of phenol from the interface to bulk solution. Indeed, as shown in Figure 7.16, the predicted phenol degradation rate constants at low initial phenol concentrations are reasonably similar to those measured. However, the model suggests a significantly lower effect of phenol concentration on degradation rate than is actually observed with this difference particularly evident at high initial phenol concentrations. No attempt has

been made to rationalise this effect further given the complexity of the phenol degradation mechanism, particularly at high phenol concentrations where the intermediates that are formed may compete strongly with phenol for hydroxyl radicals.

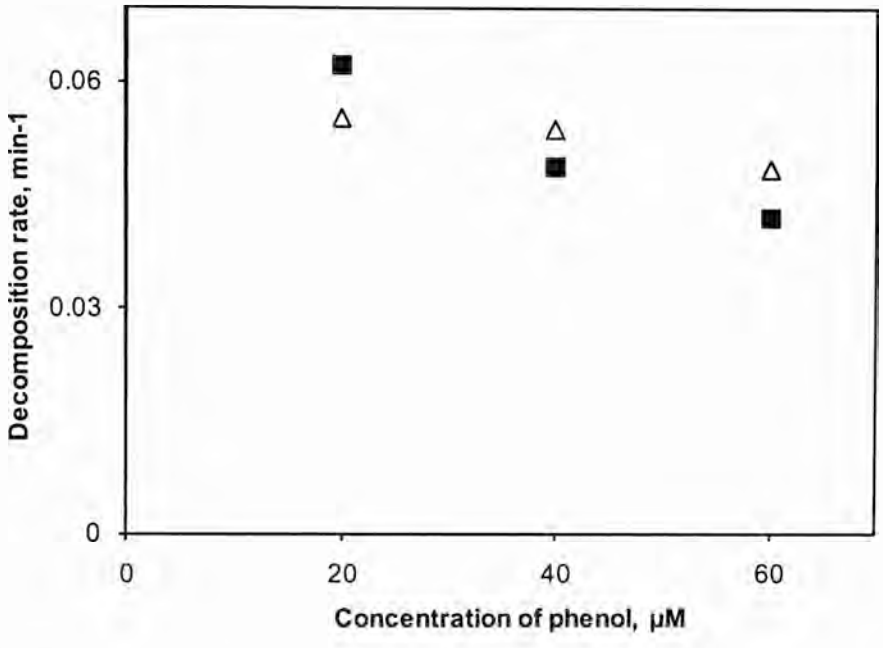

Figure 7.16 Concentration dependence profile on decomposition rate at low concentration range from 20 μM to 60 μM (■ : decomposition rate observed Δ: decomposition rate simulated). Condition : 300 kHz, 30 W(acoustic power), pH 3.5, and air saturated solutions.

We also modelled the effect of Fe(II) addition on phenol degradation under air saturated solutions. As proposed in Chapter 6, Fenton-like reactions mediated by Fe(II) are expected to occur in the bulk solution. Reactions for the redox cycling of iron in the presence of free radicals that are used here are the same as those used in Chapter 6. The rate constant for the initiation reaction and the diffusion rate constant of free radicals that are used here are the same as those proposed for use under nitrogen saturated solutions because the physical properties (solubility, specific heat ratio and thermal conductivity) of both gases are quite similar. In this case, the diffusion rate of phenol is simulated as 3×10^{-4} sec^{-1} through best fitting to the obtained data. The model determined phenol degradation rates in the presence of various concentrations of Fe(II) are shown

in Figure 7.17. The model shows that there is no significant increase in phenol degradation rate by Fenton-like reactions at the phenol concentrations examined here.

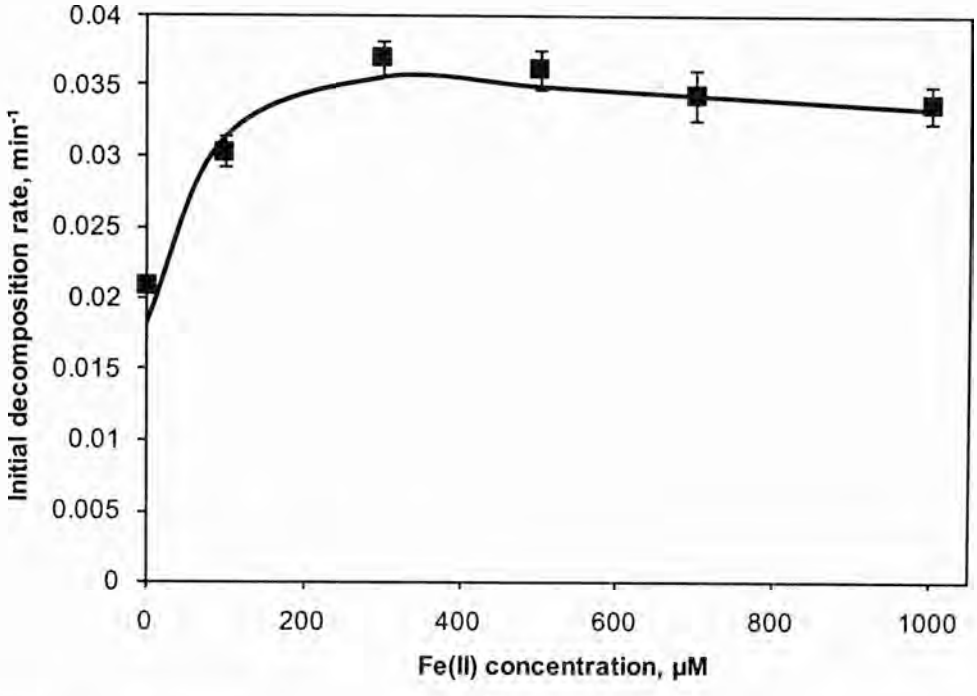

Figure 7.17 Effect of Fe(II) addition on phenol degradation under air saturated at 300 kHz. Solid line and closed symbols represent the model prediction and experimental data. Condition : 300 kHz, 30 W(acoustic power), pH 3.5, air saturated solutions, and 200 μM of phenol.

7.4 Conclusion

In this chapter, the effect on sonolytic degradation of phenol of various parameters such as frequency, dissolved gas, initial pH and initial concentration of phenol have been investigated. Phenol degradation followed the pseudo first order kinetics at all conditions examined. The maximum phenol degradation by ultrasonic irradiation was observed at 300 kHz under air saturated solutions and 600 kHz under argon saturated solutions. The experimental results of phenol degradation in the presence of scavenger (tert-butanol) support the conclusion that phenol is decomposed by the hydroxyl radical generated by ultrasound irradiation. Hydroquinone and catechol have been identified as the major intermediates under all conditions examined. The effect of solution pH in the

range 3-8 was not significant on sonolytic degradation of phenol. This clearly shows that ionized organic molecules are relatively difficult to accumulate at the interface, since uncharged forms of phenol dominate in solution as well as at interface in the pH range examined. The degradation of phenol was enhanced in the presence of Fe(II) with the maximum increase observed in the presence of 300 μM of Fe(II).

A free radical reaction mechanism for phenol degradation at the interface and in the bulk solution is proposed and a kinetic model developed. The proposed model satisfactorily predicts the effect of sonolysis on the concentration profile of phenol and its by-products under argon saturated solutions. Model predictions were carried out assuming that the diffusion of phenol and intermediates to the interface. The success of the kinetic model supports the conclusion that phenol degradation occurs both at the interface and in bulk solution. The kinetic model also satisfactorily describes the effect of Fe(II) on phenol degradation with an enhancement in degradation rate at low Fe(II) concentrations. It should be noted that the model reactions were simplified considerably by ignoring the formation and fate of potentially important species such as phenoxyl radical and dicyclodihexadienyl radical intermediates. However, despite these simplifications the model results still provide useful insight into the reaction mechanism of phenol degradation by ultrasonic irradiation under the conditions used in this study.

Chapter 8

Summary and Conclusions

A comprehensive set of experiments has been undertaken using a simple, well-defined model system over a range of operating conditions in order to gain added insight into the key free radical reactions occurring on sonolysis of solutions containing low concentrations of target organic compounds. Based on the experimental results obtained and our knowledge of likely free radical processes operating in such systems, a relatively simple kinetic model that reasonably accounts for most of the results obtained has been developed.

In particular, the formation of hydrogen peroxide, an entity that provides indirect evidence of the formation of hydroxyl radicals, has been investigated over a range of conditions including three ultrasonic frequencies and different dissolved gases. Through the analysis of the experimental results obtained, the effect of physical properties on hydrogen peroxide formation rate and hydrogen peroxide formation mechanism has been examined. The minimal effect of hydrogen peroxide addition on hydrogen peroxide formation rate suggests that the presence of hydrogen peroxide in the bulk solution results from diffusion of hydrogen peroxide from the bubble interfaces where it is formed by recombination of free radicals. Free radicals (hydroxyl, hydrogen atom, and hydroperoxyl radicals) may diffuse to some extent into the bulk solution leading to reactions with species present in the bulk though it is expected that the extent of diffusion will be limited due to the high reactivity of these species. Formic acid degradation and its degradation mechanism by ultrasonic irradiation were also investigated at different frequencies and dissolved gases. Effects of hydroxyl radical

scavengers (t-butanol and phenol) on formic acid degradation suggest that formic acid degradation by ultrasonic irradiation occurs principally at the interface.

As noted above, a kinetic model has been developed which describes hydrogen peroxide formation and formic acid degradation on ultrasonic irradiation. The model provides excellent fits to our experimental data under all conditions investigated. The model also identifies the important reactions controlling hydrogen peroxide formation and formic acid degradation. Hydrogen peroxide formation is shown to be controlled by recombination of hydroxyl radicals and, in the presence of oxygen, hydroperoxyl radicals. Under all conditions investigated, the water decomposition reaction and diffusion of hydrogen peroxide from the bubble interface to the bulk solution are the key reactions controlling hydrogen peroxide formation.

The model also shows that reaction of formic acid with hydroxyl radicals at both the interface and in the bulk solution are key to its degradation. The rate of formic acid degradation is controlled by diffusion of formic acid from bulk solution to bubble interfaces. Slow diffusion rate of formic acid from bulk solution to bubble interfaces explains the slow decomposition rate of formic acid observed experimentally. This result also supports the observation of no effect of formic acid addition on hydrogen peroxide formation.

The effect of ferrous iron addition on formic acid degradation and hydrogen peroxide production by ultrasonic irradiation has also been investigated in this study and, at pH 3.5, found to increase the rate of formic acid degradation by a factor of up to 3 under argon and oxygen saturated solutions. The effect of ferrous iron addition on formic acid degradation was shown to be minor under air saturated solutions, possibly as result of hydroxyl radical scavenging by nitrogen species. Addition of Fenton reactions to the kinetic model developed earlier was found to give reasonable predictions of the effect of Fe(II) addition under argon and oxygen saturation. The ability of the model to describe the results obtained suggested that higher rate constants for formic acid degradation in the presence of oxygen could be accounted for due to i) enhancement of the extent of iron redox cycling as a result of the hydroperoxyl radical-mediated reduction of Fe(III) and ii) the presence of higher hydrogen peroxide concentrations.

While the mechanism of sonolytic degradation of phenol is considerably more complex than that of formic acid, a model similar to that used to describe formic acid degradation was found to give a reasonable description of phenol degradation, at least at low phenol concentrations. At high phenol concentrations (>100 μM), complexities due to the intermediates formed preclude reliable modeling, at least within the constraints of this project.

Further refinement of the model developed here could be envisaged with scope for more elaborate account to be taken of temperature effects at the bubble interfaces where the bulk of the free radical reactions described in this work are likely to occur. Additionally, it is recommended that more work be undertaken using simple probe organic molecules to further clarify the key processes involved in degradation.

While not within the charter of this thesis, it would also be of interest to examine the cost of scale-up of sonolysis technology in order to assess the possibility of full scale implementation. While the complexity of the reactors required and the power costs associated with this technology may limit its use for treatment of large volumes of water, application for batch treatment of small volumes of waste (e.g., ballast water treatment on ships, treatment of in-house wastewater prior to reuse, pre-treatment of industrial wastes prior to biological treatment) would seem worthy of further investigation.

REFERENCES

ABDELSALAM, M. E. & BIRKIN, P. R. (2002) A Study Investigating the Sonoelectrochemical Dedradation of an Organic Compound Employing Fenton's Reagent. *Physical Chemistry Chemical Physics,* **4**, 5340-5345.

ABU-HASSAN, M. A., KIM, J. K., METCALFE, I. S. & MANTZAVINOS, D. (2006) Kinetics of Low Frequency Sonodegradation of Linear Alkylbenzene Sulfonate Solutions. *Chemosphere,* **62**, 749-755.

ADAMS, G. E., BOAG, J. W., CURRANT, J. & MICHEAL, B. D. (1965) *Pulse Radiolysis,* New York, Academic Press.

ADEWUYI, Y. G. (2001) Sonochemistry: Environmental Science and Engineering Applications. *Industrial & Engineering Chemistry Research,* **40**, 4681-4715.

ADEWUYI, Y. G. (2005) Sonochemistry in Environmental Remediation. 1. Combinative and Hybrid Sonophotochemical Oxidation Processes for the Treatment of Pollutants in Water. *Environmental Science and Technology,* **39**, 3409-3420.

ADEWUYI, Y. G. & OWUSU, S. O. (2006) Ultrasound-induced aqueous removal of nitric oxide from flue gases; Effects of sulfur dioxide, chloride, and chemical oxidant. *J. Phys. Chem. A,* **110**, 11098-11107.

ALLEN, A. O., HOCHANADEL, C. J., GHORMLEY, J. A. & DAVIS, T. W. (1952) Decomposition of Water and Aqueous Solutions Under Mixed Fast Neutron and Gamma Radiation. *Journal of Physical Chemistry,* **56**, 575-586.

ALNAIZY, R. & AKGERMAN, A. (2000) Advanced Oxidation of Phenolic Compounds. *Advances in Environmental Research,* **4**, 233-244.

ANBAR, M. & PECHT, I. (1964) On the Sonochemical Formation of Hydrogen Peroxide in Water. *The Journal of Physical Chemistry,* **68**, 352-355.

ASHOKKUMAR, M. & GRIESER, F. (1999) Ultrasound Assisted Chemical Processes. *Reveiws in Chemical Engineering,* **15**, 41-83.

ASHOKKUMAR, M., MULVANEY, P. & GRIESER, F. (1999) The Effect of pH on Multibubble Sonoluminescence from Aqeous Solutions Containing Simple Organic Weak Acids and Bases. *Journal of Americal Chemical Society,* **121**, 7355-7359.

ATKINS, P. W. (1995) *Physical Chemistry,* Oxford, UK, Oxford University Press.

AYYILDIZ, O., PETERS, R. & ANDERSON, P. (2007) Sonolytic Degradation of Halogenated Organic Compounds in Groundwater: Mass Transfer Effects. *Ultrasonics Sonochemistry,* **14**, 163-172.

BADER, H., STURZENEGGER, V. & HOIGNE, J. (1988) Photometric Method for the Determination of Low Concentrations of Hydrogen Peroxide by the Peroxidase Catalyzed Oxidation of N,N-Diethyl-p-Phenylenediamine(DPD). *Water Research,* **22**, 1109-1115.

BAPAT, P. S., GOGATE, P. R. & PANDIT, A. B. (2008) Theoretical Analysis of Sonochemical Degradation of Phenol and its Chloro-Derivatives. *Ultrasonics Sonochemistry,* **15**, 564-570.

BARBIER, P. F. & P TRIER, C. (1996) Study at 20 kHz and 500 kHz of the Ultrasound-Ozone Advanced Oxidation System: 4-Nitrophenol Degradation. *Journal of Advanced Oxidation Technology,* **1**, 154-159.

BECKETT, M. A. & HUA, I. (2000) Elucidation of the 1,4-Dioxane Decomposition Pathway at Discrete Ultrasonic Frequencies. *Environmental Science and Technology,*

34, 3944-3953.

BECKETT, M. A. & HUA, I. (2001) Impact of Ultrasonic Frequency on Aqueous Sonoluminescence and Sonochemistry. *Journal of Physical Chemistry A,* 2001, 3796-3802.

BECKETT, M. A. & HUA, I. (2003) Enhanced Sonochemical Decomposition of 1,4-Dioxane by Ferrous Iron. *Water Research,* **37**, 2372-2376.

BEHNAJADY, M. A., MODIRSHAHLA, I. N., TABRIZI, S. B. & MOLANEE, S. (2008) Ultrasonic Degradation of Rhodamine B in Aqueous Solution: Influence of Operational Parameters. *Journal of Hazardous Materials,* **152**, 381-386.

BERLAN, J., TRABELSI, F., DELMAS, H., WILHELM, A. M. & PETRIGNANI, J. F. (1994) Oxidative Degradation of Phenol in Aqueous Media Using Ultrasound. *Ultrasonics Sonochemistry,* **1**, S97-S102.

BRAUN, W., HERRON, J. T. & KAHANER, D. K. (1988) ACUCHEM: A computer program for modeling complex chemical reaction systems. *International Journal of Chemical Kinetics,* **20**, 51-60.

BROTCHIE, A., GRIESER, F. & ASHOKKUMAR, M. (2008) Sonochemistry and Sonoluminescence under Dual-Frequency Ultrasound Irradiation in the Presence of Water-Soluble Solutes. *Journal of Physical Chemistry. C,* **112**, 10247 -10250.

BUXTON, G. V., GREENSTOCK, C. L., HELMAN, W. P. & ROSS, A. B. (1988) Critical Review of Rate Constants for Reactions of Hydrated Electrons, Hydrogen Atoms and Hydroxyl Radicals in Aqueous Solution. *Journal of Physical and Chemical Reference Data,* **17**, 513-886.

CHEN, R. & PIGNATELLO, J. J. (1997) Role of Quinone Intermediates as Electron Shuttles

in Fenton and Photoassisted Fenton Oxidations of Aromatic Compounds. *Abstracts of Papers of the American Chemical Society*, **213**, 19.

COLARUSSO, P. & SERPONE, N. (1996) Sonochemistry II. - Effect of Ultrasounds on Homogeneous Chemical Reactions and in Environmental Detoxification. *Research on Chemical Intermediates,* **22**, 61-89.

COLUSSI, A. J., WEAVERS, L. K. & HOFFMANN, M. R. (1998) Chemical Bubble Dynamics and Quantitative Sonochemistry. *Journal of Physical Chemistry A,* **102**, 6927-6934.

CORPORATION, S. R. (2006) Interactive PhysProp Database. http://www.syrres.com/esc/phys- demo.html.

CUM, G., G, G., GALLO, R. & SPADARO, A. (1991) Role of Frequency in the Ultrasonic Activation of Chemical Reactions. *Ultrasonics,* **30**, 267-270.

DESTAILLATS, H., COLUSSI, A. J., JOSEPH, J. M. & HOFFMANN, M. R. (2000) Synergistic Effects of Sonolysis Combined with Ozonolysis for the Oxidation of Azobenzene and Methyl Orange. *Journal of Physical Chemistry A,* **104**, 8930-8935.

DESTAILLATS, H., II, T. W. A. & HOFFMANN, M. R. (2001) Applications of Ultrasound in NAPL remediation: Sonochemical Degradation of TCE in Aqueous Surfactant solutions. *Environmental Science and Technology,* **35**, 3019-3024.

DESTAILLATS, H., TURJANSKI, A. G., ESTRIN, D. A. & HOFFMANN, M. R. (2002) Molecular Structure Effects on the Kinetics of Hydroxyl Radical Addition to Azo Dyes. *Journal of Physical Organic Chemistry,* **15**, 287-292.

DEWULF, J., LANGENHOVE, H. V., VISSCHER, A. D. & SABBE, S. (2001) Ultrasonic Degradation of Trichloroethylene and Chlorobenzene at Micromolar Concentrations:

Kinetics and Modelling. *Ultrasonics Sonochemistry,* **8**, 143-150.

DIDENKO, Y. T., III, W. B. M. & SUSLICK, K. S. (1999) Hot Spot Conditions during Cavitation in Water. *Journal of the American Chemical Society,* **121**, 5817-5818.

DIDENKO, Y. T. & SUSLICK, K. S. (2002) The Energy Efficiency of Formation of Photons, Radicals and Ions During Single-Bubble Cavitation. *Nature,* **418**, 394-397.

DRIJVERS, D., BAETS, R. D., VISSCHER, A. D. & LANGENHOVE, H. V. (1996) Sonolysis of Trichloroethylene in Aqueous Solution: Volatile Organic Intermediates. *Ultrasonics Sonochemistry,* **3**, S83-S90.

DRIJVERS, D., LANGENHOVE, H. V. & HERRYGERS, V. (2000) Sonolysis of Fluoro-, Chloro-, Bromo- and Iodobenzne: A Comparative Study. *Ultrasonics Sonochemistry,* **7**, 87-95.

DRIJVERS, D., LANGENHOVE, H. V., KIM, L. N. T. & BRAY, L. (1999) Sonolysis of an Aqueous Mixture of Trichloroethylene and Chlorobenzene. *Ultrasonics Sonochemistry,* **6**, 115-121.

DRIJVERS, D., LANGENHOVE, H. V. & VERVAET, K. (1998) Sonolysis of Chlorobenzene in Aqueous Solution: Organic Intermediates. *Ultrasonics Sonochemistry,* **5**, 13-19.

DUESTERBERG, C. K., COOPER, W. J. & WAITE, T. D. (2006) Fenton-Mediated Oxidation in the Presence and Absence of Oxygen. *Environmental Science and Technology,* **39**, 5052-5058.

DUTTA, K., BHATTACHARJEE, S., CHAUDHURI, B. & MUKHOPADHYAY, S. (2002) Chemical Oxidation of C.I. Reactive Red 2 Using Fenton-like Reactions. *Journal of*

Environmental Monitoring, **4**, 754-760.

ELLIOT, A. J. & SIMSON, A. S. (1984) Rate Constants for Reactions of Hydroxyl Radicals as a Function of Temperature. *Radiation Physics and Chemistry,* **24**, 229-231.

EMERY, R. J., PAPADAKI, M. & MANTZAVINOS, D. (2003) Sonochemical Degradation of Phenolic Pollutants in Aqueous Solutions. *Environmental Technology,* **24**, 1491-1500.

ENSMINGER, D. (1973) *Ultrasonic: The Low and High-Intensity Application,* New York, Marcel Dekker.

ENTEZARI, M. H. & KRUUS, P. (1994) Effect of Frequency on Sonochemical Reactions. I : Oxidation of Iodide. *Ultrasonics Sonochemistry,* **1**, S75-S79.

ENTEZARI, M. H., KRUUS, P. & OTSON, R. (1997) Effect of Frequency on Sonochemical Reactions. III : Dissociation of Carbon Disulfide. *Ultrasonics sonochemistry,* **4**, 49-54.

ERSHOV, B. G., GORDEEV, A. V., KELM, M. & JANATA, E. (2003) Rate Constant for the Reaction of the H atom with H_2O_2 in Aqueous Solution. *Radiatiion Physics and Chemistry,* **67**, 613-616.

FISCHER, C.-H., HART, E. J. & HENGLEIN, A. (1986) Ultrasonic Irradication of Water in the Presence of $^{18,18}O_2$: Isotope Exchange and Isotopic Distribution of H_2O_2. *Journal of Physical Chemistry,* **90**, 1954-1956.

FLYUNT, R., SCHUCHMANN, M. N. & SONNTAG, C. V. (2001) A Common Carbanion Intermediate in Recombination and Proton-Catalysed Disproportionation of the Caboxyl Radical Anion, $CO_2^{\bullet-}$, in Aqueous Solution. *Chemistry-A European Journal,* **7**, 796-799.

FORTUNE, W. B. & MELLON, M. G. (1938) Determination of Iron with o-Phenanthroline - A Spectrophotometric Study. *Industical and Engineering Chemistry-Analytical Editioin,* **10**, 60-64.

FRANCONY, A. & P TRIER, C. (1996) Sonochemical Degradation of Carbon Tetrachloride in Aqueous Solutions at Two Frequencies: 20kHz and 500kHz. *Ultrasonics Sonochemistry,* **3**, S77-S82.

FUNG, P. C., POON, C. S., CHU, C. W. & TSUI, S. M. (2001) Degradation Kinetics of Reactive Dye by UV/H_2O_2/US Process Under Continuous Mode Operation. *Water Science and Technology,* **44**, 67-72.

GAUTIER, O., CARR JR., R. W. & SEIGNEUR, C. (1985) Variational Sensitivity Analysis of a Photochemical Smog Mechanism. *Internatioanl Journal of Chemical Kinetics,* **17**, 1347-1364.

GOEL, M., HONGQIANG, H., MUJUMDAR, A. S. & RAY, M. B. (2004) Sonochemical Decompostion of Volatile and Non-Volatile Organic Compounds-a Comparative Study. *Water Research,* **38**, 4247-4261.

GONDREXON, N., RENAUDIN, V., P TRIER, C., BOLDO, P., BERNIS, A. & GONTHIER, Y. (1999) Degradation of Pentacholorphenol Aqueous Solutions Using a Continuous Flow Ultrasonic Reactor: Experimental Performance and Modelling. *Ultrasonics Sonochemistry,* **5**, 125-131.

GONG, C. L. & HART, D. P. (1998) Ultrasound Induced Caviation and Sonochemical Yields. *Journal of the Acoustical Society of America,* 104, 2675-2682.

GUTIERREZ, M. & HENGLEIN, A. (1990) Chemical Action of Pulsed Ultrasound: Observation of an Unprecedented Intensity Effect. *J. Phys. Chem.,* **94**, 3625-3628.

GUTIERREZ, M. & HENGLEIN, A. (1991) Radical Scavenging in the Sonolysis of Aqueous Solutions of I^-, Br^-, and N_3^-. *Journal of Physical Chemistry,* **95**, 6044-6047.

GUTIERREZ, M., HENGLEIN, A. & FISCHER, C.-H. (1986) Hot Spot Kinetics of the Sonolysis of Aqueous Acetate Solutions. *International Journal of Radiation Biology,* **50**, 313-321.

HARADA, H. (2005) Synergistic Effect of Combining Sonolysis and Photocatalysis of Oxalic Acid. *Electrochemistry,* **73**, 202-204.

HARADA, H. & KUMAGAI, H. (2003) Effect of Dissolved Oxygen in Water on H_2O_2 Production Rate by Sonication. *Japanese Journal of Applied Physics Part 1 - Regular Papers Short Notes & Review Papers,* **42**, 2958-2962.

HARRIS, G. W. & WAYNE, R. P. (1975) Reaction of Hydroxyl Radicals with NO, NO_2 and SO_2. *Journal of the Chemical Society-Faraday Transactions I,* **71**, 610-617.

HART, E. J. & HENGLEIN, A. (1985) Free Redical and Free Atom Reactions in the Sonolysis of Aqueous Iodide and Formate Solutions. *Journal of Physical Chemistry,* **89**, 4342-4347.

HART, E. J. & HENGLEIN, A. (1987) Sonochemistry of Aqueous Solutions : H_2-O_2 Combustion in Cavitation Bubbles. *Journal of Physical Chemistry,* **91**, 3654-3655.

HART, E. J. & HENGLEIN, A. (1988) Sonolysis of Formic Acid-Water Mixtures. *Radiatiion Physics and Chemistry,* **32**, 11-13.

HENGLEIN, A. (1993) Contributions to Various Aspects of Cavitation Chemistry. IN MASON, T. J. (Ed.) *Advances in Sonochemistry.* London, JAI Press Ltd.

HENGLEIN, A. & KORMANN, C. (1985) Scavenging of OH Radicals Produced in the Sonolysis of Water. *International Journal of Radiation Biology,* **48**, 251-258.

HOFFMANN, M. R., HUA, I. & HOCHEMER, R. (1996) Applications of Ultrasonic Irradiation for the Degradation of Chemical Contaminants in Water. *Ultrasonics Sonochemistry,* **3**, S163-S172.

HOWARD, P. H. & MEYLAN, W. M. (1997) *Handbook of Physical Properties of Organic Chemical,* Environ. Sci. Center, Syracuse Res. Corporation, CRC Press Inc.

HUA, I., HOCHEMER, R. H. & HOFFMANN, M. R. (1995) Sonolytic Hydrolysis of p-Nitrophenyl Acetate: The Role of Supercritical Water. *Journal of Physical Chemistry,* **99**, 2335-2342.

HUA, I. & HOFFMANN, M. R. (1996) Kinetics and Mechanism of the Sonolytic Degradation of CCl_4: Intermediated and Byproducts. *Environmental Science and Technology,* **30**, 864-871.

HUA, I. & HOFFMANN, M. R. (1997) Optimization of Ultrasonic Irradiation as an Advanced Oxidation Technology. *Environmental Science and Technology,* **31**, 2237-2243.

HUNG, H.-M. & HOFFMANN, M. R. (1998) Kinetics and Mechanism of the Enhanced Reductive Degradation of CCl_4 by Element Iron in the Presence of Ultrasound. *Environmental Science and Technology,* **32**, 3011-3016.

HUNG, H.-M. & HOFFMANN, M. R. (1999) Kinetics and Mechanism of the Sonolytic Degradation of Chlorinated Hydrocarbons: Frequency Effects. *Journal of Physical Chemistry A,* **103**, 2734-2739.

HUNG, H.-M., KANG, J.-W. & HOFFMANN, M. R. (2002) The Sonolytic Destruction of Methyl Tert-Butyl Ether Present in Contaminated Groundwater. *Water Environment Research,* **74**, 545-556.

HUNG, H.-M., LING, F. H. & HOFFMANN, M. R. (2000) Kinetics and Mechanism of the Enhanced Reductive Degradation of Nitrobenzene by Elemental Iron in the Presence of Ultrasound. *Environmental Science and Technology,* **34**, 1758-1763.

IANNI, J. C. (2002) KINTECUS. Windows Version 3.0 ed., www.kintecus.com.

IOAN, I., WILSON, S. & LUNDANES, E. (2007) Comparison of Fenton and sono-Fenton Bisphenol A Degradation. *Journal of Hazardous Materials,* **142**, 559-563.

JIANG, Y., PETRIER, C. & WAITE, T. D. (2002) Effect of pH on the Ultrasonic Degradation of Ionic Aromatic Compounds in Aqueous Solution. *Ultrasonics Sonochemistry,* **9**, 163-168.

JIANG, Y., PETRIER, C. & WAITE, T. D. (2002) Kinetics and Mechanisms of Ultrasonic Degradation of Volatile Chlorinated Aromatics in Aqueous Solutions. *Ultrasonics Sonochemistry,* **9**, 317-323.

JIANG, Y., PETRIER, C. & WAITE, T. D. (2006) Sonolysis of 4-Chlorophenol in Aqueous Solution: Effects of Substrate Concentration, Aqueous Temperature and Ultrasonic Frequency. *Ultrasonics Sonochemistry,* **13**, 415-422.

JIANG, Y. & WAITE, T. D. (2003) Degradation of Trace Contaminants using Coupled Sonochemistry and Fenton's Reagent. *Water Science and Technology,* **47**, 85-92.

JOSEPH, J. M., DESTAILLATS, H., HUNG, H.-M. & HOFFMANN, M. R. (2000) The Sonochemical Degradation of Azobenzene and Related Azo Dyes: Rate

Enhancements via Fenton's Reactions. *Journal of Physical Chemistry A,* **104**, 301-307.

JUNBO, F., AKI, S. N. V. K., CHATEAUNEUF, J. E. & BRENNECKE, J. F. (2002) Hydroxyl Radical Reactivity with Nitrobenzene in Subcritical and Supercritical Water. *Journal of Americal Chemical Society,* **124**, 6304-6311.

KANG, J.-W. & HOFFMANN, M. R. (1998) Kinetics and Mechanism of the Sonolytic Destruction of Methyl tert-Butyl Ether by Ultrasonic Irradiation in the Presence of Ozone. *Environmental Science and Technology,* **32**, 3194-3199.

KANG, J.-W., HUNG, H.-M., LIN, A. & HOFFMANN, M. R. (1999) Sonolytic Destruction of Methyl tert-Butyl Ether by Ultrasonic Irradiation: The Role of O_3, H_2O_2, Frequency, and Power Density. *Environmental Science and Technology,* **33**, 3199-3205.

KANTHALEA, M. P., BROTCHIEA, A., ASHOKKUMAR, M. & GRIESERA, F. (2008) Experimental and Theoretical Investigations on Sonoluminescence under Dual Frequency Conditions. *Ultrasonics Sonochemistry,* **15**, 629-635.

KATSUMURA, Y., JIANG, P. Y., NAGAISHI, R., OISHI, T. & ISHIGURE, K. (1991) Pulse Radiolysis Study of aqueous nitric acid solutions. Formation mechanism, Yield, and reactivity of NO_3 radical. *J. Phys. Chem.,* **95**, 4435-4439.

KIM, D. K., O'SHEA, K. E. & COOPER, W. J. (2002) Degradation of MTBE and Related Gasoline Oxygenates in Aqueous Media by Ultrasound Irradiation. *Journal of Environmental Engineering,* **128**, 806-812.

KIM, J. K., MARTINEZ, F. & METCALFE, I. S. (2007) The Beneficial Role of Use of Ultrasound in Heterogeneous Fenton-like System over Supported Copper Catalysts for Degradation of *p*-Chlorophenol. *Catalysis Today,* **124**, 224-231.

KIWI, J., LOPEZ, A. & NADTOCHENKO, V. (2000) Mechanism and Kinetics of the OH-Radical Intervention during Fenton Oxidation in the Presence of a Significant Amount of Radical Scavenger(Cl^-). *Environmental Science and Technology,* **34**, 2162-2168.

KODA, S., KIMURA, T., KONDO, T. & MITOME, H. (2003) A Standard Method to Calibrate Sonochemical Efficiency of an Individual Reaction System. *Ultrasonics Sonochemistry,* **10**, 149-156.

KONDO, K., KRISHNA, C. M. & RIESZ, P. (1989) Pyrolysis Radicals Formed by Ultrasound in Aqueous Solutions of Nucleotides: A Spin-Trapping Study. *International Journal of Radiation Biology,* **57**, 23-33.

KOTRONAROU, A., MILLS, G. & HOFFMANN, M. R. (1991) Ultrasonic Irradiation of p-Nitrophenol in Aqueous Solution. *Journal of Physical Chemistry,* **95**, 3630-3638.

KROSCHWITZ, J. I. (2004) *Kirk-Othmer Encyclopedia of Chemical Technology,* N. J., John Wiley & Sons Inc.

KRUUS, P., BURK, R. C., ENTEZARI, M. H. & OTSON, R. (1997) Sonication of Aqueous Solutions of Chlorobenzene. *Ultrasonics Sonochemistry,* **4**, 229-233.

KUBO, M., MATSUOKA, K., TAKAHASHI, A., SHIBASAKI-KITAKAWA, N. & YONEMOTO, T. (2005) Kinetics of Ultrasonic Degradation of Phenol in the Presence of TiO_2 Particles. *Ultrasonics Sonochemistry,* **12**, 263-269.

KUIJPERS, M. W. A., KEMMERE, M. F. & KEURENTJES, J. T. F. (2002) Calorimetric Study of the Energy Efficiency for Ultrasound-Induced Radical Formation. *Ultrasonics,* **40**, 675-678.

KWAN, W. P. & VOELKER, B. M. (2002) Decomposition of Hydrogen Peroxide and Organic Compounds in the Presence of Dissolved Iron and Ferrihydrite. *Environmental Science and Technology,* **36**, 1467-1476.

LEIGHTON, T. G. (1994) *The Acoustic Bubble,* London, Harcourt Brace & Co..

LESKO, T., COLUSSI, A. J. & HOFFMANN, M. R. (2006) Sonochemical Decomposition of Phenol: Evidence for a Synergistic Effect of Ozone and Ultrasound for the Elimination of Total Organic Carbon from Water. *Environmental Science and Technology,* **40,** 6818-6823.

LIDE, D. R. (2004-2005) *CRC handbook of chemistry and physics.,* Cleveland, Ohio, CRC Press.

LIM, M., KIM, S., KIM, Y. & KHIM, J. (2007) Sonolysis of Chlorinated Compounds in Aqueous Solution. *Ultrasonics Sonochemistry,* **14**, 93-98.

LIN, J.-G. & MA, Y.-S. (2000) Oxidation of 2-Chlorophenol in Water by Ultrasound/Fenton Method. *Journal of Environmental Engineering,* **126**, 130-137.

LORIMER, J. P., MASON, T. J. & FIDDY, K. (1991) Enhancement of Chemical Reactivity by Power Ultrasound: An Alternative Interpretation of the Hot Spot. *Ultrasonics,* **29**, 338-343.

LORIMER, J. P., MASON, T. J., PLATTES, M., PHULL, S. S. & WALTON, D. J. (2001) Degradation of Dye Effluent. *Pure and Applied Chemistry,* **73**, 1957-1968.

MACK, J. & BOLTON, J. R. (1999) Photochemistry of Nitrite and Nitrate in Aqeous Solution : A Review. *Journal of Phtochemistry and Photobiology A: Chemistry,* **128**, 1-13.

MAKINO, K., MOSSOBA, M. M. & RIESZ, P. (1983) Chemical Effects of Ultrasound on

Aqueous Solutions. Formations of Hydroxyl Radicals and Hydrogen Atoms. *Journal of Physical Chemistry* **87**, 1369-1377.

MARGULIS, M. A. (1993) *Sonochemistry and Cavitation,* London, Gordon and Breach Publishers.

MASON, T. J. (1991) *Practical Sonochemistry : User's Guide to Applications in Chemistry and Chemical Engineering,* Chichester, Ellis Horwood Limited.

MASON, T. J. (1992) *Sonochemistry: Current Trends and Future Prospects,* Cambridge, U.K., Royal Society of Chemistry.

MASON, T. J. (1990b) *A Survey of Commercially Available Sources of Ultrasound Suitable for Sonochemistry,* Cambridge, Royal Society of Chemistry.

MASON, T. J. & LORIMER, J. P. (1988) *Sonochemicstry : Theory, applications and uses of Ultrasound in Chemistry,* Chichester, U.K., Ellis Horwood Limited.

MASON, T. J., LORIMER, J. P. & BATES, D. M. (1992) Quantifying Sonochemistry -Casting Some Lights on a Black Art. *Ultrasonics,* **30**, 40-42.

MASON, T. J. & TIEHM, A. (2001) Ultrasound in Envrionmental Protection. IN MASON, T. J. (Ed.) *Advances in Sonochemistry.* JAI Press.

MEAD, E. L., SUTHERLAND, R. G. & VERRALL, R. E. (1976) The Effect of Ultrasound on Water in the Presence of Dissolved Gases. *Journal of Physical Chemistry,* **54**, 1114-1120.

MINERO, C., LUCCHIARI, M., VIONE, D. & MAURINO, V. (2005) Fe(III)-Enhanced Sonochemical Degradation of methylene Blue in Aqueous Solution. *Environmental Science and Technology,* **39**, 8936-8942.

MISIK, V. & RIESZ, P. (1996) Nitric Oxide Formation by Ultrasound in Aqueous Solutions. *Journal of Physical Chemistry,* **100**, 17986-17994.

MROWETZ, M., PIROLA, C. & SELLI, E. (2003) Degradation of Organic Water Pollutants Through Sonophotocatalysis in the Presence of TiO2 *Ultrasonics Sonochemistry,* **10**, 247-254.

NAGATA, Y., MIZUKOSHI, Y., OKITSU, K. & MAEDA, Y. (1996) Sonochemical Formation of Gold Particles in Aqueous Solution. *Radiation Research,* **146**, 333-338.

NAGATA, Y., NAKAGAWA, M., OKUNO, H., MIZUKOSHI, Y., YIM, B. & MAEDA, Y. (2000) Sonochemical Degradation of Chlorophenol in Water. *Ultrasonics Sonochemistry,* **7**, 115-120.

NAM, S.-N., HAN, S.-K., KANG, J.-W. & CHOI, H. (2003) Kinetics and Mechanisms of the Sonolytic Destruction of Non-Volatile Organic Compounds: Investigation of the Sonochemical Reaction Zone Using Several $OH^{\cdot}$ Monitoring Techniques. *Ultrasonics Sonochemistry,* **10**, 139-147.

NANZAI, B., OKITSU, K., TAKENAKA, N., BANDOW, H. & MAEDA, Y. (2008) Sonochemical Degradation of Various Monocyclic Aromatic Compounds: Relation between Hydrophobicities of Organic Compounds and the Decomposition Rates. *Ultrasonics Sonochemistry,* **15**, 478-483.

NEPPOLIAN, B., JUNG, H., CHOI, H., LEE, J. H. & KANG, J.-W. (2002) Sonolytic Degradation of Methyl *tert*-Butyl Ether: The Role of Coupled Fenton Process and Persulphate Ion. *Water Research,* **36**, 4699-4708.

NEPPOLIAN, B., PARK, J.-S. & CHOI, H. (2003) Effect of Fenton-like Oxidation on Enhanced Oxidative Degradation of para-Chlorobenzoic Acid by Ultrasonic Irradiation. *Ultrasonics Sonochemistry,* **11**, 273-279.

NIKITENKO, S. I., VENAULT, L. & MOISY, P. (2004) Scavenging of OH Radicals

Produced from H_2O Sonolysis with Nitrate Ions. *Ultrasonics Sonochemistry,* **11**, 139-142.

NOLTINGK, B. E. & NEPPIRAS, E. A. (1950) Cavitation Produced by Ultrasonics. *Proceedings of the Physical Society of London Section B,* **63**, 674-685.

OKITSU, K., IWASAKI, K., YOBIKO, Y., BANDOW, H., NISHIMURA, R. & MAEDA, Y. (2005) Sonochemical Degradatioin of Azo Dyes in Aqueous Solution: A New Heterogenous Kinetics Model taking into account The Local Concentratiion of OH Radicals and Azo Dyes. *Ultrasonics Sonochemistry,* **12,** 255-262.

OKOUCHI, S., NOJIMA, O. & ARAI, T. (1992) Cavitation-Induced Degradation of Phenol by Ultrasound. *Water Science and Technology,* **26**, 2053-2056.

OKUNO, H., KIM, B., MIZUKOSHI, Y., NAGATA, Y. & MAEDA, Y. (2000) Sonolytic Degradation of Hazardous Organic Compounds in Aqueous Solution. *Ultrasonics Sonochemistry,* **7**, 261-264.

OLSON, T. M. & BARBIER, P. F. (1994) Oxidation Kinetics of Natural Organic Matter by Sonolysis and Ozone. *Water Research,* **28**, 1383-1391.

PETRIER, C., COMBET, E. & MASON, T. (2007) Oxygen-induced concurrent ultrasonic degradation of volatile and non-volatile aromatic compounds. *Ultrasonics Sonochemistry,* **14**, 117-121.

PETRIER, C. & FRANCONY, A. (1997) Ultrasonic Waste-water Treatment: Incidence of Ultrasonic Frequency on the Rate of Phenol and Carbon Tetrachloride Degradation. *Ultrasonics Sonochemistry,* **4**, 295-300.

PETRIER, C., JEUNET, A., LUCHE, J.-L. & REVERDY, G. (1992) Unexpected Frequency Effects on the Rate of Oxidative Processes Induced by Ultrasound. *Journal of*

Americal Chemical Society, **114**, 3148-3150.

PETRIER, C., JIANG, Y., FRANCONY, A. & LAMY, M.-F. (1999) Ultrasound in Environmental Engineering. IN A., T. & U., N. (Eds.) *TU Harmburg-Harburg Reports on Sanitary Engineering.*

PETRIER, C., JIANG, Y. & LAMY, M.-F. (1998) Ultrasound and Environment: Sonochemical Destruction of Chloroaromatic Derivaties. *Environmental Science and Technology,* **32**, 1316-1318.

PETRIER, C., LAMY, M.-F., FRANCONY, A., BENAHCENE, A. & DAVID, B. (1994) Sonochemical Degradation of Phenol in Dilute Aqueous Solutions: Comparison of the Reaction Rates at 20 and 487 kHz. *Journal of Physical Chemistry,* **98**, 10514-10520.

PETRIER, C., MICOLLE, M., MERILN, G., LUCHE, J.-L. & REVERDY, G. (1992) Characteristics of Pentachlorophenate Degradation in Aqeous Solution by Means of Ultrasound. *Environmental Science and Technology,* **26**, 1639-1642.

PETRIER, C., NAFFRECHOUX, E., GIMENO, C. H. & HACHEMI, M. E. E. (2002) *Combined Processes Ultrasound/Ozone and Ultrasound/UV for Liquid Waste Treatment*, Neis U..

PRICE, G. (1990) The Use of Ultrasound for the Controlled Degradation of Polymer Solutions. IN MASON, T. J. (Ed.) *Advances in Sonochemistry.* JAI Press.

RAGAINI, V., SELLI, E., BIANCHI, C. L. & PIROLA, C. (2001) Sono-Photocatalytic Degradation of 2-Chlorophenol in Water: Kinetic and Energetic Comparison with Other Techniques. *Ultrasonics Sonochemistry,* **8**, 251-258.

RAJAN, R., KUMAR, R. & GANDHI, K. S. (1998) Modeling of Sonochemical

Decomposition of CCl_4 in aqueous solutions. *Environmental Science and Technology,* **32**, 1128-1133.

RASSOKHIN, D. N., GOKZHAEV, M. B., BUGAENKO, L. T. & KOVALEV, G. V. (1994) Sonolysis of Aqueous Solutions under Argon: Dependence of the Rate of Hydrogen Peroxide Formation on Hydroxyl radical Scavenger Concentration. *Mendeleev Communications*, 25-27.

RATOARINORO, N., CONTAMINE, F., WILHELM, A. M., BERLAN, J. & DELMAS, H. (1995) Power Measurment in Sonochemistry. *Ultrasonics Sonochemistry,* **2**, S43-S47.

RIESZ, P., BERDAHL, D. & CHRISTMAN, C. L. (1985) Free Radical Generation by Ultrasound in Aqueous and Nonaqueous Solutions. *Environ. Health Perspect,* **64**, 233-238.

RIESZ, P. & KONDO, T. (1992) Free Radical Formation Induced by Ultrasound and Its Biological Implications. *Free Radical Biology & Medicine,* **13**, 247-270.

RIESZ, P., KONDO, T. & KRISHNA, C. M. (1990) Sonochemistry of Volatile and Non-volatile Solutes in Aqueous Solutions: E.P.R. and Spin Trapping Studies. *Ultrasonics,* **28**, 295-303.

RONG, L., YASUDA, K., BANDO, Y. & NAKAMURA, M. (2002) Ultrasonic Decomposition of a Mixture of Phenol and p-Chlorophenol in Aqueous Solution. *Japanese Journal of Applied Physics Part 1,* **41**, 3272-3276.

ROSE, A. R. & WAITE, T. D. (2002) Kinetic Model for Fe(II) Oxidation in Seawater in the Absence and Presence of Natural Organic Matter. *Environmental Science and Technology,* **36**, 433-444.

ROSS, F. & ROSS, A. B. (1977) *Selected Specific Rates of Reactions of Transients from Water in Aqueous Solution; (NSRDS-NBS59),* Gaithersburg, MD, U.S. National Bureau of Standards.

SEHGAL, C. M. & WANG, S. Y. (1981) Threshold Intensities and Kinetics of Sonoreaction of Thymine in Aqueous Solutions at Low Ultrasonic Intensities. *Journal of Americal Chemical Society,* **103**, 6606-6611.

SERPONE, N. & COLARUSSO, P. (1994) Sonochemistry I. Effects of Ultrasounds on Heterogeneous Chemical Reactions-A Useful Tool to Generate Radicals and to Examine Reaction Mechanisms. *Research on Chemical Intermediates,* **20**, 635-679.

SERPONE, N., TERZIAN, R., COLARUSSO, P., MINERO, C., PELIZZETTI, E. & HIDAKA, H. (1992) Sonochemical Oxidation of Phenol and Three of Its Intermediate Products in Aqueous Media: Catechol, Hydroquinone, and Benzoquinone. Kinetic and Mechanistic Aspects. *Research on Chemical Intermediates,* **18**, 183-202.

SERPONE, N., TERZIAN, R., HIDAKA, H. & PELIZZETTI, E. (1994) Ultrasonic Induced Dehalogenation and Oxidation of 2-, 3-, and 4-Chlorophenol in Air-Equilibrated Aqueous Media. Similarities with Irradiated Semiconductor Particulates. *Journal of Physical Chemistry,* **98**, 2634-2640.

SERVANT, G., CALTAGIRONE, J. P., GERARD, A., LABORDE, J. L. & HITA, A. (2000) Numerical Simulation of Cavitation Bubble Dynamics Induced by Ultrasound Waves in a High Frequency Reactor. *Ultrasonics Sonochemistry,* **7**, 217-227.

SHIRGAONKAR, I. Z. & PANDIT, A. B. (1998) Sonophotochemical Destructionof Aqueous Solutionof 2,4,6-Trichlorophenol. *Ultrasonics Sonochemistry,* **5**, 53-61.

SIERKA, R. A. & AMY, G. L. (1985) Catalytic Effects of Ultraviolet-Light and or Ultrasound on the Ozone Oxidation of Humic-Acid and Trihalomethane Precursors. *Ozone-Sicence & Engineering,* **7**, 47-62.

SINGLA, R., ASHOKKUMAR, M. & GRIESER, F. (2004) The Mechanism of the Sonochemical Degradation of Benzoic Acid in Aqueous Solutions. *Res. Chem. Intermed.,* **30**, 723-733.

SIVAKUMAR, M. & PANDIT, A. B. (2001) Ultrasound Enhanced Degradation of Rhodamine B: Optimization with Power Density. *Ultrasonics Sonochemistry,* **8**, 233-240.

SIVAKUMAR, M., TATAKE, P. A. & PANDIT, A. B. (2002) Kinetics of p-Nitrophenol Degradation: Effect of Reaction Conditions and Cavitational Parameters for a Multiple Frequency System. *Chemical Engineering Journal,* **85**, 327-338.

Standard Methods for the Examination of Water and Wastewater, Washington DC, 1992 American Public Health Association.

STAVARACHE, C., YIM, B., VINATORU, M. & MAEDA, Y. (2002) Sonolysis of Chlorobenzene in Fenton-type Aqueous Systems. *Ultrasonics Sonochemistry,* **9**, 291-296.

SUPENO & KRUUS, P. (2000) Sonochemical Formation of Nitrate and Nitrite in Water. *Ultrasonics Sonochemistry,* **7**, 109-113.

SUSLICK, K. S. (1988) *Ultrasound; Its Chemical, Physical, and Biological Effects,* New York, VCH Pubilishers.

SUSLICK, K. S. (1989) The Chemical Effect of Ultrasound. *Scientific American,* **260**,

80-86.

SUSLICK, K. S. (1990) Sonochemistry. *Science,* **247**, 1493-1495.

SUSLICK, K. S. & HAMMERTON, D. A. (1986) The Site of Sonochemical Reactions. *IEEE Transactions on Ultrasonics, Ferroelectrics, and Frequency Control,* **UFFC-33**, 143-146.

SUSLICK, K. S., HAMMERTON, D. A. & RAYMOND E. CHLINE, J. (1986) The Sonochemical Hot Spot. *Journal of Americal Chemical Society,* **108**, 5641-5642.

SWIATLA-WOJCIK, D. & BUXTON, G. V. (2005) On the Possible Role of the Reaction $H\bullet + H_2O \rightarrow H_2 + OH\bullet$ in the Radiolysis of Water at High Temperatures. *Radiatiion Physics and Chemistry,* **74**, 210-219.

THOMAS, J. K. (1965) Rates of Reaction of the Hydroxyl Radical. *Transactions of the Faraday Society,* **61**, 702-707.

THOMPSON, L. H. & DORAISWAMY, L. K. (1999) Sonochemistry: Science and Engineering. *Industrial & Engineering Chemistry Research,* **38,** 1215-1249.

TORII, T., YASUI, K., YASUDA, K., IIDA, Y., TUZIUTI, T., SUZUKI, T. & NAKAMURA, M. (2004) Generation and Consumption Rates of OH radicals in Sonochemical Reactions. *Research on Chemical Intermediates,* **30**, 713-721.

TORRES, R. A., PETRIER, C., COMBET, E., CARRIER, M. & PULGARIN, C. (2007) Ultrasonic Cavitation Applied to the Treatment of Bisphenol A. Effect of Sonochemical Parameters and Analysis of BPA By-products *Ultrasonics Sonochemistry,* **15**, 605-611.

TOY, M. S. (1990) Photosonochemical Decompostion of Aqeous 1,1,1-Trichloroethane. *Environmetal Technology,* **11**, 837-842.

TRAPIDO, M., VERESSININA, Y. & MUNTER, R. (1998) Advanced Oxidation Processes for Degradation of 2,4-Dichloro- and 2,4-Demethylphenol. *Journal of Environmental Engineering,* **124**, 690-694.

TUŔANYI, T. (1990) Sensitivity analysis of complex kinetic systems. Tools and applications. *Journal of Mathematical Chemistry,* **5**, 203-248.

VAJDA, S., VALKO, P. & TUŔANYI, T. (1985) Principal Component Analysis of Kinetic Models. *International Journal of Chemical Kinetics,* **17**, 55-81.

VENAULT, L., PH., M., NIKITENKO, S. I. & MADIC, C. (1997) Kinetics of Nitrous Acid Formation in Nitric Acid Solutions under the Effect of Power Ultrasound. *Ultrasonics Sonochemistry,* **4**, 195-204.

VIONE, D., MAURINO, V., MINERO, C., BORGHESI, D., LUCCHIARI, M. & PELIZZETTI, E. (2003) New Processes in the Environmental Chemistry of Nitrite. 2. The Role of Hydrogen Peroxide. *Environmental Science and Technology,* **37**, 4635-4641.

VISSCHER, A. D. (2003) Kinetic Model for the Sonochemical Degradation of Monocyclic Aromatic Compounds in Aqueous Solution: New sights. *Ultrasonics Sonochemistry,* **10**, 157-165.

VISSCHER, A. D., EENOO, P. V., DRIJVERS, D. & LANGENHOVE, H. V. (1996) Kinetic Model for the Sonochemical Degradation of Monocyclic Aromatic Compounds in Aqueous Solution. *Journal of Physical Chemistry,* **100**, 11636-11642.

WAKEFORD, C. A., BLACKBURN, R. & LICKISS, P. D. (1999) Effect of Ionic Strength

on the Acoustic Generation of Nitrite, Nitrate and Hydrogen Peroxide. *Ultrasonics Sonochemistry,* **6**, 141-148.

WALLING, C. (1975) Fenton's Reagent Revisited. *Acc. Chem. Res.,* **8**, 125-131.

WEAST, R. C. (1988-1989) *HandBook of Chemistry and Physics*, CRC Press.

WEAVERS, L. K. & HOFFMANN, M. R. (1998) Sonolytic Decomposition of Ozone in Aqueous Solution: Mass Transfer Effects. *Environmental Science and Technology,* **32**, 3941-3947.

WEAVERS, L. K., LING, F. H. & HOFFMANN, M. R. (1998) Aromatic Compound Degradation in Water Using a Combination of Sonolysis and Ozonolysis. *Environmental Science and Technology,* **32**, 2727-2733.

WEAVERS, L. K., MALMSTADT, N. & HOFFMANN, M. R. (2000) Kinetics and Mechanism of Pentachlorophenol Degradation by Sonication, Ozonation, and Sonolytic Ozonation. *Environmental Science and Technology,* **34**, 1280-1285.

WEISSLER, A. (1958) Formation of Hydrogen Peroxide by Ultrasonic Waves: Free Radicals. *Journal of the American Chemical Society,* **81**, 1077-1081.

WHILLOCK, G. O. H. & HARVEY, B. F. (1997b) Ultrasonically Enhanced Corrosion of 304L Stainless Steel. II: The Effect of Frequency, Acoustic Power and Horn to Specimen Distance. *Ultrasonics Sonochemistry,* **4**, 33-38.

WU, C., LIU, X., WE, D., FAN, J. & WANG, L. (2001) Photosonochemical Degradation of Phenol in Water *Water Research,* **35**, 3927-3933.

WU, J., HUANG, H. & LIVENGOOD, C. (1992) Ultrasonic Destruction of Chlorinated Compounds in Aqueous Solution. *Environmental Progress,* **11**, 195-201.

WU, Z. & ONDRUSCHKA, B. (2005) Roles of Hydrophobicity and Volatility of Organic Substrates on Sonolytic Kinetics in Aqueous Solutions. *Journal of Physical Chemistry A,* **109**, 6521-6526.

YIM, B., YOO, Y. & MAEDA, Y. (2003) Sonolysis of Alkylphenols in Aqueous Solution with Fe(II) and Fe(III). *Chemosphere,* **50**, 1015-1023.

AND UB